APPLICATION SPECIFIC DESIGN OF PHOTONIC CRYSTAL FIBERS, WAVEGUIDES AND DEVICES

A thesis submitted to the Faculty of Technology,
University of Delhi for the award of degree of

DOCTOR OF PHILOSOPHY

in

APPLIED PHYSICS

by

JITEN BORUAH

Under the supervision of

Prof. R.K. SINHA

Department of Applied Physics,
Delhi College of Engineering (Now, Delhi Technological University),
Faculty of Technology, University of Delhi,
Shahabad Daulatpur, Bawana Road, Delhi-110042, India.

CERTIFICATE

This is to certify that the thesis entitled **"Application Specific Design of Photonic Crystal Fibers, Waveguides and Devices"** which is being submitted by Mr. Jiten Boruah for the award of degree of Doctor of Philosophy to the Faculty of Technology, University of Delhi, India, is entirely based on the work carried out by him under my supervision. The work reported in this thesis embodies the work of the candidate himself and is original one and has not been submitted to any other University or Institution for the award of any degree or diploma.

(Prof. R. K. Sinha)
Supervisor
Department of Applied Physics,
Delhi College of Engineering (Now, Delhi Technological University),
Faculty of Technology, University of Delhi,
Delhi-110042

CERTIFICATE

This is to certify that the thesis titled, **"Application Specific Design of Photonic Crystal Fibers, Waveguides and Devices"** being submitted to the Faculty of Technology, University of Delhi, India, is based on the research work carried out by me under the supervision of Prof. R.K. Sinha. Department of Applied Physics,Delhi College of Engineering (Now, DTU), Faculty of Technology, University of Delhi, Delhi, India.

The Results obtained in this thesis is an original work and has not been submitted in part or full to any other university or institute for the award of any degree or diploma.

(Jiten Boruah)
Candidate

Place:
Date:

(Prof. R. K. Sinha)
Supervisor
Department of Applied Physics,
Delhi College of Engineering
(Now, Delhi Technological University),
Faculty of Technology
University of Delhi, Delhi – 110078, India

(Prof. Sachin Maheshwari)
Head
Applied Sciences & Humanities
& Dean, Faculty of Technology
University of Delhi
Delhi – 110078, India

DEPARTMENT OF APPLIED SCIENCES & HUMANITIES,
FACULTY OF TECHNOLOGY, UNIVERSITY OF DELHI,
DELHI – 110078, INDIA

Date:

CERTIFICATE OF ORIGINALITY

The research work embodied in this thesis entitled "Application Specific Design of Photonic Crystal Fibers, Waveguides and Devices" has been carried out by me at the Department of Applied Science and Humanities, Faculty of Technology, University of Delhi, India. The manuscript has been subjected to plagiarism check by CheckForPlagarism.net software. I declare that the work and language included in this thesis are free from any kind of plagiarism.

Jiten Boruah
Name and Signature of the Candidate

STUDENT APPROVAL FORM

Name of the Author	Jiten Boruah
Department	Department of Applied Sciences and Humanities
Degree	Doctor of Philosophy
University	University of Delhi
Guide	Prof. R.K. Sinha
Thesis Title	Application Specific Design of Photonic Crystal Fibers, Waveguides and Devices
Year of Award	

Agreement

1. I hereby certify that, if appropriate, I have obtained and attached hereto a written permission/statement from the owner(s) of each third party copyrighted matter to be included in my thesis/dissertation, allowing distribution as specified below.
2. I hereby grant to the university and its agents the non-exclusive license to archive and make accessible, under the condition specified below, my thesis/dissertation, in the whole or in part in all forms of media, now or hereafter now. I retain all other ownership right to the copyright of the thesis/dissertation. I also retain to use in future works (such as article or books) all or part of this thesis, dissertation, or project report.

Conditions:

1. Release the entire work for access worldwide.	
2. Release the entire work for 'My University' only for 1 Year 2 Year 3 Year	

After this time release the work for access worldwide.	
3. Release the entire work for 'My university' only while at the same time releasing the following parts of the work (e.g. because other parts relate to publications) for the worldwide access. a) Bibliographic details and synopsis only. b) Bibliography details, synopsis and the following chapters only. c) Preview/Table of Contents/24 pages only.	
4. View only (No Downloads) (worldwide).	

Jiten Boruah

Signature of the Scholar

Prof. R.K. Sinha

Signature and Seal of the Guide

Place:

Date :

Dedicated to my Parents

ACKNOWLEDGEMENT

I am intensely obliged to Prof. (Dr.) Ravindra Kumar Sinha, Professor, Department of Applied Physics, Delhi College of Engineering (Now, Delhi Technological University), Faculty of Technology, University of Delhi, Delhi, India and presently in lien as Director, CSIO, Chandigarh, India for his worthy and insightful guidance and his steady stimulating motivation to induce something new and innovative in the research work in each of our discussions. I would also like to thank him for establishing, procuring and providing the requisite updated research infrastructure to carry out the research work placidly and ardently and at par with the international research community at the "Technology Information, Forecasting and Assessment Council (TIFAC)-Centre of Relevance and Excellence in Fiber Optics and Optical Communication (CORE)", in the department of Applied Physics, Delhi College of Engineering (now Delhi Technological University) Faculty of Technology, University of Delhi, Delhi, India.

It is my privilege to acknowledge the valuable inputs of Dr. Yogita Kalra, Asst. Professor, Department of Applied Physics, Delhi Technological University, Delhi, India, in respect of designing of photonic crystal in the very beginning of this work that increased my motivation level and interest in the subject matter manifold. I also thank her for her active support throughout the course of this research work.

I shall always be grateful to Dr. Than Singh Saini, Post Doctoral Fellow at Optical Functional Materials Laboratory, Toyota Technological Institute (TTI), Nagoya 468-8511, Japan, for his invaluable suggestions and the active support in respect of design and analyses of photonic crystal fiber.

I take this opportunity to thank my fellow research scholars and the technical staff at TIFAC, Department of Applied Physics, Delhi Technological University for their cooperation in the laboratory and boosting my moral.

I would also like to thank my family, friends and colleagues and all well wishers for their support in carrying out this research work. Last but not least, I thank my wife 'Papari' for her patience, constant encouragement and moral support in completing this research work.

Place: **Jiten Boruah**

Date: Candidate

ABSTRACT

Photonic Crystals (PhC) are micro-structured materials with periodic variation of dielectric constant in one, two, or three dimensional length scale and periodicity comparable to the wavelength of light. Because of the periodicity, the PhC exhibit strong reflection for a range of wavelengths resulting in the formation of Photonic Band Gap (PBG). By selecting an appropriate crystal structure of certain materials, one can get a PBG or a frequency range in which propagation or existence of electromagnetic waves is forbidden. Light with frequency that falls within this forbidden frequency range or PBG can be guided through such PhC by creating a waveguide. Similarly, light can be confined or trapped inside such a PhC by creating a cavity. The confined modes of a photonic cavity could be used in optical resonators, laser cavities, filters, switches, demultiplexers, sensors etc. Waveguide and cavity can be created by introducing defects in the periodic structure of PhC on different platforms like Silicon Carbide (SiC), Gallium Arsenide (GaAs) etc predicted for use in all optical networks.

The most significant application of PhC is the design of a novel waveguide known as Photonic Crystal Fiber (PCF) which is essentially a fused silica optical fiber with a periodic distribution of voids or air holes in the cladding that run parallel to its axis. PCF has the extraordinary ability to carry more light in the core, confinement characteristics not possible in conventional optical fiber and characterized by simpler and economic fabrication technique. Nowadays, PCF is finding applications in optical fiber communications, fiber lasers, nonlinear devices, high-power transmission, and highly sensitive gas sensors. Since its inception, PCF is mainly fabricated from silica glass material. But today, researchers have been profusely using materials like fluoride glass, polymer-based and chalcogenide glass in fabrication of PCF. Use of these materials in PCF offer advance characteristics like high non-linearity, high refractive index, high mode confinement, Raman amplification etc.

In this thesis, first, introductions of PhC and PCF have been given and discussed regarding PhC and PCF based devices. This is followed by detailed discussion of theory of light guidance through PhC and PCF, Photonic band gap engineering in PhC, analysis of PhC and PCF structures and different PhC and PCF fabrication

methods. Computational methods utilized in the analysis of PhC and PCF including an overview of the thesis work have been discussed in the introduction.

Investigating photonic structures which are less sensitive to environmental fluctuations like temperature is a valuable area of research. Here, in this thesis, it has been proposed to design photonic crystals using temperature resilient material Silicon Carbide (SiC) and study the variation of width of photonic band gaps in SiC photonic crystals with change in temperature and a comparison with Silicon (Si) photonic crystals using Plane Wave Expansion (PWE) method. Further, SiC point defect cavity has been created in the PhC and analysis of the SiC photonic crystal cavity defect modes have been carried out using Finite Difference Time Domain (FDTD) method. The effect of temperature on different parameters of the proposed designs like band gap width, defect cavity mode dispersion, the resonance mode and quality factor of resonant mode have been studied. The SiC PhC devices can be used for high temperature and power transmission which is difficult to achieve with conventional Si or GaAs based photonic crystals and devices. Apart from applications in optical communication, various other SiC based devices such as optical filters, switches and lasers etc can be designed. The SiC based devices are stable at high power and high temperature, at which the silicon based devices, cannot sustain such high power and temperature.

Apropos of the recent trend of using new fabrication material in PCF, in this thesis, the application specific design of PCF having solid core with regular and irregular cladding geometries, using different and new material and doping the cladding have been studied. First, the design of a PCF in Fluoropolymer material has been done and analyses of the proposed PCF has been carried out in terms of the parameters like effective refractive index of the guided mode and dispersion for wavelength range 10μm to 300μm using full vectorial Finite Element Method (FEM) and MATLAB computational tool. The transmission characteristics of Fluoropolymer PCF are found to be comparable with the earlier published result. The proposed Fluoropolymer PCF may find applications in long distance telecommunication and in mid-infrared region.

Next, the design of a PCF with irregular cladding geometry has been proposed. The PCF has been named after its W letter shaped refractive index profile as W-type PCF. The analysis of the proposed W-type PCF have been done in terms of the parameters

like bend loss of the guided mode, effect of temperature on bend loss and nonlinearity using full vectorial FEM . The transmission characteristics of W-Type PCF obtained are found better compared with the earlier published results. The power coupling in W-type PCF is more compared to conventional PCF. The bend insensitive nature of the proposed W-type PCF structures makes them good candidate for large mode area fiber design and fit for fiber to home applications.

Then, cladding doped large mode area W-type photonic crystal fibers are designed. The analyses of these proposed structures in terms of the parameters like confinement loss, effective refractive index of the guided mode, bend loss, birefringence, sensitivity, effective area and non-linear co-efficient using full vectorial FEM have been carried out. The proposed W-type PCF structures found to possess very low confinement loss and low macro bend loss. The W-type PCF is found to be birefringent and sensitive and can find application in telecommunication and sensing.

In addition to the above proposed PCF structures, a PCF structure has been designed for nonlinear applications in novel Ga-Sb-S based chalcogenide glass which is a different and new PCF fabrication material. The propagation characteristics of the designed Ga-Sb-S based chalcogenide glass PCF structure like effective refractive index of the guided mode, dispersion, effective area, non-linear co-efficient have been investigated by employing full vectorial FEM and MATLAB computational tool. The transmission characteristics of Ga-Sb-S-PCF have been obtained for wavelength range 0.8μm to 14μm. The nonlinear coefficient as high as 14.92 $W^{-1}m^{-1}$ with effective mode area of 3.37μm^2 at the operating wavelength of 1.55μm for the proposed photonic crystal fiber structure has been found. The proposed PCF structure exhibit flat and low dispersion value between spectral spanning 2.4μm - 2.7μm with maximum dispersion variation of 20 ps/nm km. The PCF structure possesses zero dispersion wavelength value at 2.6μm. This novel Ga-Sb-S material based PCF structure has been studied for the first time since the inception of the novel material Ga-Sb-S and can be a promising candidate for nonlinear applications such as mid-infrared supercontinuum generation, slow light generation, and mid-infrared fiber lasers.

In the last, the thesis includes summery and future scope of the research work reported.

LIST OF ABBREVIATIONS

PhC	Photonic Crystal
PBG	Photonic Band Gap
1D	One Dimension
2D	Two Dimension
3D	Three Dimension
SOI	Silicon On Insulator
TE	Transverse Electric
TM	Transverse Magnetic
SiC	Silicon Carbide
Si	Silicon
PCF	Photonic Crystal Fiber
FDTD	Finite Difference Time Domain method
FTTH	Fiber To The Home
FWHM	Full Wave at Half Maximum
GVD	Group Velocity Dispersion
WDM	Wavelength Division Multiplexing
PWE	Plane Wave Expansion method
FEM	Finite Element Method
SC	Supercontinuum
HNA	high numerical aperture
LMA	Large-Mode-Area
HNL	Highly-Non-Linear
HC	Hollow Core
RIP	Refractive Index Profile

LIST OF PUBLICATIONS

A. Research Papers in Journals

1. **Jiten Boruah**, Yogita Kalra, and R. K. Sinha, "Demonstration of temperature resilient properties of 2D silicon carbide photonic crystal structures and cavity modes", OPTIK-international journal for light and electron optics, ISSN: 0030-4026, Elsevier, 125, 1663-1666, (2014).

2. **Jiten Boruah**, Bhawana Dabas, Monika Rajput, and R. K. Sinha, "Characterization of Fluoropolymer Photonic Crystal Fiber for THz regime", Journal of Atomic, Molecular, Condensate & Nano Physics, ISSN: 2349-2716, RGN Publications, 1(2), 65–69, (2014).

3. **Jiten Boruah**, Than Singh Saini, Yogita Kalra, and Ravindra Kumar Sinha, "Temperature-dependent bending loss characteristics of W-type photonic crystal fibres: design and analysis", Journal of Modern Optics, ISSN: 0950-0340(Print), 1362-3044(Online),Taylor & Francis, 64(8), 855-860, (2017).

4. **Jiten Boruah**, Than Singh Saini, Yogita Kalra, and Ravindra Kumar Sinha, "Design and analyses of cladding doped large mode area W-type photonic crystal fiber for high power delivery devices and sensing applications", (2018) (under submission).

5. **Jiten Boruah**, Than Singh Saini, and Ravindra Kumar Sinha, "Low bend loss photonic crystal fiber in Ga-Sb-S based chalcogenide glass for nonlinear applications: design and analysis", Journal of Nanophotonics, ISSN: 1934-2608, SPIE, 11(3), 036002-1–036002-9, (2017).

B. Research Papers in Conferences

1. **Jiten Boruah**, "Propagation Characteristics of Solid Defect-Core W-Type Photonic Crystal Fiber**",** Workshop on Recent Advances in Photonics (WRAP), 17-18 Dec' 2013, IITD, New Delhi, India and published in IEEE *Xplore*, 14663368, 09 Oct' 2014.

2. **Jiten Boruah**, and R.K. Sinha, "Analysis of 2D hexagonal lattice SiC PhC cavity defect mode", International Conference on Optics & Optoelectronics (ICOL-

2014), XXXVIII Symposium of Optical Society of India, Instruments Research and Development Establishment (IRDE), Dehradun, Uttarakhand, India, 5-8 March'2014.

3. **Jiten Boruah**, Yogita Kalra, and Ravindra Kumar Sinha, "Cladding doped defect-core large mode area W-type photonic crystal fiber", Proc. SPIE 9958, Photonic Fiber and crystal Devices: Advances in Materials and Innovations in Device Applications X, 99580N, September 7, 2016.

4. Ambrish Kumar, **Jiten Boruah,** and R.K.Sinha, "Performance Characterization of High Speed point to point Dual Broadcast service PON system without using any source at ONUs", Presented and appeared in the proceedings (page number 171) of XXXVI OSI Symposium, Frontiers in Optics and Photonics, IIT Delhi, December 03-05, 2011.

5. Yogita kalra, **Jiten Boruah,** and R.K.Sinha, "Design of 2D Silicon Carbide based Photonic Crystal Waveguides", Proceedings of XXXVI Optical Society of India (OSI) Symposium, Frontiers in Optics and Photonics, IIT Delhi, pg.218,December 03-05, 2011.

6. Yogita Kalra, **Jiten Boruah,** and R.K. Sinha,"Thermo-optic Effect in Si and SiC Photonic Crystal Waveguides", National Conference on Recent Trends in Synthesis and Applications of Advanced Materials, Department of Applied Physics, Maharaja Agrasen Institute of Technology(MAIT), Sec-22, Rohini, Jointly with Delhi Technological University (DTU), Bawana Road, Delhi, 05-06 Dec'2011.

7. **Jiten Boruah**, Yogita Kalra, and R.K. Sinha, "Defect mode analysis of 2D SiC photonic crystal cavity", Accepted for oral presentation in Proceedings of 37th Optical Society of India (OSI) symposium, Pondicherry University, 23-25 Jan'2013.

Jiten Boruah

Name and Signature of the Candidate

Prof. R. K. Sinha

Name and signature of thesis supervisor

CONTENTS

LIST OF FIGURES

LIST OF TABLES

Chapter-I

Introduction

CHAPTER-I

INTRODUCTION

1.1 Photonic crystal

Photonic crystals have changed the scenario of light guiding and thereby the development of miniature photonic devices and circuits. In the present decade, miniature photonic devices and circuits are in the verge of completely replacing electronic devices and circuits. Photonic crystals (PhC) [1-3] are artificial manmade micro-structured materials of dielectric or semiconductor, metallo-dielectric or even superconductor in which, the dielectric constant [4,5] varies periodically on length scale in one, two, or three dimensions with periodicity comparable to the wavelength of light as shown in the figure 1.1.

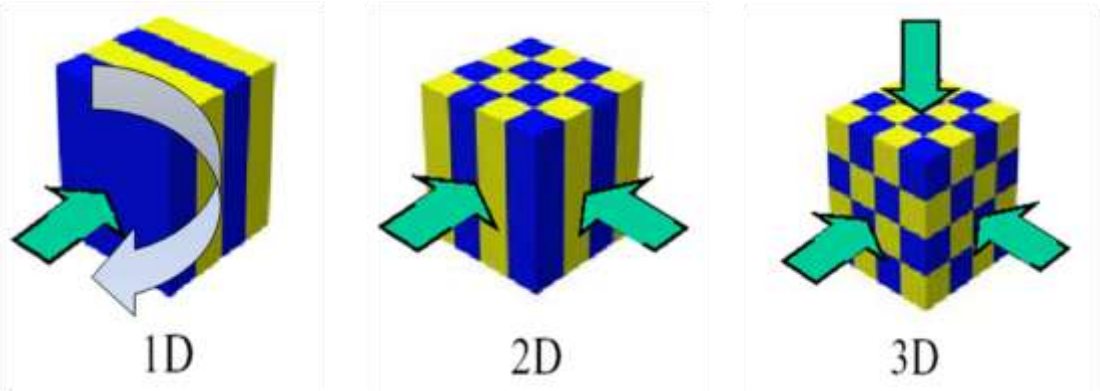

Source Fig.: http:/ab-intio.mit.edu/photons/tutorial.

Fig. 1.1: Artificial one dimensional (1D), two dimensional (2D) and three dimensional (3D) photonic crystals. The different colors represent materials having different dielectric constants.

Because of the periodicity, these crystals exhibit strong reflection for a range of wavelengths resulting in photonic band gap (PBG) [6-8] similar to electronic band gap [9] of solid. Since its inception, Photonic crystals, proposed by Prof. Eli Yablonovitch and Prof. Sajeev John in 1987 [10,11], have captured a lot of attention because of their ability of controlling and manipulating the flow of light within given frequency range of PBG. Thus, PhC or PBG structures provide the way to develop miniature photonic devices and circuits that are optical analog of electronic devices and circuits with multiple advantages like microstructure, light weight, low power and high speed data transmission.

1.1.1 Photonic crystal based devices

A photonic crystal is a periodic optical nanostructure that affects the motion of photons in much the same way that ionic lattices affect electrons in solids and hence the name photonic crystal. Photonic crystals occur in nature in the form of structural coloration like opal and reflectors in the colorful wings of butterflies and peacocks and in different forms. Artificial or manmade photonic crystals promise to be useful in a range of applications. Light can be confined or guided in such artificial or manmade PhC or PBG structure by introducing defects or disorder in the PhC or PBG structure. Creating a linear defect or line defect [12] in a PhC one can make a PhC waveguide that allows guidance of light for the frequencies inside the band gap. Similarly, light can be confined or trapped by incorporating a point defect [13,14] in the PhC to create a photonic cavity. Because of the strong photon confinement and guidance shown by these crystals they can be used in variety of applications.

PBG waveguides and cavities have been a subject of interest because of their potential ability for strongly controlling the propagation of light with the possibility of design and development of PBG based devices like Optical Filter[15], Coupler[16,17], Switches[18], Polarizer[19-21], Splitter[22-24], Multiplexers[25], Demultiplexers[26-28], Sensors[29-31] on different platforms like silicon on insulator (SOI) [32-34], Silicon Carbide (SiC) [35], Gallium Arsenide (GaAs) [36,37] etc envisaged for use in all optical networks[38]. A special attractive application of PhC is to construct localized electromagnetic modes by introducing defect in the periodic structure. These confined modes could be used in optical resonators [39], laser cavities [40] etc.

Thus, PhC based PBG materials forms a new class of optical material used in the design and development of waveguide [41,42], left-hand material [43,44], slow light [45-47], soliton propagation [48], optical register [49,50], large scale integrated circuits [51] and many more.

1.2 Theory of light guidance through photonic crystals

PhC or PBG materials are viewed as an optical analog of semiconductors that modify the properties of light similar to a microscopic atomic lattice that create a band gap for electrons in semiconductors. An electronic band gap in semiconductor is a forbidden zone

of energies that electrons cannot occupy. In PhC the periodic change in refractive index acts as partial reflection mirrors that corresponds to the formation of band structure for the wavelengths of photons. Intuitively, the photonic band gap of PhC can be understood to arise from the destructive interference of multiple reflections of light propagating in the PhC at the interfaces of the high and low dielectric constant regions, similar to the band gaps of electrons in solids. Thus, PhC provides a stimulating framework for the manipulation of light on a micrometer scale. PhC enables band engineering [52] by which one can artificially control the optical properties of solids. By selecting an appropriate crystal structure of certain materials, one can get a photonic band gap or a frequency range in which propagation or existence of electromagnetic waves is forbidden. Hence, such structures are also called photonic band gap structures.

1.2.1 Photonic band gap engineering

In order to obtain the photonic band structures of the considered PhC, the plane-wave expansion (PWE) [53, 54] method can be employed. In PWE method, both the electro-magnetic field and the periodic dielectric structure are expanded in Fourier series. For which the material has to be assumed as linear, locally isotropic and periodic with lattice vector R. The relative permeability (μ) is taken as 1 and the relative permittivity ($\in(r)$) is defined as,

$$\in(r) = \in_b + (\in_s - \in_b) f(r), \tag{1.1}$$

where, $\in_s$ is the dielectric constant of the columns and $\in_b$ is the dielectric constant of the background respectively and f(r) = 1 inside the column and f(r) = 0 outside it.

For two-dimensional lattice periodicity, the dielectric constant $\in$ can be described as,

$$\in(r) = \in(r+R) \tag{1.2}$$

where, r and R are the vectors of the 2D lattice.

Solving Maxwell's equations for the magnetic field (H_w) leads to the following vector wave equation,

$$\nabla \times \left(\frac{1}{\in(r)} \nabla \times H_w(r) \right) = \left(\frac{w}{c} \right)^2 H_w(r) \tag{1.3}$$

The magnetic field (H_w) is then expanded into plane waves of wave vector k with respect to the 2D reciprocal lattice vector G.

$$\mathbf{H_w(r)} = \sum_{G\lambda} \mathbf{h_{G\lambda} e_\lambda e^{[i(k+G)R]}} \tag{1.4}$$

where, the polarization vector e_λ characterize two independent polarizations and e is ellipticity ($e = \frac{a_e}{b_e}$) of the constituent dielectric rods or air holes.

Substituting eq.(1.4) in the vector wave eq.(1.3) impart an equation for the coefficient $h_{G\lambda}$ given by,

$$\sum_{G'\lambda'} E^k_{G\lambda,G'\lambda'} h_{G'\lambda'} = w^2 h_{G\lambda} \tag{1.5}$$

The matrix E in the eigenvalue equation is defined as,

$$E^k_{G\lambda,G'\lambda'} = [(k+G)\times e_\lambda][(k+G')\times e_{\lambda'}] \in^{-1} (G,G') \tag{1.6}$$

The Fourier transform of the inverse dielectric constant,

$$\in^{-1} (G,G') = \in^{-1} (G - G') \tag{1.7}$$

depends on the difference of the reciprocal lattice vectors only. The properties of $\in(r)$ are given by,

$$\in^{-1} (G) = \frac{1}{A} \iint_A \in^{-1} (r)\, e^{-iG(r)} d^2 r \tag{1.8}$$

where, A is the area of the unit cell.

By solving Eq.1.6 for 2D photonic crystals for in-plane propagation, the photonic band diagrams can be obtained for the two polarization states, namely, Transverse Electric (TE) polarization and Transverse Magnetic (TM) polarization.

To explore the possibility of existence of photonic band gaps in optical materials like Silicon (Si), Silicon Carbide (SiC) usually first, photonic crystals gap maps [54,82] are being plotted. Gap maps are basically a plot of band gap and radius of rods or holes of the proposed PhC structure. As for example, figure 1.2(a) and figure 1.2(a) show the gap maps for two types of photonic crystals namely, PhC composed of hexagonal arrangement of SiC rods in air and PhC composed of hexagonal arrangement of holes in SiC.

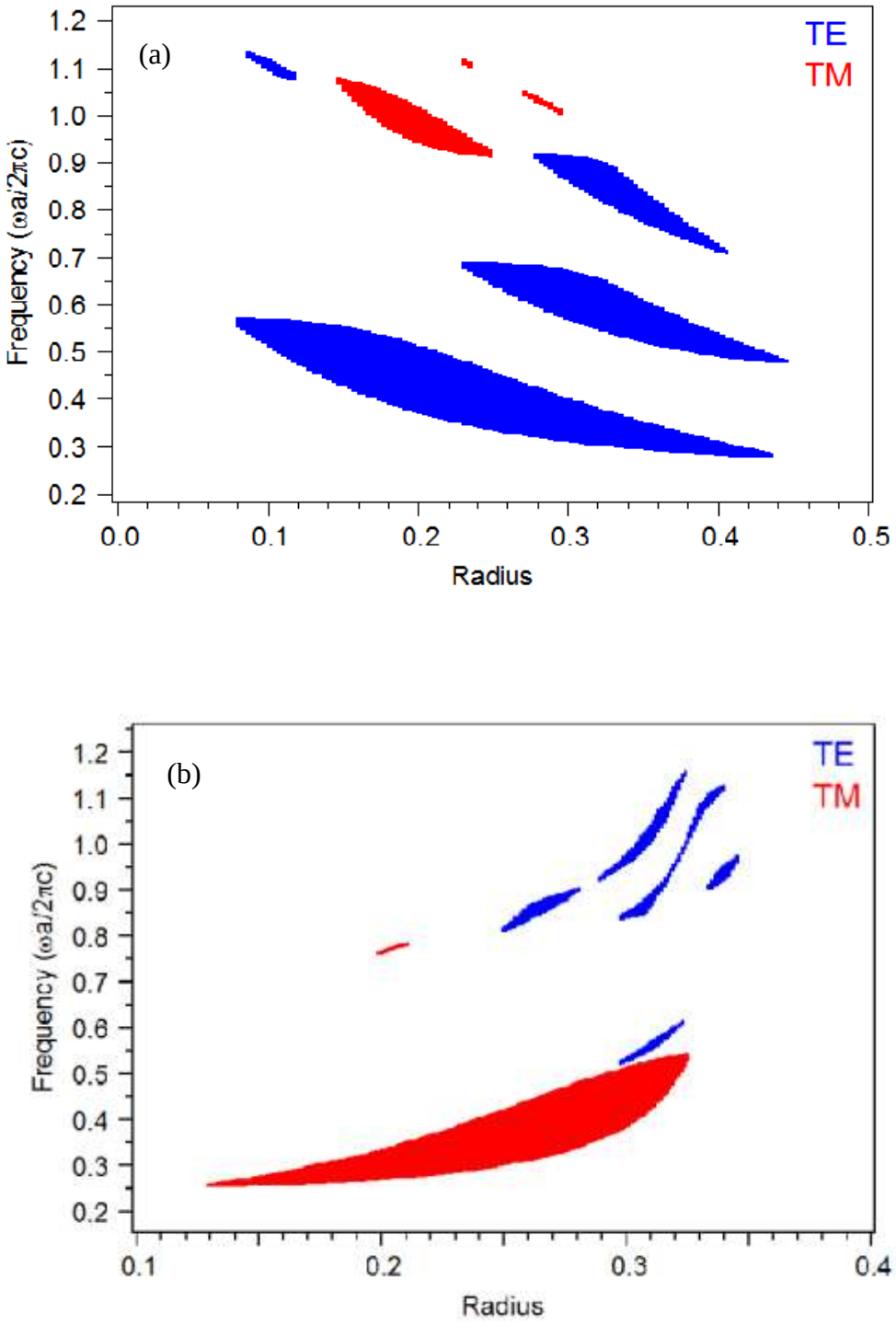

Fig. 1.2: Gap map of: (a) hexagonal arrangement of SiC rods in air PhC and (b) hexagonal arrangement of air holes in SiC PhC.

The gap maps for both these structures have been obtained using the plane wave expansion method. The gap maps indicate that the band gaps do open up in the designed photonic crystal structures.

After finding the gap maps, the band gaps of PhC structures are calculated. Different computational methods like Plane-Wave Expansion (PWE), Finite Difference Time Domain (FDTD) etc can be utilized to calculate gap maps and band gaps of PhC structures.

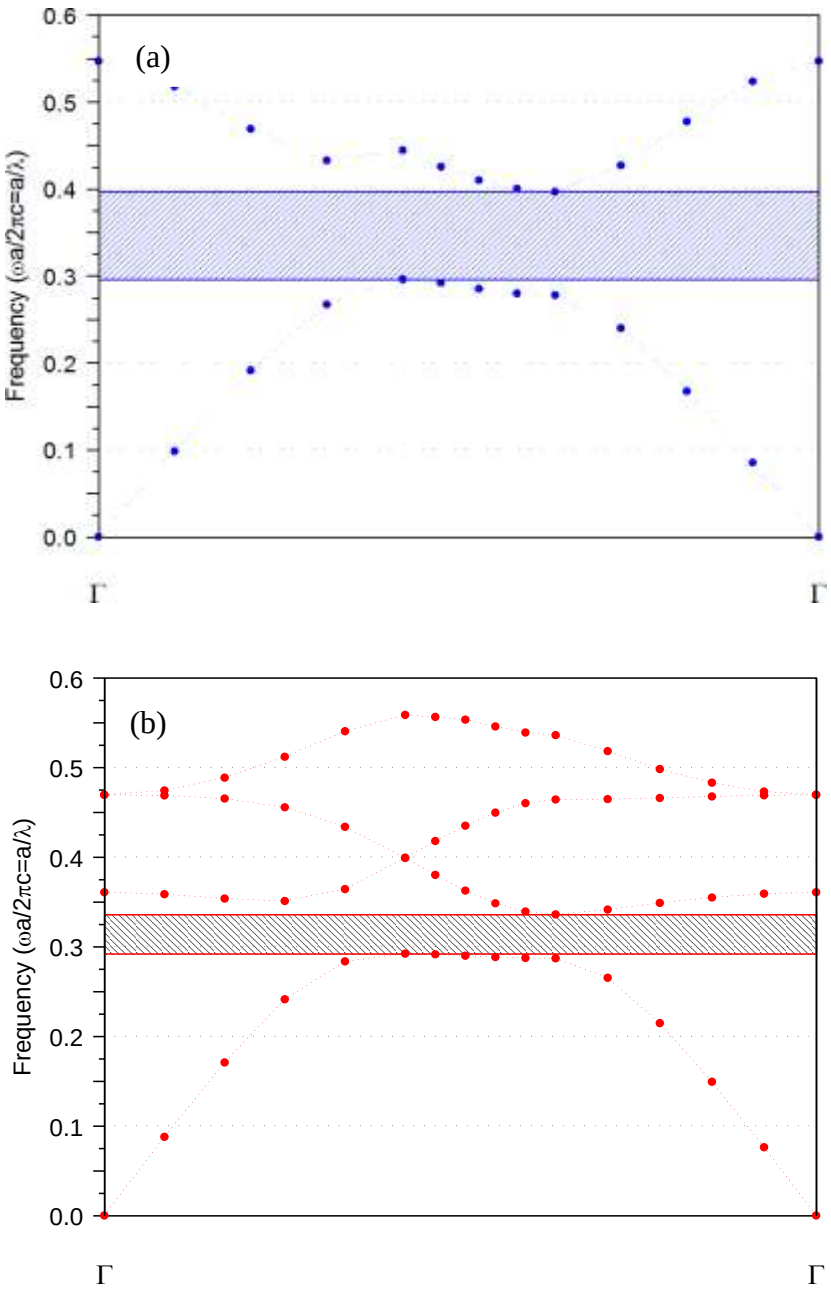

Fig. 1.3: (a) TE band Gap of hexagonal lattice of SiC rods in air PhC, (b) TM band Gap of hexagonal lattice air holes in SiC PhC.

Figure 1.3(a) and figure 1.3(b) show the band gaps of two types of photonic crystals namely, PhC composed of hexagonal arrangement of SiC rods in air and PhC

composed of hexagonal arrangement of holes in SiC. A band gap diagram gives the forbidden frequency range or PBG of such designed PhC that can not propagate through such PhC structure.

1.2.2 Analyses of photonic crystal: Helmholtz master equation

The propagation of light in a photonic crystal is governed by the following four Maxwell's equations (1864) 1.9 to 1.12 of classical electrodynamics,

$$\nabla.D = \rho \tag{1.9}$$

Equation (1.9) is the point or differential form of Gauss's law in electrostatics for the static charges. This law ratifies the source of electric field or physical meaning of how q produces E i.e. E or electric filed lines of force begin and end on q's. This law states that the electric flux through any closed hypothetical surface is equal to 1/ε times the total charge enclosed by the surface.

$$\nabla.B = 0 \tag{1.10}$$

Equation (1.10) is the point or differential form of Gauss's law for magnetism. It states that B never diverges it just loops around on itself i.e. the net magnetic flux through any closed surface is zero that confirms the nonexistence of magnetic charges or magnetic monopoles and B lines only forms loops.

$$\nabla \times E = -\frac{\partial B}{\partial t} \tag{1.11}$$

which is point or differential form of Faraday's law which tells that a changing magnetic field results in an electric field or changing magnetic flux (Φ_B) gives electro motif force or emf.

$$\nabla \times H = \frac{\partial D}{\partial t} + \sigma E$$

$$\nabla \times H = \frac{\partial D}{\partial t} + \mathrm{J} \tag{1.12}$$

which is point or differential form of Ampere-Maxwell's law which tells that a changing magnetic field results in an electric field or changing electric flux (Φ_E) gives magnetic field.

where,

$$D = \varepsilon E \tag{1.13}$$

$$B = \mu H \tag{1.14}$$

$$J = \sigma E \tag{1.15}$$

where, E is the electric field, H is the magnetic field, ρ is the charge density and σ is the conductivity. In an isotropic medium, the permittivity is written as $\varepsilon = \varepsilon_0 \varepsilon_r$ where, ε_0 is the permittivity of vacuum and ε_r is the relative permittivity. The materials used in this work are considered as non-magnetic insulators i.e. $\mu = \mu_0$ and $\sigma = 0$, therefore, equation (1.3) and (1.4) are written as:

$$\nabla \times E(r,t) = -\frac{\partial}{\partial t}[\mu_0 H(r,t)] \tag{1.16}$$

$$\nabla \times H(r,t) = \frac{\partial}{\partial t}[\varepsilon_0 \varepsilon_r(r) E(r,t)] \tag{1.17}$$

Solving equation (1.16) for E and inserting it into time derivative of equation (1.17) gives:

$$\nabla \times \left(\frac{1}{\varepsilon_0 \varepsilon_r(r)} \nabla \times H(r,t) \right) = -\frac{\partial}{\partial t} \mu_0 H(r,t) \tag{1.18}$$

The time dependent solutions of the magnetic field given by,

$$H(r,t) = H(r) e^{-i\omega t}$$

Therefore, equation (1.18) becomes,

$$\nabla \times \left(\frac{1}{\varepsilon_0 \varepsilon_r(r)} \nabla \times H(r) \right) = \left(\frac{\omega}{c} \right)^2 H(r) \tag{1.19}$$

where, $c = \frac{1}{\sqrt{\mu_0 \varepsilon_0}}$ is the speed of light in vacuum. Thus, by taking double curl of the Maxwell equations we get the eigenvalue equation (1.19) known as the **Helmholtz master equation** [55] for the magnetic field. This equation is solved by employing different computational methods like Plane-Wave Expansion (PWE) [52,54], Finite Difference Time Domain (FDTD) [56], Finite Element Method(FEM) [57] etc to find the band gap and other parameters of the photonic crystal structures and further theoretical analyses of the same.

In homogeneous medium, equation (1.19) becomes:

$$\nabla^2 H(r) = - n^2 \left(\frac{\omega}{c} \right)^2 H(r) \tag{1.20}$$

where, $n = \sqrt{\varepsilon_r}$ is the refractive index of the medium. Solution of equation (1.20) gives the superposition of plane waves of the form,

$$H(r,t) = H_0 e^{i(k.r - \omega t)} \tag{1.21}$$

where, wave vector, $k = \left| \vec{k} \right| = \frac{n\omega}{c} = n\frac{2\pi}{\lambda}$, and λ is the wavelength in vacuum.

Therefore, the plane wave is travelling in a direction defined by *k* with phase velocity v_p given by,

$$v_p = \frac{\omega}{k} = \frac{c}{n} \tag{1.22}$$

However, for group index n_g , group velocity is given by,

$$v_g = \frac{\partial \omega}{\partial k} = \frac{c}{n_g} \tag{1.23}$$

Since, *n* depends on ω, therefore dispersion relation ω(*k*) is not linear. $\Rightarrow v_p \neq v_g$.

Thus, group velocity is the velocity at which the envelope of a short pulse propagates through space.

Group velocity dispersion (GVD) is defined as the derivative of the inverse group velocity and is given by,

$$\beta = \frac{d^2k}{d\omega^2} = \frac{d}{d\omega}\left(\frac{1}{\frac{d\omega}{dk}}\right) = -\frac{1}{\left(\frac{d\omega}{dk}\right)^3}\frac{d^2\omega}{dk^2} = -\frac{1}{v_g{}^3}\frac{d^2\omega}{dk^2} \qquad (1.24)$$

Equation (1.24) implies that when group velocity converges to zero, the GVD parameter goes to infinity and that in turn causes the spreading of an optical pulse in time and as a result different frequency components of the pulse travelling at different velocities may merge together.

1.3 Fabrication of photonic crystal

PhC can be fabricated for one, two, or three dimensions. A number of methods for fabrication of photonic crystals have been developed till today. One dimensional PhC can be made of layers deposited or stuck together. Two dimensional PhC can be fabricated by photolithography, or by drilling holes in a suitable substrate. Three-dimensional PhC fabrication methods include: drilling under different angles, stacking multiple 2D layers on top of each other, direct laser writing, and instigating self-assembly of spheres in a matrix and dissolving the spheres. Photo lithography [58] and electron beam lithography (EBL) [59] were the first methods for fabrication of photonic crystals.

Another technique which has been developed recently is the holographic lithography [60] which utilizes the interference between two or more coherent light waves to produce a periodic intensity pattern to produce a periodic photonic structure in a photo resist. Self assembly [61] is the most popular approach to fabricate 3D photonic crystals. It is based on the natural tendency of the mono dispersive colloidal particles to self assemble into ordered arrays called artificial opals. Auto cloning technique [62] is another fabrication

technique which includes three processes occurring simultaneously; the sputtering deposition of dielectric layers, their physical etching by ions accelerated perpendicularly to the surface and the re-deposition of the neutral particles torn from the deposited layer by accelerated ions. The subtle balance achieved between these processes result in repetition of the topology of a pre-structured growth substrate from one deposited layer to other. Two main methods of fabrication of photonic crystal and photonic crystal based devices are discussed here.

1.3.1 Photolithography

Optical lithography or photolithography also termed as ultra violet (UV) lithography is an optical means for transferring patterns or geometric shapes on a mask onto a substrate. It is based on the principle that certain materials, such as polymers are sensitive enough to light that trigger chemical or physical changes in the material structure with nanoscale resolution in three dimensions. It is a technique that is used to define the shape of micro machined structures on a wafer. The steps involved in photolithography process are preparation of the wafer, coating with photoresist, soft baking, mask alignment, exposure, development (etch, implant and stripresist) and hard baking.

In photolithography, the sample is covered with a chemical called photoresist which is sensitive to UV light. When exposed to UV light its chemical composition changes. The mask consists of transparent and opaque regions that define the desired patterns. Mask is aligned with respect to the previously defined alignment marks. Then the sample is exposed to the UV light.

Exposed photoresist changes its composition. The chemical called developer is used to take away exposed photoresist. After the development, desired regions are ready for further treatment. Figure 1.4 shows the fabrication of photonic crystals using photolithography technique.

Photo-lithography is a technique of high speed for large shapes with parallel exposure but light diffraction limits minimum size of structure 50nm at best.

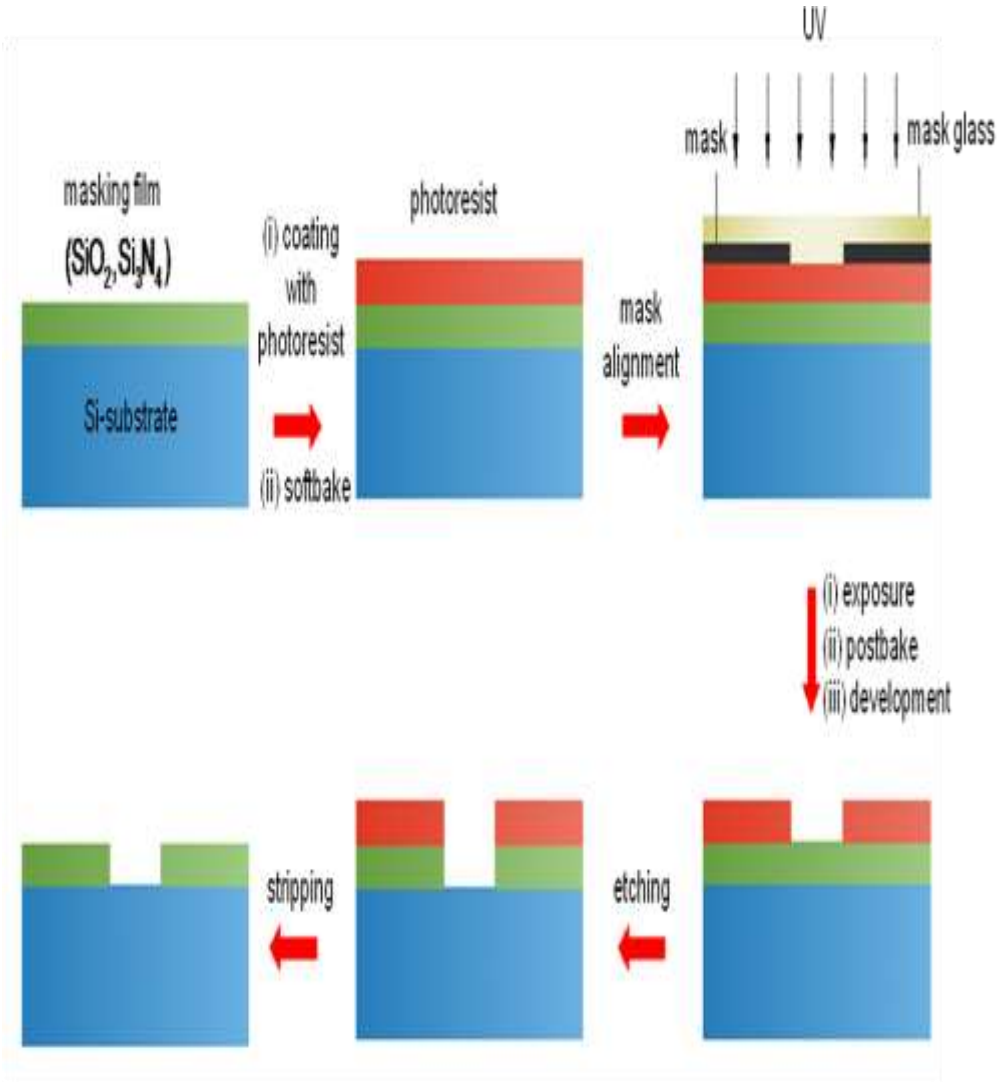

Fig. 1.4: Fabrication of photonic crystals using photolithography technique.

1.3.2 Electron beam lithography

Electron beam lithography abbreviated as e-beam lithography (EBL) is a very flexible technique of emitting a beam of electrons in a specific pattern across a sample surface covered with a film which is an electron sensitive material called the resist and then exposing the resist with electron beam and of selectively removing either exposed or non-exposed regions of the resist in the developing process. Similar to photolithography, its aim is to create micro structures in the resist that can subsequently be transferred to the substrate material, often by etching. It was developed for manufacturing integrated circuits, and is also used for creating photonic nano structures. Figure 1.5 shows the fabrication of photonic crystals using e-beam lithography technique.

Electron beam lithography has the advantages of printing complex patterns directly on wafers with high speed but point by point exposure limits speed. It eliminates the diffraction problem prevalent in photolithography, and it has high resolution up to 20nm in comparison to photolithography~50nm. Electron beam lithography is slower than photolithography and develops approximately 5 wafers/hour at less than 0.1 μ resolution, expensive and complicated. It has the disadvantages of forward scattering, backward scattering and secondary electrons.

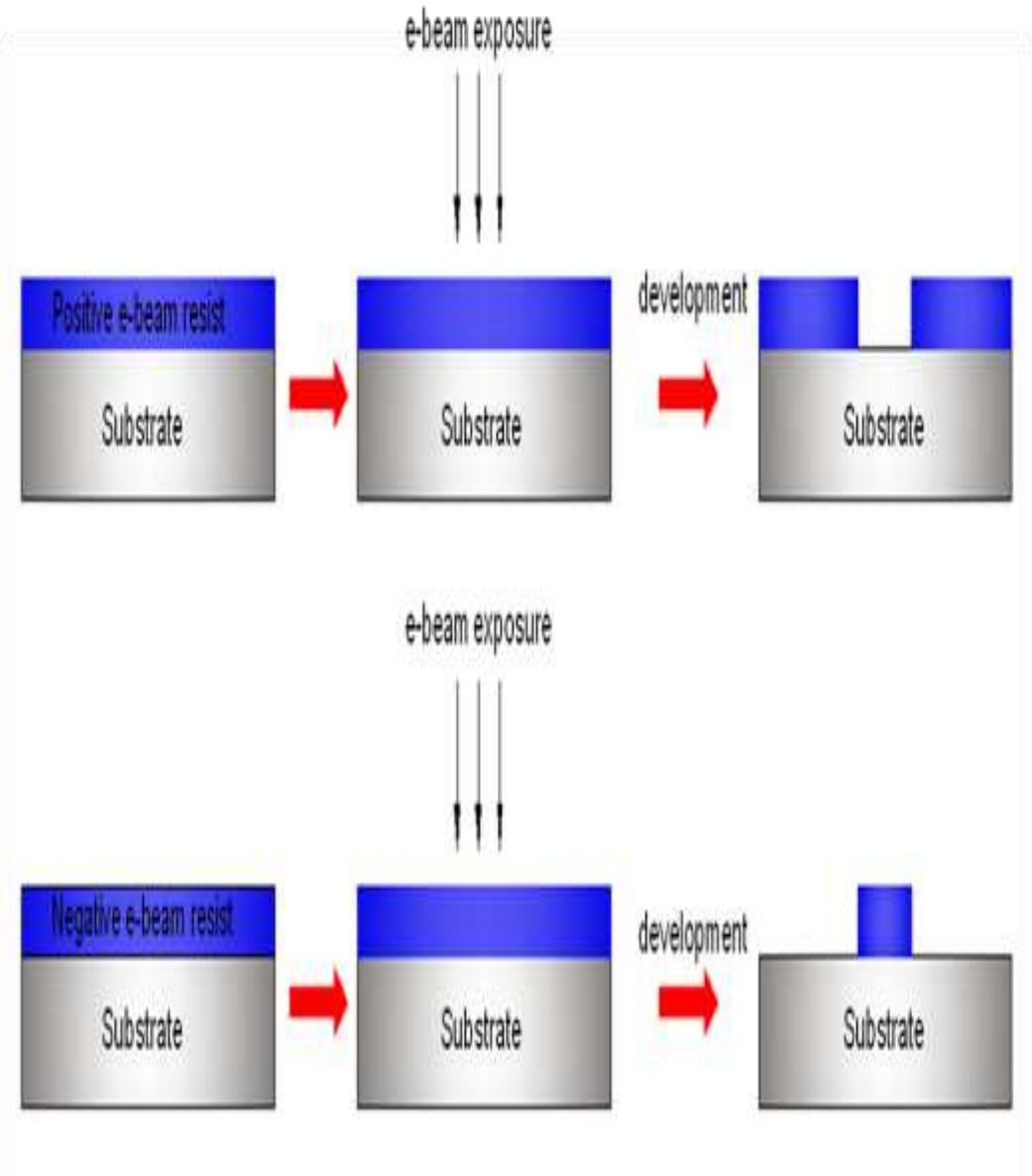

Fig. 1.5: Fabrication of photonic crystals using e-beam lithography technique.

1.4 Photonic Crystal Fiber

The most important application of photonic crystal is the design of a novel waveguide known as Photonic Crystal Fiber (PCF) or Holey Fiber or micro structured fiber [63-65]. The basic PCF is a fused silica optical fiber with a periodic distribution of voids or air holes in the cladding that run parallel to its axis. PCF can also be recognized as an optical fiber having a high or low index core surrounded by the 2D photonic crystal cladding. The name photonic crystal fiber is due to the fact that photonic crystal is being employed as cladding and is drawn in the form of an optical fiber. PCF shows unusual and unique properties due to the wavelength dependence of cladding index. The presence of air holes in the cladding makes PCF unlike conventional optical fibers and is responsible for many unusual properties, like single mode operation from the UV to IR with large mode-field diameters, highly nonlinear performance for super continuum generation, numerical aperture (NA) values ranging from very low to about 0.9, optimized and tunable dispersion properties, and air core guidance and many more. This has opened the road to solve all the severe limits faced by the conventional optical fibers. Due to its extraordinary ability to carry light in cores or with confinement characteristics not possible in conventional optical fiber, PCF is now finding applications in optical fiber communications, fiber lasers, nonlinear devices, high-power transmission, highly sensitive gas sensors and other areas.

Conventional fibers [66-72] guide light in the core by total internal reflection (TIR) principle. However, Phillip Russell and co-workers demonstrated fibers with a so-called photonic crystal cladding in 1995 and coined the term “Photonic Crystal Fiber”. PCF guide light by a new physical mechanism different from traditional fibers. Optical fibers have been fabricated from solid glass or silica (SiO_2) for more than last three decades. A radical change that took place, when researchers in the late 90's started to fabricate hair-thin optical fibers with numerous microscopic air holes running along the length of the fibers, with a central guiding core called the photonic crystal fiber or holey fibers made up of nano-photonic crystals. These micro structured fibers did not only mark the introduction of tailored materials with unique spectral properties in fiber optics, but it also opened the perspective of the applicability of photonic band gap materials at optical wave lengths. In this respect, a completely new guiding mechanism was demonstrated, and a revolution in fiber optics had started.

1.4.1 Photonic crystal fiber types

Two distinct methods determined by the arrangement pattern of voids or air holes exist for confining light in a photonic crystal fiber and that classifies the same into two major types. One is **index guiding PCF** [73-75] in which light guidance is by total internal reflection between a solid high index core and a low index cladding region with several air-holes. The other type of photonic crystal fiber is called the **photonic band gap guiding PCF** also called the **photonic band gap fiber (PBGF)** [76] uses a perfectly periodic structure exhibiting a PBG effect at the operating wavelength to guide light in a low index core-region. Figure 1.6 and 1.7 shows the schematic diagrams of the two major types of photonic crystal fibers along with their corresponding refractive index profile. The refractive index profile (RIP) is a plot between refractive index along y axis and distance from the core along x axis [77].

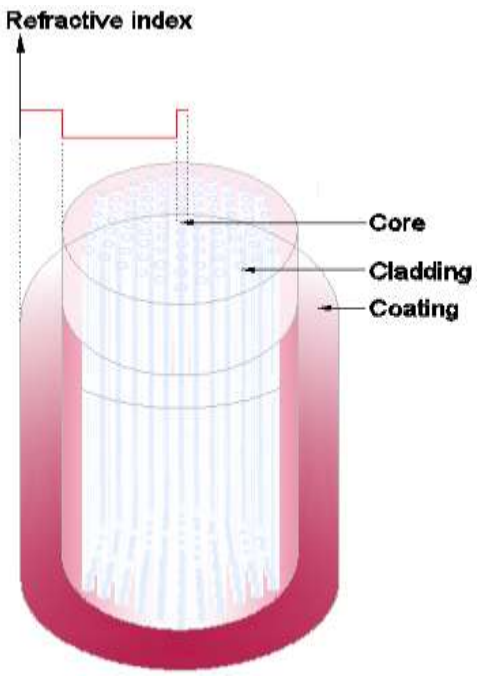

Fig. 1.6: Photonic crystal fiber (PCF) and its refractive index profile.

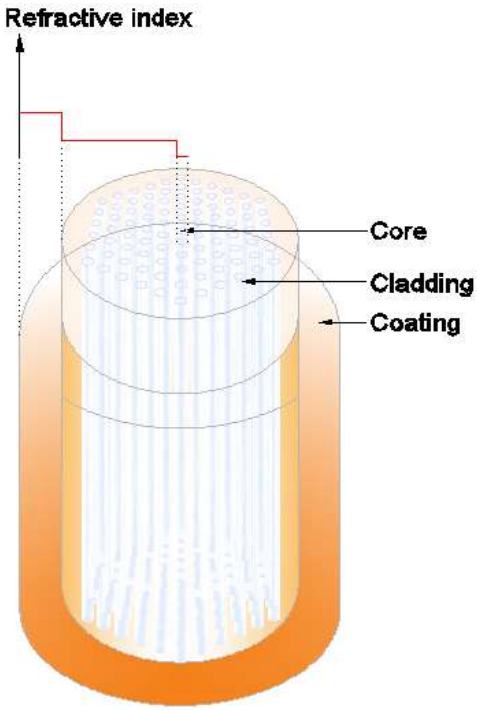

Fig 1.7: Photonic band gap fiber (PBGF) and its refractive index profile.

Each of the two main types of PCF can be divided into a number of subtypes determined by the cladding pattern, dimension of the fiber structure and their specific application. The high index core photonic crystal fiber has the subtypes of specialty PCFs namely high numerical aperture (HNA) PCF [78], Large-Mode-Area (LMA) PCF [79], Highly-Non-Linear (HNL) PCF [80, 81]. The low index core photonic band gap fiber has the following subtypes: low index core PCF [82], hollow core (HC) PCF [83] and Bragg fiber [84]. The Bragg fiber is composed of periodic layers of one dimensional photonic crystal in which light guidance obeys the Bragg's law. Figure 1.8 shows the transverse cross sectional scanning electron microscope (SEM) images of different PCF types [85].

Recent trend of research in PCF shows that special emphasis is on the specialty PCFs. In the domain of high index core PCF, the specialty PCF types that have been found reported are Endlessly single-mode PCF, Hi-Bi PCF, W-type PCF. Similarly, under hollow core PBG PCF the reported specialty PCF types are Suspended core PCF, Kagome HC-PCF, Polarization maintaining single-mode HC-PCF, Broadband single-mode HC-PCF and PCF with a sub-wavelength air-hole in the core.

Endlessly single-mode photonic crystal fibers are un-doped silica fibers that use a triangular or hexagonal pattern of air holes to form the cladding as shown in figure 1.8(i)(a). Since the index contrast between the core and the cladding, Δn, is determined only by the geometry of the air holes, it is possible to fabricate fibers with a very small and accurate Δn, and thus obtain very low numerical apertures and very large mode areas. Endlessly single-mode photonic crystal fibers are characterized by low fiber loss over broad wavelength range, single-mode at all wavelengths, radiation less pure silica fiber, wavelength independent MFD with a practically constant mode-field diameter (MFD). Endlessly single-mode photonic crystal fibers find applications in sensors, spectroscopy, interferometry or RGB displays.

PCF can be made highly birefringent by having different air hole diameters along the two orthogonal axes or by introducing asymmetries in core design. Such PCF structures are called **Hi-Bi PCF** as shown in figure 1.8(i)(b). Hi-Bi PCFs have modal birefringence of an order of magnitude higher than that of the conventional high-birefringent fiber and have potential for a number of applications such as high bit rate communication systems, polarization maintaining (PM) pigtailing of photonic devices, and PM fiber loops for gyroscopes.

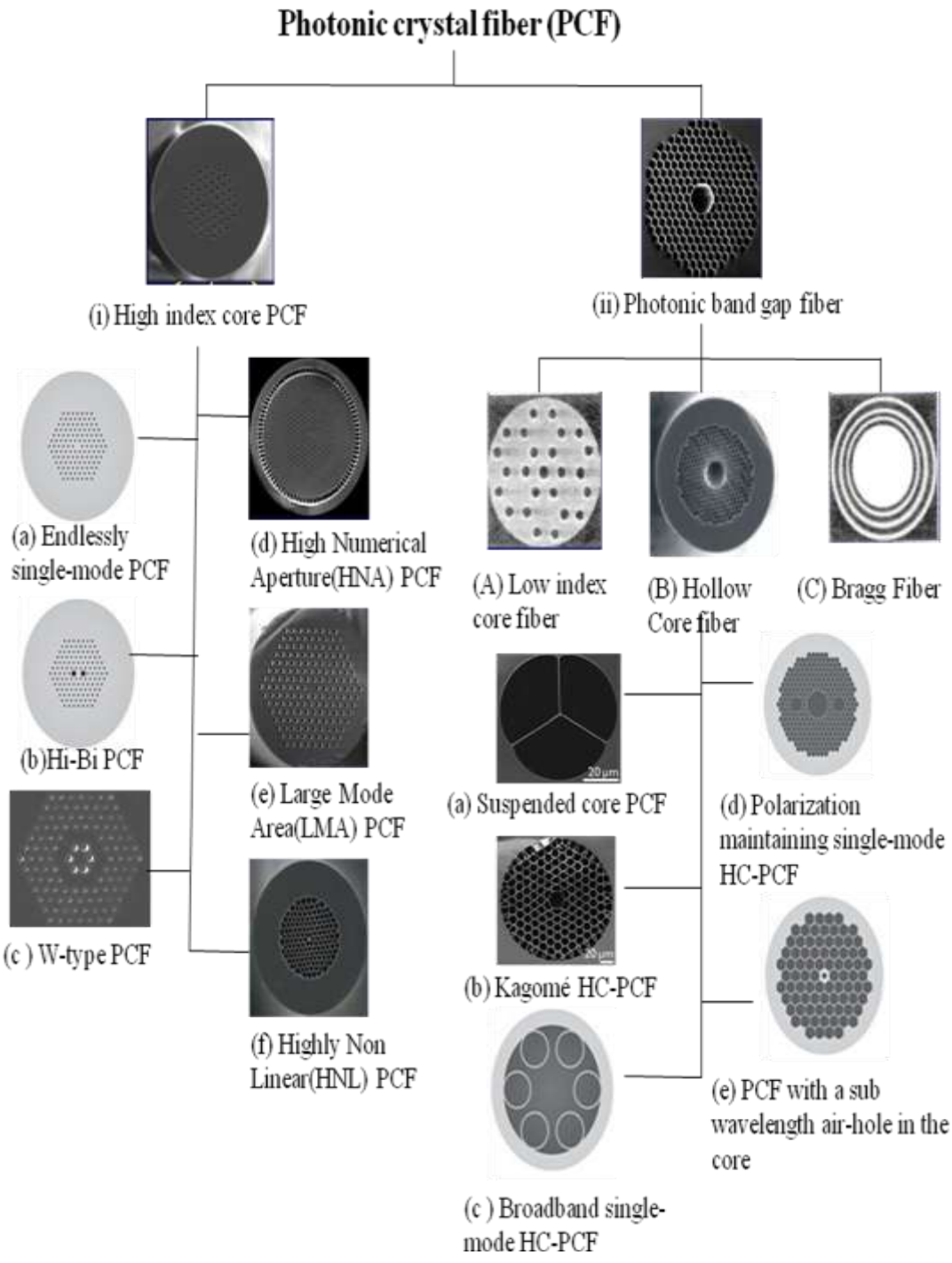

(Source: www.slideplayer.com slide of École polytechnique fédérale de Lausanne; www.iopscience.iop.org, www. pubs.rsc.org, www.researchgate.net and [85]).

Fig. 1.8: Transverse cross sectional SEM images of different PCF types.

The RIP of photonic crystal fibers plays an important role in the design and confinement of light for specific applications. As for example, in W-type specialty

PCFs, there is an additional zone between core and cladding having it's own lower refractive index. Then the cross sectional refractive index profile resembles the letter "W", hence the name **W-fiber** [77] also called the **DIC fiber or depressed index cladding fiber** as shown in figure 1.8(i)(c). The W type RIP provides ample freedom for designing the dispersion variation of such fiber.

Air-silica microstructured fibers designed and fabricated to yield Numerical Aperture (NA) greater than 0.9 are termed as **High Numerical Aperture (HNA) PCF** as shown in figure 1.8(i)(d). In order to achieve a large NA, one must arrange for a core and cladding material of widely differing indexes. The range of indexes available in transparent solids including glass and plastics is relatively small, the lowest attainable value being approximately 1.3. For a core of silica glass, this yields a maximum NA of the order of 0.6. In practice, NAs above 0.4 are extremely uncommon in silica fibers. Therefore, in recent years use of chalcogenide glass, tellurite and even plastic material to design HNA PCF have been observed. HNA PCF structures have applications in lasers and laser-induced-fluorescence systems. In optical coherence tomography (OCT) system, high numerical aperture PCF is required for collecting back scattering light for detailed information from body tissue. The HNA PCF can be designed for 0.83 μm, 1.06 μm and 1.31 μm wavelengths which are used for ophthalmology, dermatology and dentistry, respectively.

Large Mode Area (LMA) photonic crystal fibers offer diffraction limited high power delivery as shown in figure 1.8(i)(e). The very large mode area usually greater than 10 μm enables high power levels to be transmitted through the fiber without the effects caused by the fiber's non-linear properties, or material damage. LMA PCF applications are high power delivery, short pulse delivery, mode filtering, laser pigtailing, multiwavelength guidance, broadband interferometry.

An optical fiber required to be optically linear so that its properties remain same irrespective of how much power it carries. But, at high power, unwanted nonlinear effects crept into optical fiber. The nonlinearities in optical fibers can be made useful for amplification and switching of light propagating through them and that has been made possible by **Highly Nonlinear (HNA) PCF**. The nonlinear effects in such highly

nonlinear PCFs have been enhanced by concentrating light in small core as shown in figure 1.8(i)(f). Highly nonlinear fibers are characterized by positive dispersion at shorter wavelengths, formation of solitons at visible and near infrared wavelengths. To design a highly non linear fiber following four different approaches employed: (i) In Narrow-core fibers with Silica cladding a narrow core and high doping level reduce Aeff and enhance γ, (ii) In Tapered fibers with air cladding: the standard fibers are stretched by a factor of 50 or more and the surrounding air acts as the cladding, (iii) In Microstructured fibers: air holes are introduced within the cladding, (iv) In Non-Silica fibers: Use a different material with large values of n_2 like lead silicates, chalcogenides, tellurite oxide, bismuth oxide.

Hollow Core (HC) PCF or Hollow Core Photonic Band Gap (HC-PBG) fibers (figure 1.8(ii)(B)) guide light in a hollow core that is surrounded by a microstructured cladding based on the photonic band gap effect so that only a minor portion of the optical power propagates in the microstructured glass-air cladding. The attractions of hollow-core PCF are mainly that the primary guidance in air minimizes nonlinear effects and makes possible a high damage threshold. With the advent of HC PCF it has become possible even to guide light at wavelengths where the transparency of the glass material is relatively poor. Also, one may exploit the high optical intensity in air or in some other gas filled into the fiber. Another attractive feature of HC Photonic band gap fibers is zero dispersion close to design wavelength.

One limitation of hollow-core PCF is that their propagation losses are substantially higher than for solid-core PCF and specifically, for single-mode guidance. Another limitation is that the photonic band gap guiding mechanism works for a small wavelength range. This wavelength range can be substantially broadened by using a different kind of hollow-core fibers.

The hollow-core PCFs are useful for transporting high optical powers, as all nonlinear effects are much weaker due to the presence of air inside the core for which non linear refractive index, n_2 is smaller by a factor of 1000 compared to that of silica. However, most such fibers exhibit relatively high losses (~1 dB/m) compared to conventional silica PCFs that depend on many design factors, including the shape and size of air holes.

Suspended core PCFs with a thin suspended core as shown in figure 1.8(ii)(B)(a) have a large evanescent field extended into the air-holes. Suspended core PCFs facilitates all-fiber evanescent wave spectroscopic and refractive index sensors and distributed sensing over the entire length of the fiber.

PCF with a Kagomé lattice design can increase the band gap guiding wavelength range. Hollow-core PCF whose cladding is designed in the form of a kagome lattice is termed as the **kagome PCF** as shown in figure 1.8(ii) (B)(b). A kagome lattice consists of interlaced triangles such that each crossing has four nearest neighbours. In kagome PCF, the use of a kagome lattice results in a cladding filled mostly with air. The operation principle of the Kagome fiber design profoundly differs from that of a photonic bandgap fiber; it does not rely on a photonic band gap. Some optical properties also differ substantially from those of photonic bandgap fibers. Namely, the wavelength range with good transmission can be much broader, which is useful for many applications, including supercontinuum generation. Some designs exhibit very small overlap of light with the silica structures (order of 0.01%), allowing the guidance of beams with rather high optical peak powers. The advent of kagome PCF has reduced losses of hollow-core PCFs to ~1 dB/km. The kagome PCF employ a relatively large hollow core having diameter 20 μm or more and increase the pitch of the kagome lattice to beyond 10 μm. Because such a PCF consists of mostly air, the nonlinear effects are reduced dramatically inside them. Narrower-core PCFs exhibit higher losses but they are still useful for applications such as pulse compression as the slope of the chromatic dispersion is lower.

Shown in figure 1.8(ii)(B)(c) is a **broadband single mode HC PCF** which has a broadband guiding wavelength range in spite of single mode.

Polarization maintaining HC PCF incorporate a non-circular core in combination with a large refractive index step between silica and the periodic air hole giving rise to birefringence and which becomes larger at longer wavelengths. This results in a shorter beat length that reduces the bend or other deformation induced variations of the state of polarization (SOP) compared with conventional fibers and thereby preserving the SOP of light. The polarization maintaining HC PCF finds applications in communication and sensing. Figure 1.8(ii)(B)(d) shows a polarization maintaining HC PCF.

Similarly, **PCF with a sub wavelength air hole** in the core increases the band gap guiding wavelength range, SEM image of which is as shown in figure 1.8(ii)(B)(e).

1.4.2 Photonic crystal fiber based devices

The optical properties such as band gap and light propagation characteristics of PBGF and PCF can be manipulated by structural design and defect engineering [86]. Both PCF and PBGF have 2D periodic structures with designed defect structure in the center. Hence light can be confined and guided by special defect modes in PhC. PCFs are new class of optical fibers combining properties of optical fiber and PhC. A great deal of interest has been generated in PCF due to its attractive optical properties like endlessly single mode behavior [87], unique group velocity dispersion [88] characteristics, large mode area [89], enhanced non-linear effect [90], supercontinum generation [91-98], soliton propagation [99], high birefringence [100-103], polarization-maintaining[104], lasing action [105], optical coherence tomography [106] and high precision optical frequency measurement [107]. The applications of PCF are increasing swiftly and are expected to replace conventional optical fibers used in optical communication. In recent years, main work in the field of PCFs has focused on silica glasses, but now the researches are diverting toward using different non silica materials like fluoride glass [108], germanium [109], lead-silicate [110], tellurite [111], bismuth-oxide [112], polymer-based [113], chalcogenide (As–S, As–Se, Ge–Se–Te, etc.) [114] and soft glasses [115] etc in PCF because they offer advance characteristics like high non-linearity [80], high refractive index [78], high mode confinement [116], Raman amplification [117] etc. Therefore, in this proposed thesis it is planned to study the application specific design of Photonic crystal fibers, waveguides and devices with PCFs having solid core, regular or irregular geometries and using different materials.

The properties of PCF can also be altered by external stimuli that can be thermal, optical, chemical, electrical, magnetic, biological, nuclear etc. Hence, the propagation of electromagnetic pulses through PBG crystals and PCF has to be probed and this study is important for understanding propagation characteristics in specialty photonic crystal fiber, which have potential applications in telecommunication, sensing, transporting high optical power etc.

1.5 Theory of light guidance through photonic crystal fiber

In conventional optical fiber the light guidance takes place obeying the principle of total internal reflection (TIR) at the edge of the high refractive index core and low refractive index cladding.

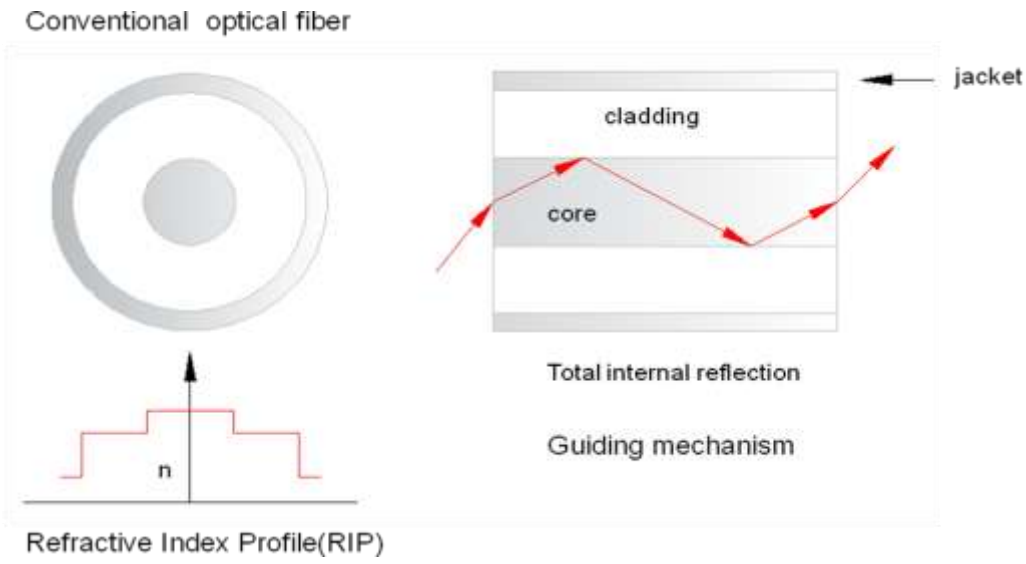

(a)

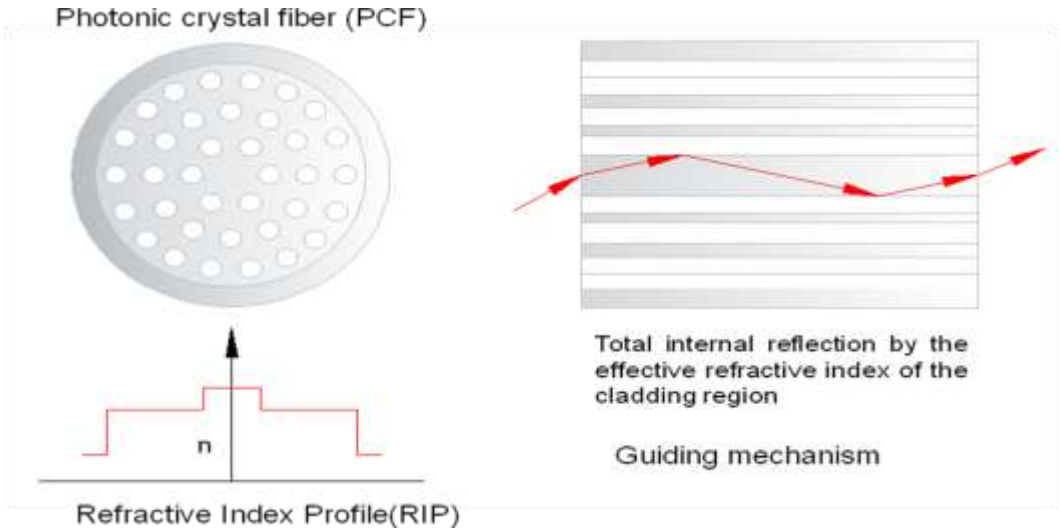

(b)

Fig. 1.9: Schematic diagrams of: (a) Conventional optical fiber with its RIP and guiding mechanism, (b) Photonic crystal fiber with its RIP and guiding mechanism.

The light guidance mechanism in conventional optical fiber has been illustrated in figure 1.9(a) along with its refractive index profile (RIP). Whereas, in PCF, the light guidance takes place obeying the principle of total internal reflection (TIR) by the effective refractive index of the cladding region. The light guidance mechanism in PCF has been illustrated in figure 1.9(b) along with its refractive index profile (RIP). The effective refractive index of the cladding of the PCF is the average refractive index of the cladding with multiple air holes.

To achieve field confinement in the core, index guiding Photonic crystal fibers depend on the total internal reflection and photonic band gap fibers depend on photonic band gap (PBG) effect discussed in section 1.1. But very recently, there has been report of the discovery of a new light trapping technique within fibers by the so-called Dirac point of photonic band structures by Kang Xie et al. [118]. It has been claimed that the Dirac point can establish suppression of radiation losses and consequently a novel guided mode for propagation in photonic crystal fibers. The mentioned Dirac point is a conical singularity of a photonic band structure where wave motion obeys the famous Dirac equation. The unexpected phenomenon of wave localization at this point beyond photonic bandgaps has been reported. This guiding relies on the Dirac point rather than total internal reflection or photonic bandgaps, thus providing a sort of advancement in conceptual understanding over the traditional fiber guiding.

1.6 Fabrication of PCF

Fiber stack and draw technique [119] has been utilized to fabricate photonic crystal fibers since its inception. Successive stages of fabrication of PCF are shown in figure 1.10(a) to 1.10(f). Like in conventional optical fiber fabrication, fabrication of PCF starts with preparation of a fiber preform. PCF preforms are formed by stacking a number of capillary silica tubes and rods to form the desired air-silica structure. For which, first, silica tubes and rods are drawn down to capillaries using an optical fiber draw tower with precise outer diameters. These are then stacked into a hexagonal, square or other format of arrays as per requirement and by inserting solid rods or removing capillaries at selected site (s) to form cores. The creating of PCF preform allows a high level of design flexibility as the core size and shape as well as the index

profile throughout the cladding region can be controlled. The finished preform stack is fused together and drawn down into fiber in one or more stages in a high-temperature drawing tower and hair-thin photonic crystal fibers are readily produced in desired lengths and spooled as shown in figure 1.10(g).

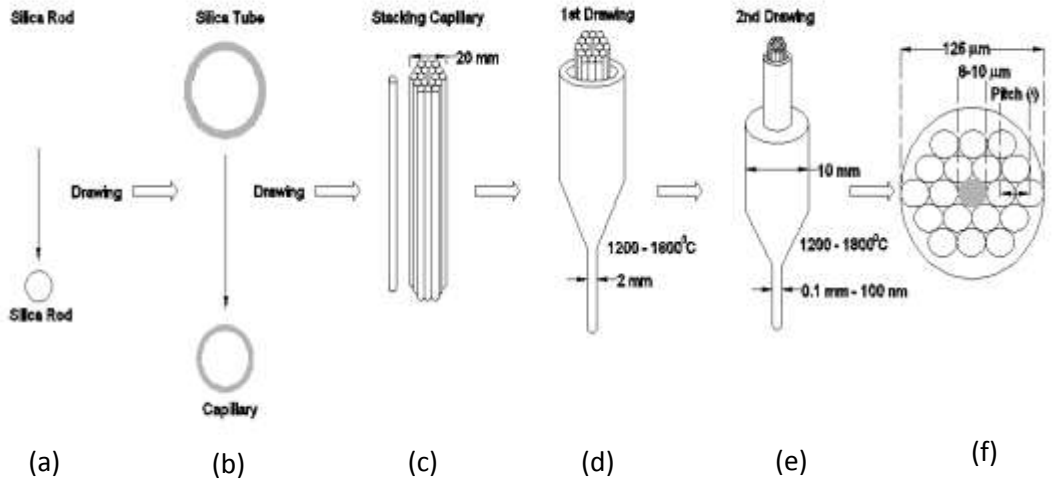

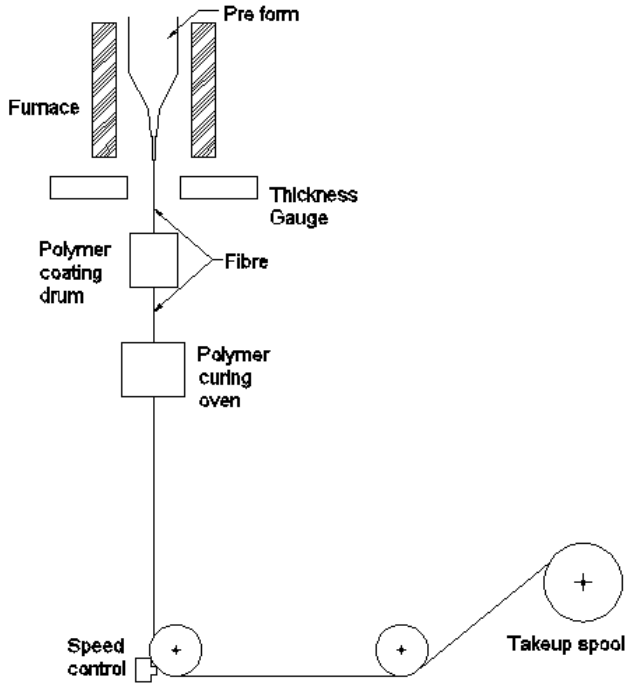

(g)

Fig. 1.10: Schematic diagrams of: (a) to (f) different stages of preform fabrication during the production of a solid core photonic crystal fiber, (g) Fiber draw tower.

Through careful process control, the air holes retain their arrangement all through the drawing process, fibers with very complex designs and high air filling fraction can be produced. Finally, the fibers are coated with polymer to provide a protective standard jacket that allows robust handling of the fibers. The final fibers are comparable to standard fiber in both robustness and physical dimensions and can be both striped and cleaved using standard tools. Figure 1.11 shows the captured images of (a) Pre form fabricator, (b) Fabricated performs, (c) Fiber draw tower, and (c) Microscopic (10X) view of solid core photonic crystal fiber drawn at Fiber Optics and Photonics division, Central Glass and ceramic Research Institute (CGCRI), CSIR- Laboratory, Kolkata, India and collected during one of the visit to the establishment.

Apart from the above discussed capillary stack and draw technique, polymer PCF preform can be prepared using techniques like extrusion polymer casting, polymerization in a mould and injection moulding.

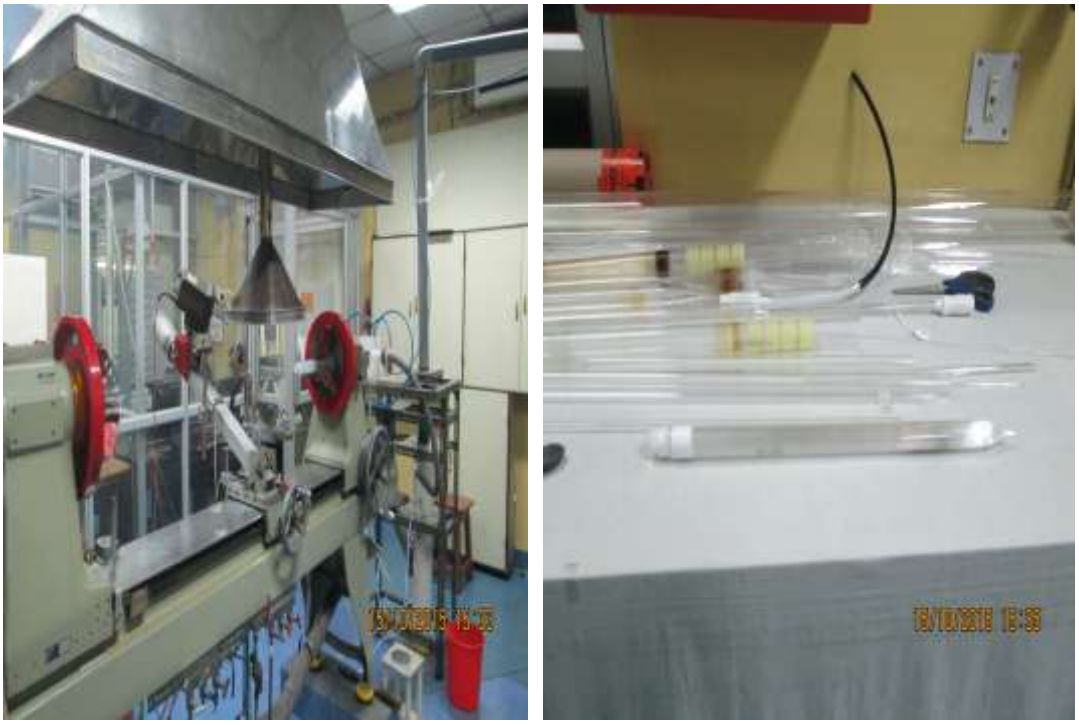

(a) (b)

(c)

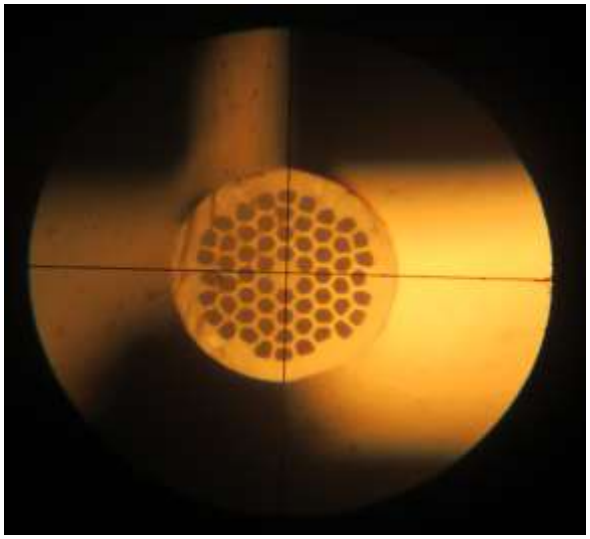

(d)

Courtesy: Fiber Optics and Photonics division, Central Glass and ceramic Research Institute(CGCRI), CSIR- Laboratory, Kolkata, India.

Fig. 1.11: (a) Pre form fabricator, (b) Fabricated performs, (c) Fiber draw tower, and (d) Microscopic (10X) view of solid core photonic crystal fiber.

1.7 Analyses of photonic crystal fiber

The following parameters of the designed PCF structures have been analysed.

1.7.1 Dispersion

The wavelength dependent refractive index of the pure silica glass material has been calculated by employing the Sellmeier equation [120,73] as described in Eq. 1.25.

$$n^2(\lambda) = 1 + \frac{a_1\lambda^2}{\lambda^2 - b_1^2} + \frac{a_2\lambda^2}{\lambda^2 - b_2^2} + \frac{a_3\lambda^2}{\lambda^2 - b_3^2} \qquad (1.25)$$

where, λ is the resonance wavelength, the values of the Sellmeier coefficients are: a_1= 0.004679148, a_2= 0.01351206, a_3= 97.93400, b_1= 0.6961663, b_2= 0.4079426 and b_2= 0.8974794.

The group velocity dispersion [121-129] is very important characteristic of any PCF structure. The group velocity dispersion D (λ) has been calculated from wavelength dependent effective indices of propagating mode by employing the following relation,

$$D(\lambda) = -\frac{\lambda}{c}\frac{d^2 Re(n_{eff})}{d\lambda^2} \quad (1.26)$$

where, *c* is the velocity of light in free space, $Re(n_{eff})$ is the real part of the effective index (n_{eff}) of the guided mode. Both material and waveguide dispersion can be included in the Eq. 1.26 considering Sellmeier equation while calculating n_{eff}.

1.7.2 Effective area

The effective mode area [130-132] of the propagating mode which is essential feature to suppress the nonlinear effects in the proposed design has been calculated by using the Eq.1.27.

$$A_{eff} = \frac{(\iint E^2 dxdy)^2}{\iint E^4 dxdy} \quad (1.27)$$

where, E is the amplitude of the transverse electric field propagating inside the PCF structure.

1.7.3 Nonlinear coefficient

Many non-linear effects inside PCF depend on the parameter, nonlinear coefficient (γ). The nonlinear coefficient [133] (γ), offered by PCF structure related to the nonlinear refractive index of material of the PCF and represented by the following equation.

$$\gamma = \frac{2\pi n_2}{A_{eff}\lambda} \quad (1.28)$$

where, n_2 is the nonlinear refractive index of material, A_{eff} is the effective mode area of propagating mode, and λ is the operating wavelength of light in μm. The silica glass which is the usual material for fabrication of PCF, is a weak non-linear medium with a measured value of nonlinear refractive index, $n_2 \sim 2.7 \times 10^{-20}$ m ^{2}/W. For silica fibers this value of n_2 can vary in the range $2.2–3.0\times10^{-20}$ m ^{2}/W depending on the density of dopants and on whether the fiber preserves polarization of light [120]. For

telecommunication fibers, $\gamma \sim 1\ W^{-1}/Km$ which is too small for most applications and that forces one to employ high peak powers and long fiber lengths. This problem has been solved by designing of highly non linear fibers ($\gamma > 10W^{-1}/Km$). PCF could have ultra high nonlinear coefficient, $\gamma \sim 245\ W^{-1}/Km$ and above.

1.7.4 Confinement loss and Bend loss

The confinement loss arises due to the leakage of power from the core of the PCF. The PCF being a leaky structure has complex effective indices, n_{eff} of the modes. The confinement loss [134,122] can be extracted from the imaginary part of the n_{eff} by using the following relation.

$$L\ [dB/m] = (40\pi/\ln(10)\times\lambda)\,\mathrm{Im}(n_{eff}) = 8.686 k_0 \mathrm{Im}(n_{eff}) \qquad (1.29)$$

where, $\mathrm{Im}(n_{eff})$ is the imaginary part of the mode effective index, n_{eff} and λ is the operating wavelength of light in μm.

While using the fiber for free space communications, bending of the PCF is inevitable. The PCF needs to be spooled at certain radius for this purpose and during this the fiber gets bent. Therefore, it is essential to study the bending performance of the design. In bent fibers the field profile deforms outwards in the direction of the bend. The presence of air holes around the core makes the design of effective refractive index more flexible. Bending loss [135,136] of the proposed PCF has been calculated by using the equivalent index model as shown in figure 1.12.

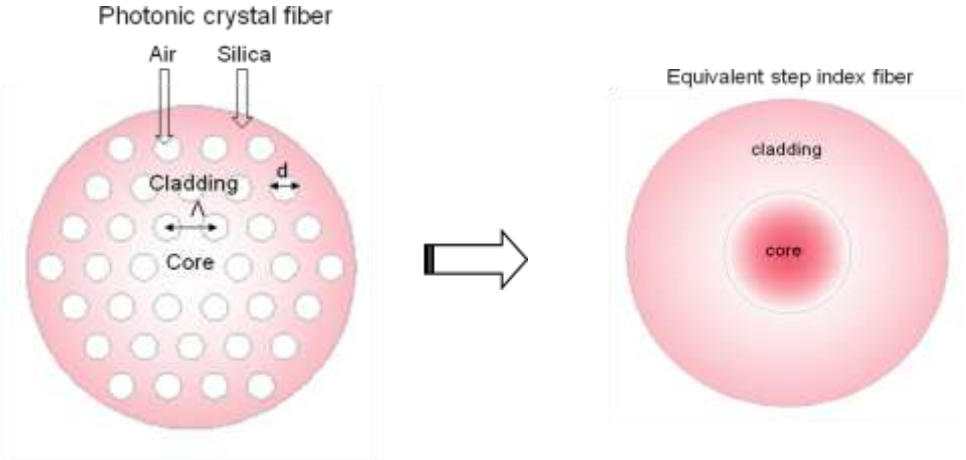

Fig. 1.12: Conventional PCF and equivalent step index fiber.

In this method, in order to simulate the effects of bending, the bent PCF is transformed into a straight PCF with an equivalent refractive index [137] defined in the following equation 1.30.

$$n_{eq}^2 = n^2(x,y)\left(1+\frac{2x}{R}\right) \qquad (1.30)$$

where, n(x,y) represents the refractive index profile of the straight PCF, x is the transverse distance from the centre of the fiber in the direction of bending and R is the bend radius.

The bend loss of photonic crystal fiber can be calculated by applying perfectly matched layer (PML) [57] boundary condition. For which, a rectangular perfectly matched layer (PML) is introduced at the surface of the proposed PCF structures to simulate the effect of an infinite domain in the finite element method. With the introduction of the PML the propagation constant of modes of the proposed PCF structure becomes complex [138]. The bending loss of the mode has been can be calculated by using the imaginary part of propagation constant or complex effective index of the bent fiber using the equivalent refractive index.

1.8 Computational methods utilized

Various computational methods have been used to get the results for application specific design of Photonic crystal fibers, waveguides and devices. A brief introduction of the computational methods utilized to analyze the characteristics of the proposed PhC and PCF structures has been included hereunder.

1.8.1 Plane wave expansion (PWE) method

The plane wave expansion (PWE) [53,54] method is a frequency-domain approach based on the expansion of the fields as definite-frequency states in some truncation of a complete basis (e.g. plane waves with a finite cutoff) and then finding solution of the resulting linear eigen problem. This method solves for a number of frequency eigen values ($\frac{\omega a}{2\pi c}$) at a given wave vector (k) and the optical modes are solved in the vector space or in the reciprocal space. The PWE method has the twin advantages of

accuracy and efficiency. The method is applicable to optical waveguides with arbitrary cross-sections, resonators, photonic band-gap materials, and photonic crystal structures, or for calculations of optical dispersion relations and eigen states for conventional and specialty optical fibers. One disadvantage of the PWE method is that the wave vector serves as the free parameter, whereas the frequency eigen values follow from the calculation. For certain applications, especially for finding waveguide modes, it is often more convenient to specify the frequency and solve for the required propagation constant. Precisely, such an approach would make it much easier to include the effects of dispersion, which is perpetually specified as a function of frequency. For some problems, such as defect modes in PhC and PCF, the plane wave expansion method may be extremely time-consuming. Moreover, the PWE method is unable to treat loss and so the PWE method can not account for materials with loss or obtain complex eigenvalues representing decaying modes in a lossy dielectric material structure. Band gap calculations in this work have been carried out using Rsofts' Bandsolve software using PWE.

1.8.2 Finite element method (FEM)

The finite element method (FEM) [139,140] is a numerical technique for finding approximate solutions of partial differential equations (PDE) as well as of integral equations that deal with complex geometries and boundaries, such as waveguides with arbitrary cross-sections, with relative ease. The field region is divided into elements of various shapes, such as triangles and rectangles, allowing the use of an irregular grid. The solution approach is based either on eliminating the differential equation completely in steady state problems, or turning the PDE into an approximating system of ordinary differential equations, which are then numerically integrated using standard techniques such as finite differences, Euler's method, Runge-Kutta, etc. In optical waveguides, the FEM can be used for mode solving and propagation problems. Two approaches to solve waveguide problem include the variational method and the weighted residual method. Both methods lead to the same eigenvalue equation that needs to be solved.

In solving partial differential equations, the key challenge is to create an equation that approximates the equation to be studied, but is numerically stable, meaning that errors in the input and intermediate calculations do not mount up and cause the resulting output to be meaningless. There are many ways of doing this, all with advantages and disadvantages. In this thesis, effective index, confinement loss and bend loss of PCF structures have been calculated using FEM.

1.8.3 Finite difference time domain (FDTD) method

The FDTD [141,142] technique is based on a discrete representation of time-dependent Maxwell's equations on a grid that is exact in the limit that the grid spacing goes to zero. Since, the FDTD is a time-domain technique that solves Maxwell's equations without any assumptions, so, the response of the system over a wide range of frequencies can be obtained with a single simulation and is flexible towards geometry of the device under study. Various optical materials can be used with FDTD algorithms. Modal properties can be extracted in a single simulation by Fourier-transformation of the time-varying response of the system to some input. Then, the peaks in the resulting spectrum correspond to the eigenfrequencies. The primary limitation of FDTD is that it is computationally intensive, especially in the three-dimensional case, but the method is readily applicable to the two-dimensional structures. In practice, FDTD needs to have at least 10 to 20 cells per minimum wavelength in every direction, depending on the application and accuracy required. Also, even higher sampling rates may be required to reduce the combined numerical dispersion error, which is proportional to the length of wave propagation. This makes FDTD impractical for large devices. Various techniques have been proposed to make the FDTD method more efficient, including pseudo-spectral time-domain techniques, non uniform and adaptive mesh refinement, hybrid FDTD-Finite Element techniques, and hardware acceleration concepts. Different software providers take various approaches to optimize the performance of their software in solving problems that require clustering. The approaches include parallel processing features in the software and, most recently, dedicated hardware to increase single system processing speeds. Typical applications for optical software based on an FDTD algorithm include the

modeling of high-index-contrast waveguides, photonic-bandgap structures for photonic crystals, ring resonators, nano-plasmonic devices, gratings and other diffractive structures, dispersive, nonlinear and gain materials, and biophotonics. Defect mode analysis, Dispersion, Q factor of PhC structure discussed in chapter II of this thesis have been calculated using FDTD.

There are other mode solvers software packages containing multiple-mode solving techniques including analytical methods, such as the beam propagation method(BPM) [143,144] effective index method [145-147], and numerical approaches, such as the finite-difference method and meshless techniques etc that can be taken into consideration depending on the type of analysis. Moreover, MATLAB [148,149] computational commands can also be used for calculating band gap, gap map and dispersion of PhC structures [82]. In this thesis, MATLAB codes have been utilized to calculate dispersion in PhC and PCF structures [120].

1.9 Overview of the thesis

In this thesis work, first, the design and analyses of silicon carbide based photonic crystal cavity has been done using PWE and FDTD techniques. Further, four specialty photonic crystal fibers are designed and the propagation characteristics of these photonic crystal fibers have been investigated. The geometrical and wave guiding parameters of the PCFs have been calculated using different computational methods like PWE, FDTD, FEM etc.

The thesis has been divided into seven chapters and a brief inclusion of each chapter has been given hereunder.

Chapter 1: This chapter includes the importance of photonic crystal and photonic crystal fiber based photonic devices for potential applications. It includes detailed literature review on the advances in the area of photonic crystal and the photonic crystal fiber based photonic devices for potential applications and method of fabrication. This chapter also includes the theory, analytical techniques and numerical methods used for the design of photonic crystal and the photonic crystal fiber based photonic devices.

Chapter 2: This chapter includes designing of silicon carbide (SiC) based 2D photonic crystal and point defect cavity and studying the effect of temperature on key parameters of the proposed designs like band gap width, defect cavity mode dispersion, the resonance mode and quality factor of resonant mode using plane wave expansion (PWE) method and finite difference time domain (FDTD) method for telecommunication applications. It has been found that the results obtained were better compared to Si based PhC. The SiC PhC devices can be used for high temperature and power transmission which is difficult to achieve with Si or GaAs based photonic crystals and devices. Apart from applications in optical communication, various other SiC based devices such as optical filters, switches and lasers etc can be designed which are stable at high power and high temperature, at which the silicon photonics fails, which can lead to the era of silicon carbide power photonics analogous to silicon carbide power electronics.

Chapter 3: This chapter includes the design and analyses of fluoropolymer photonic crystal fiber in terms of the parameters like effective refractive index of the guided mode, dispersion, confinement loss for wavelength range 10μm to 300μm using full vectorial FEM. It has been found that the transmission characteristics of fluoropolymer photonic crystal fiber obtained are comparable with the earlier published result. The proposed fluoropolymer PCF may find applications in long distance telecommunication and in mid-infrared region.

Chapter 4: This chapter includes the design and analyses of W-type photonic crystal fibers (W-Type PCF) in terms of the parameters like bend loss of the guided mode, effect of temperature on bend loss, and nonlinearity using full vectorial FEM. It has been found that the transmission characteristics of W-Type PCF obtained with the simulation are better compared with the earlier published results. The power coupling in W-type PCF is more compared to conventional PCF. The bend insensitive nature of the proposed W-type PCF structures makes them good candidate for large mode area fiber design and fit for fiber to home applications.

Chapter 5: This chapter includes the designing of large mode area W-type photonic crystal fibers with doped cladding and analyses of the proposed structures in terms of

the parameters like confinement loss, effective refractive index of the guided mode, bend loss, birefringence, sensitivity, effective area and non-linear co-efficient using full vectorial FEM. The proposed W-type PCF structures possesses very low confinement loss and bend loss in the wavelength range of 0.6μm to 2μm. The W-type PCF is found to be birefringent and sensitive and can find possible telecommunication applications in high power delivery devices and sensing.

Chapter 6: This chapter includes the design and analyses of novel Ga-Sb-S based chalcogenide glass photonic crystal fiber (Ga-Sb-S-PCF) in terms of the parameters like effective refractive index of the guided mode, dispersion, effective area, non-linear co-efficient and bend loss using full vectorial FEM. It has been shown that the transmission characteristics of Ga-Sb-S-PCF obtained for wavelength range 0.8μm to 14μm. The novel Ga-Sb-S material PCF structure has been studied for the first time since the inception of novel material Ga-Sb-S and can be a promising candidate for nonlinear applications such as supercontinuum generation, slow light generation, and mid-infrared fiber lasers.

Chapter 7: This chapter includes summery and future scope of the research work described in the previous chapters, references and reprint of the published papers.

Chapter-II

Demonstration of temperature resilient properties of 2D silicon carbide photonic crystal structures and cavity modes

CHAPTER II

DEMONSTRATION OF TEMPERATURE RESILIENT PROPERTIES OF 2D SILICON CARBIDE PHOTONIC CRYSTAL STRUCTURES AND CAVITY MODES

2.1 Introduction

In chapter I it has been discussed that the photonic crystals (PhCs) exhibit photonic band gaps (PBG) in which electromagnetic fields cannot propagate in given directions, if the geometrical parameters and dielectric contrast of the photonic lattices are chosen appropriately [2]. Photonic Crystals can be used to control light propagation through it by using different geometry and dielectric contrast. Because of the strong photon confinement shown by these crystals they can be used in variety of applications. A special attractive application of PhCs is to construct localized electromagnetic modes by introducing defects in the periodic structure. These confined modes could be used in optical resonators, laser cavities etc.

Investigating photonic structures which are less sensitive to environmental fluctuations like high temperature is a valuable area of research. Hence, this chapter takes account of the design photonic of crystals using temperature resilient material silicon carbide [150, 35] and investigate the variation of width of photonic band gaps in SiC photonic crystals with change in temperature and a comparison with Silicon (Si) photonic crystals [151]. Further, SiC A1 point defect cavity has been created in the PhC by removing one central dielectric rod and analysis of the SiC photonic crystal cavity defect modes in comparison with Si photonic crystal cavity defect modes using plane wave expansion (PWE) method and finite difference time domain (FDTD) method has been carried out. However, the most widely used materials to design photonic crystal devices are Silicon (Si) and Gallium Arsenide (GaAs) because of the available and mature technology of fabrication and optimum refractive index contrast offered by these materials for the existence of the photonic band gaps. We here propose to design photonic crystals using silicon carbide which is one of the hardest materials known, which has found wide application in power electronics and

further the creation of photonic crystal cavity in SiC photonic crystal. The reason for using silicon carbide is its high mechanical strength, large thermal conductivity and small thermo optic coefficient that in turn induces high temperature resiliency.

In this chapter, first, a 2D PhC composed of square lattice of rods in air PhC in temperature resilient material Silicon Carbide (SiC) is realized and the PhC structures are optimized by varying different parameters like radius of the nanopillars, period of the lattice etc for telecommunication applications.

Further, defect cavities have been created in the optimized PhC structures and analysis of the cavity defect modes using plane wave expansion (PWE) method and finite difference time domain (FDTD) method has been reported. The defect A1 cavity has been created in the periodic lattice of photonic crystal by removing one central dielectric rod completely from the unperturbed lattice structure that result in localization of light in the specified defect space in the frequency range lying within the PBG of the optimized PhC [152]. The localized defect modes [56] of these A1 defect cavity structures have been extracted and the dispersion relations plotted to investigate the temperature resilient property of the localized defect modes of these structures. Also Quality factor (Q) [156] for both these structures have been calculated using finite difference time domain (FDTD) method for different temperatures ranging from 25^0C to 200^0C and studied resonant wavelength peak shift for the temperature range.

2.2. Design of 2D SiC and Si rods in air photonic crystals and cavity structures

A 2D PhC composed of square lattice of SiC rods (n=2.64) in air with radius of dielectric nanopillars, r = 0.16 μ m and distance between the center of two consecutive rods or lattice constant, a=0.55 μm has been designed as shown in the Fig. 2.1, whose PBG for TE mode lies in the range of 1.46 μm to 1.80 μm as shown in the Fig. 2.3. Similarly, a 2D Si rods (n=3.4) in air PhC with a square lattice is created with r = 0.12 μm and a=0.42 μm as shown in the Fig.2.2, whose PBG for TE mode is in between 1.34 μm to 1.77 μm as shown in the Fig.2.4. Further, point defect is

created in these proposed designs of SiC and Si photonic crystal to form PhC cavity as shown in the Fig.2.1 and Fig.2.2.

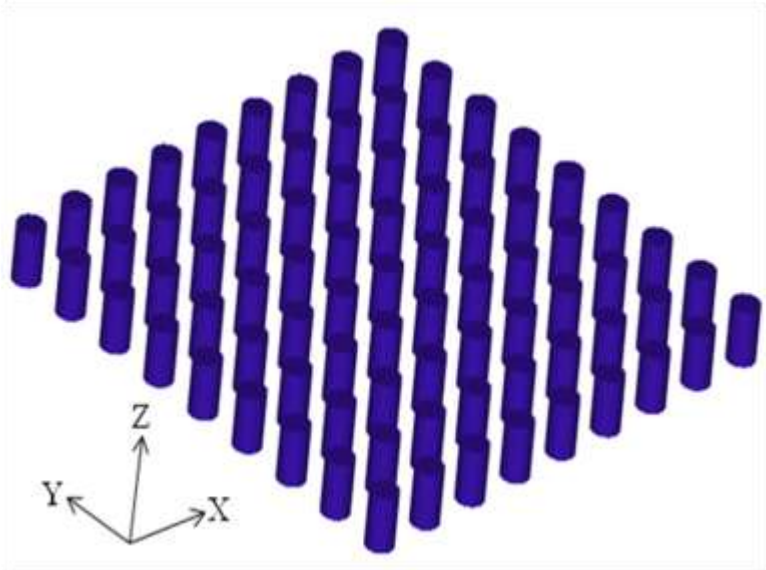

Fig. 2.1: A square lattice dielectric rods in air silicon carbide 2D PhC.

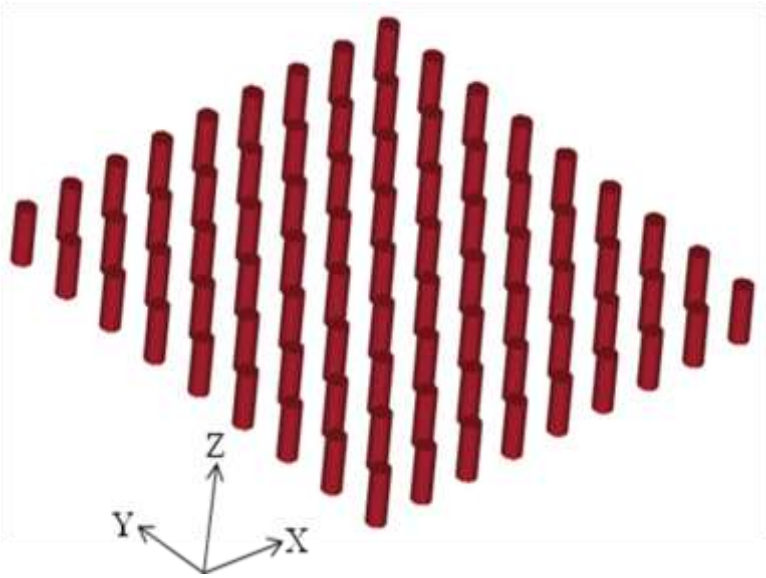

Fig. 2.2: A square lattice dielectric rods in air silicon 2D PhC.

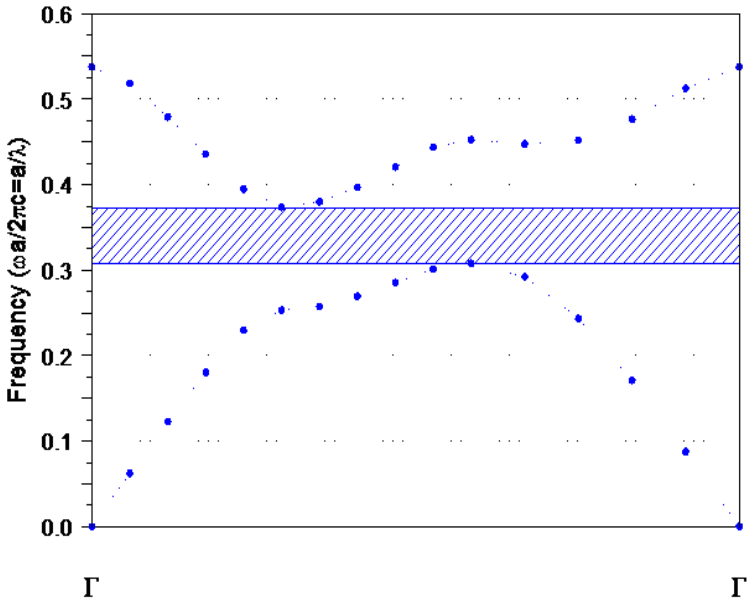

Fig. 2.3: TE band gap of square lattice of SiC rods in air PhC.

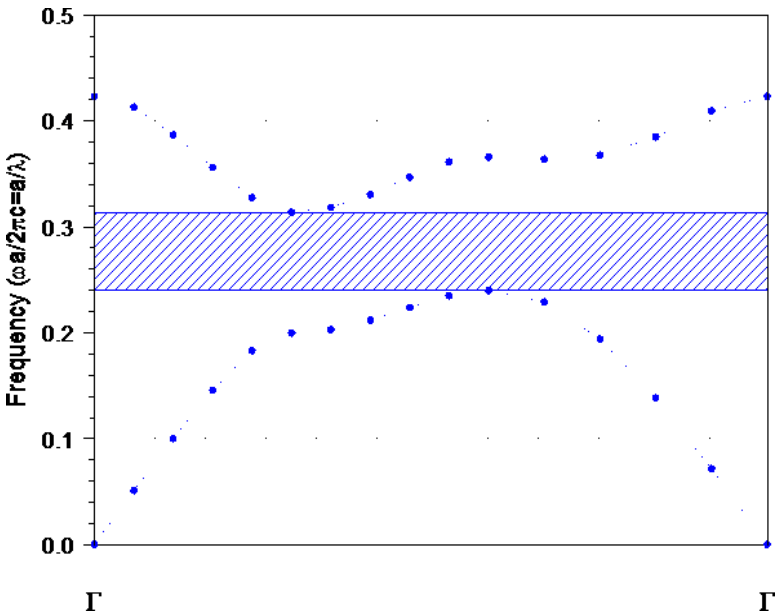

Fig. 2.4: TE band gap of square lattice of Si rods in air PhC.

Again, a 2D PhC composed of hexagonal lattice of SiC rods (n=2.64) in air with radius of dielectric nanopillars, r = 0.16 μ m and lattice constant, a=0.55 μ m has been considered as shown in the Fig.2.5, whose PBG for TE mode lies in the range of 1.38 μ m to 1.85 μ m as shown in the Fig.2.7. Similarly, a 2D Si rods in air PhC with a

hexagonal lattice is created with r = 0.12 μ m and a=0.42 μ m as shown in the Fig.2.6, whose PBG for TE mode is in between 1.28 μ m to 1.81μ m as shown in the Fig.2.8. Further, point defect is created in these proposed designs of SiC and Si photonic crystal to form PhC cavity. The figures indicate that the band gaps exhibited by SiC crystals are smaller as compared with those exhibited by Si photonic crystals because the SiC photonic crystals have lower refractive index contrast.

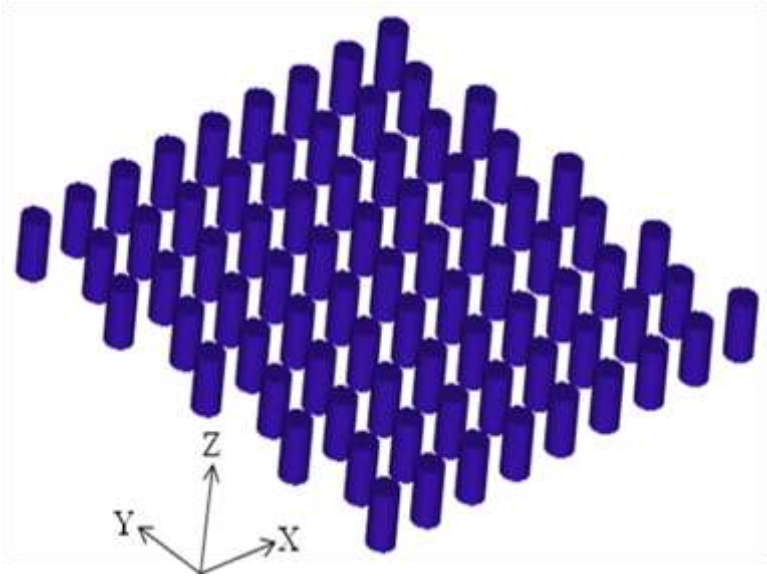

Fig. 2.5 A hexagonal lattice dielectric rods in air silicon carbide 2D PhC.

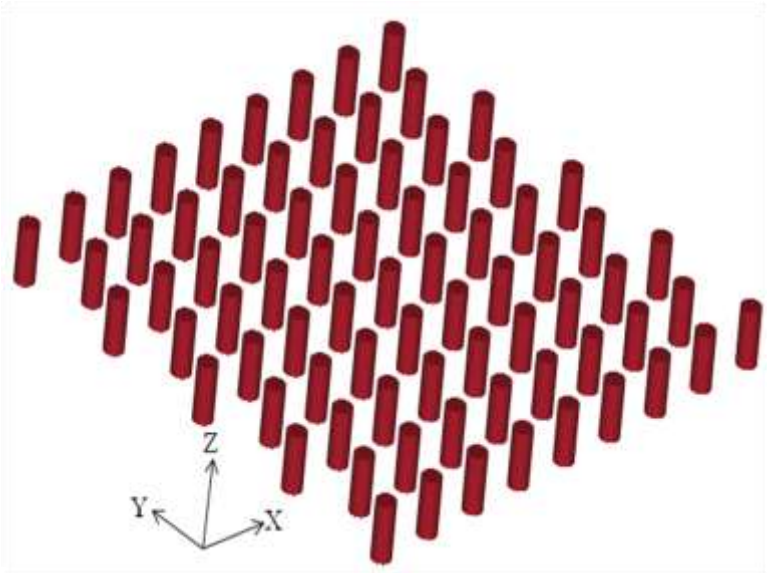

Fig. 2.6: A hexagonal lattice dielectric rods in air silicon 2D PhC.

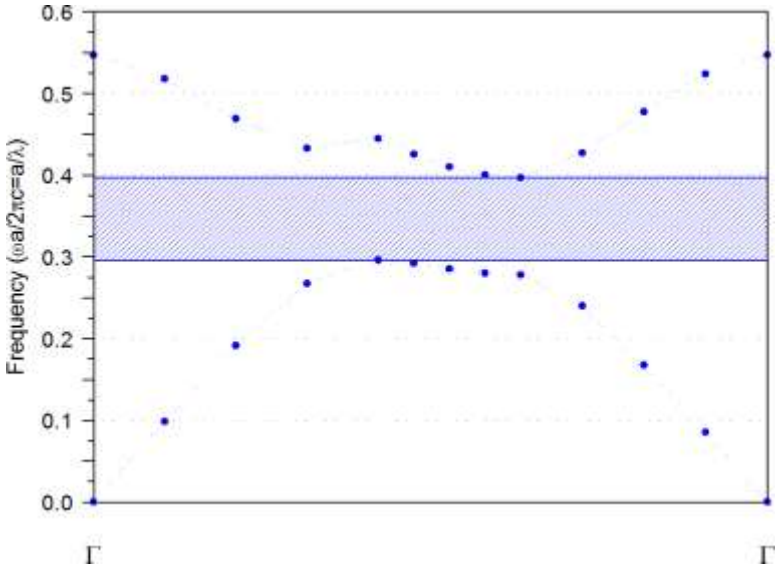

Fig. 2.7: TE band gap of hexagonal lattice of SiC rods in air PhC.

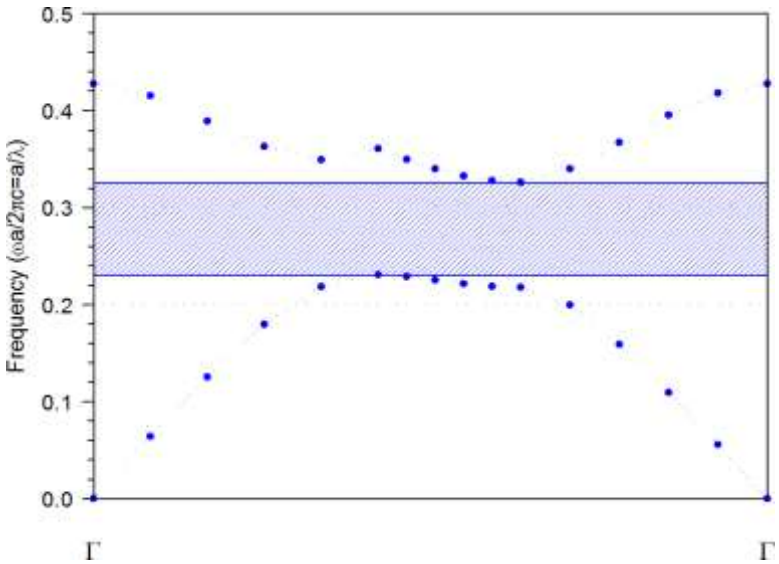

Fig. 2.8: TE band gap of hexagonal lattice of Si rods in air PhC.

2.3. Temperature resiliency study of band gap width of 2D SiC PhC

To study the effect of temperature on the photonic crystal structures, the temperature of the designed structures has been raised from 25^0C to 200^0C [153] and the band gap width has been calculated at various temperatures for both SiC PhC and Si PhC. The variation of photonic band gap with temperature for both Si and SiC based square and hexagonal lattice PhC has been shown in figure 2.9. Figure 2.9 indicates that the SiC based photonic crystal exhibited a very small variation or shallow shift in the width of

the band gap with change in temperature as compared to the Si based PhC. For the operational wavelength of 1550nm, the SiC based square lattice PhC exhibited a shift of around 2.2nm in the operational range (band gap width) while the temperature is varied from 25^0C to 200^0C, whereas the Si based photonic crystal, exhibits a shift of around 5.5nm in the same operational window, which is around three times the variation observed with respect to the SiC based PhC. Also the SiC based hexagonal lattice PhC exhibited a shift of 1nm in the operational range (band gap width) while the temperature is varied from 25^0C to 200^0C, whereas the Si based photonic crystal, exhibits a shift of around 8.2 nm in the same operational window, which is around eight times the variation observed with respect to the SiC based PhC. Thus, the results indicate that the SiC based photonic crystals are nearly three times more resilient than Si based photonic crystals over a given temperature range and hexagonal lattice SiC PhC structures are more resilient than its square counterpart. This variation in the operational range of the SiC and Si PhC indicate the difference in the thermo optic effect of SiC and Si photonic crystal. Thus, the SiC PhCs are less susceptible to the temperature fluctuations in comparison to Si PhCs that lead to the instability of the optical properties of the opto-elctronic systems and hence SiC PhCs find application in making photonic crystal nanophotonic devices almost independent of the temperature of their environment.

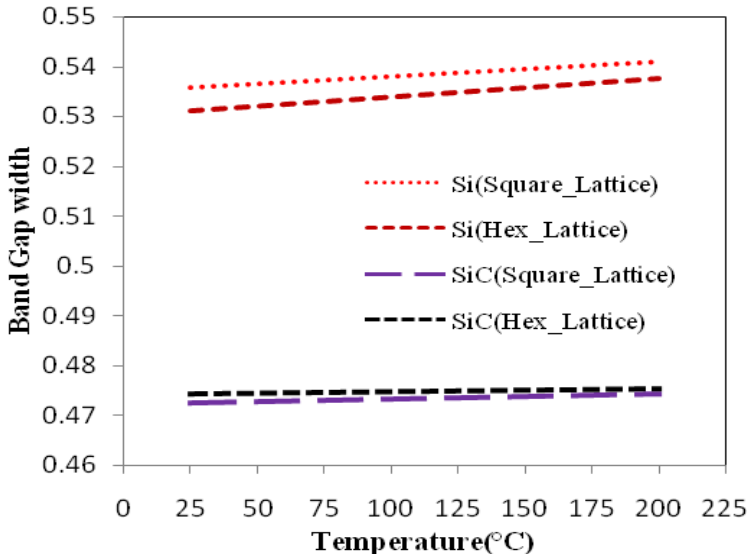

Fig. 2.9: Variation of band gap width with temperature in square and hexagonal lattice SiC and Si PhC.

2.4. Defect mode analysis of 2D SiC square lattice cavity

Photonic crystals have the potential of realizing nanoscale optical components and devices. Since the PBG structures strongly control the flow of light, therefore various types of defect cavities can be created in periodic lattice of PhC's by changing the radius of rods or holes or by removing them completely that result in confinement or localization of light in a specified defect space [13]. These cavities support localized modes in the frequency range lying within the PBG of the PhC. These localized modes are horizontally confined by PBG of the photonic crystal and vertically by total internal reflection because of the refractive index contrast between the dielectric and the cladding [154, 155].

2.4.1. Dispersion analysis of defect cavity mode

A defect A1 cavity has been created by removing a single dielectric rod from the proposed square and hexagonal lattice SiC PhC structures and it has been found that the localization or trapping of light in square lattice cavity is more compared to hexagonal lattice cavity. The defect A1 cavities of silicon carbide dielectric rods in air PhC and silicon rods in air PhC designs have been shown in the figure 2.10 and figure 2.11 respectively. It has been found that the PWE TE solutions exhibit a band gap in the range between 1.49 μm to 1.81 μm for SiC PhC cavity and the PWE TE solutions exhibit a band gap in the range between 1.30 μm to 1.78 μm for Si PhC cavity. When a point defect is created in a photonic crystal, the defect can pull light mode into the band gap. As such a state is forbidden from propagating in the bulk crystal, it is trapped. Localized defect modes have been extracted for both the SiC and Si PhC cavities. The dispersion diagram for SiC 2D PhC cavity has been plotted as shown in figure 2.12. Figure 2.13 shows the dispersion diagram for Si 2D PhC cavity. The corresponding defect mode profile of SiC and Si PhC cavity is shown in figure 2.14 (i) and figure 2.14 (ii), which indicates that modes get localized in both 2D SiC and Si PhC A1 cavity and these modes are confined vertically by total internal reflection and horizontally by the photonic band gap of the PhC.

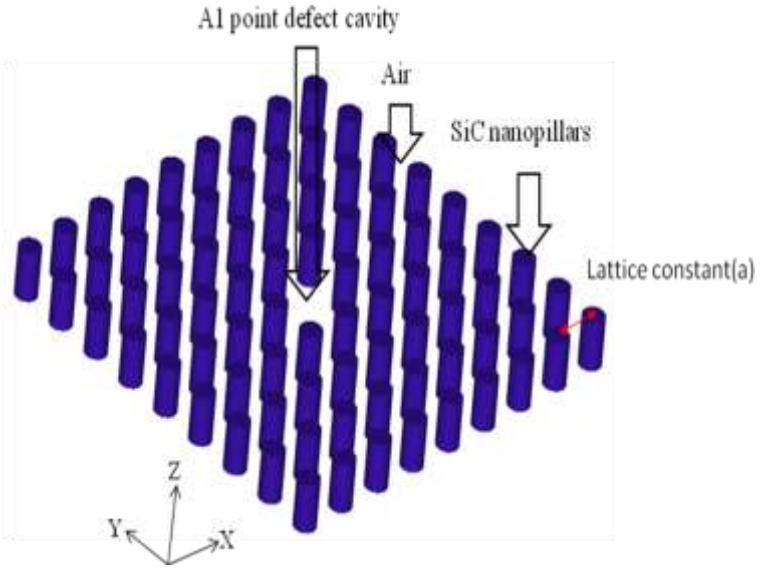

Fig. 2.10: A square lattice dielectric rods in air silicon carbide 2D A1 PhC cavity having lattice constant, a = 0.55 μ m.

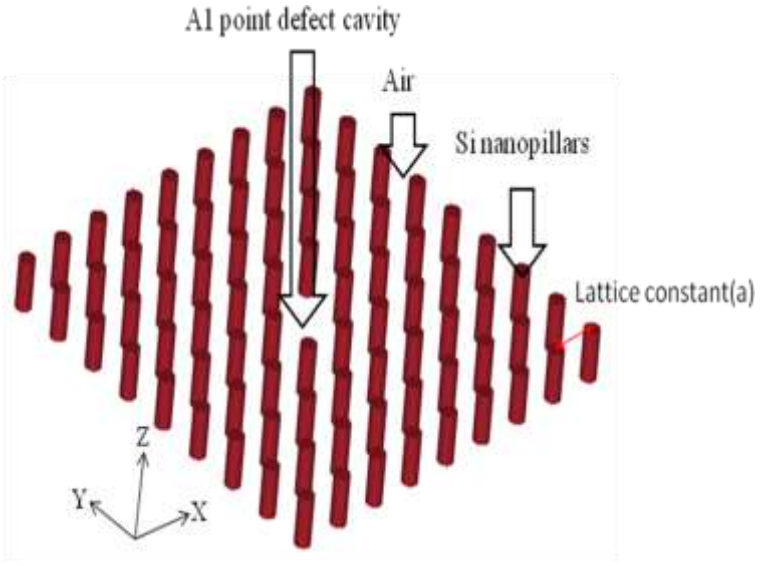

Fig. 2.11: A square lattice dielectric rods in air silicon 2D A1 PhC cavity having lattice constant, a = 0.42 μ m.

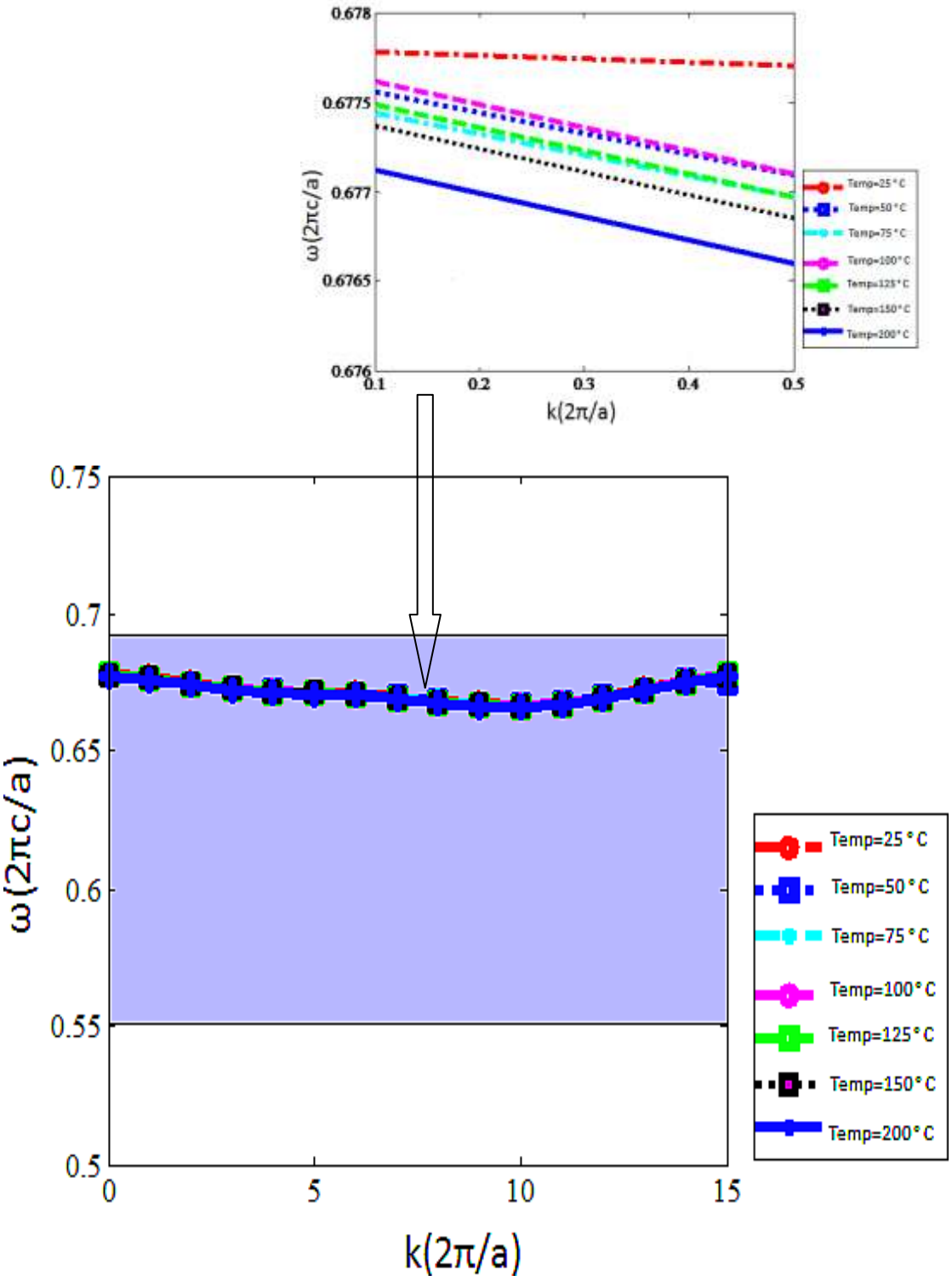

Fig. 2.12.: Dispersion graph of localized defect mode of SiC PhC A1cavity at different temperatures: the blue line is the dispersion curve. Inset: Shift in the resonant wavelength of the A1 SiC rods in air PhC micro cavity structures for different temperatures.

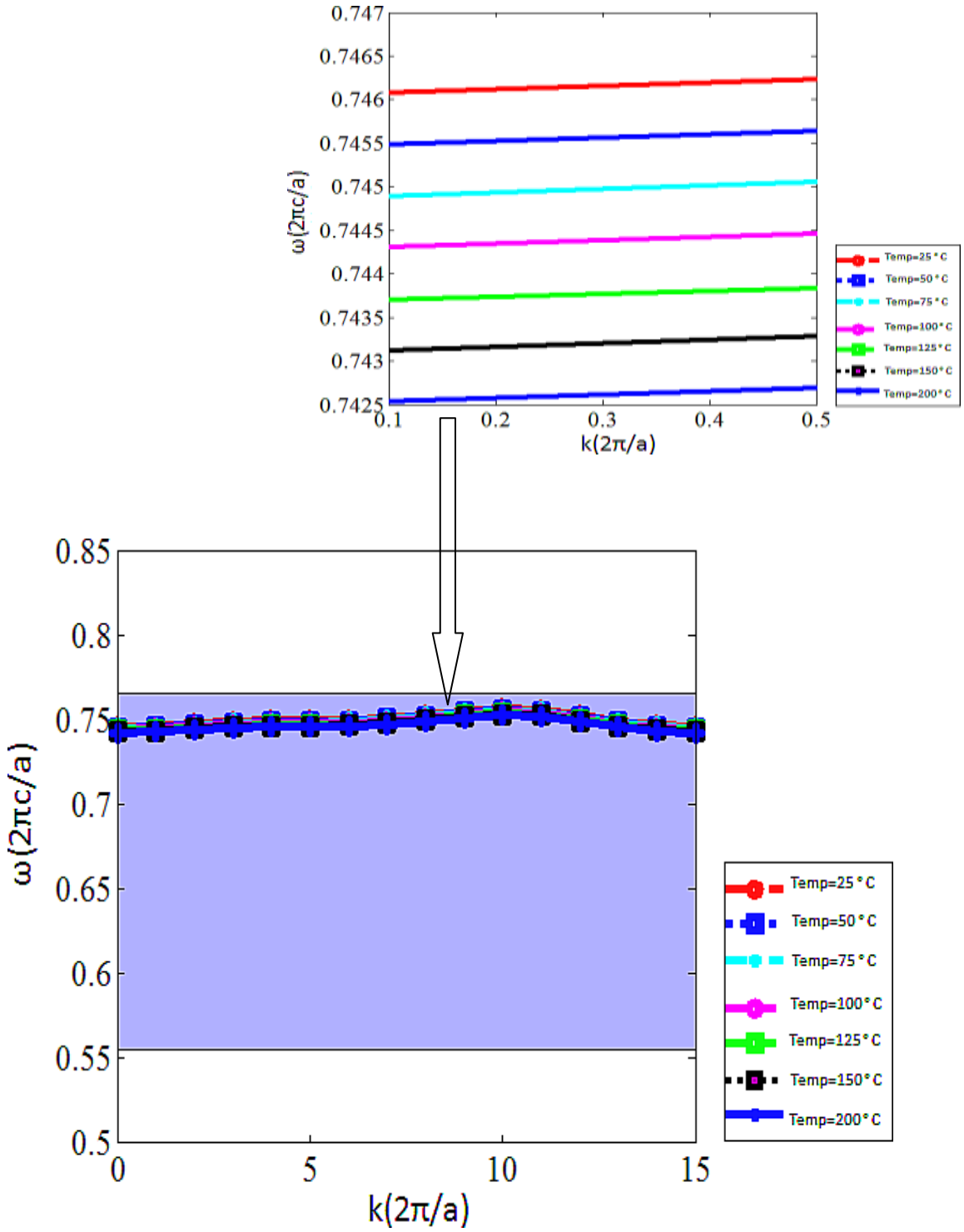

Fig. 2.13: Dispersion graph of localized defect mode of Si PhC A1cavity at different temperatures: the blue line is the dispersion curve. Inset: Shift in the resonant wavelength of the A1 Si rods in air PhC micro cavity structures for different temperatures.

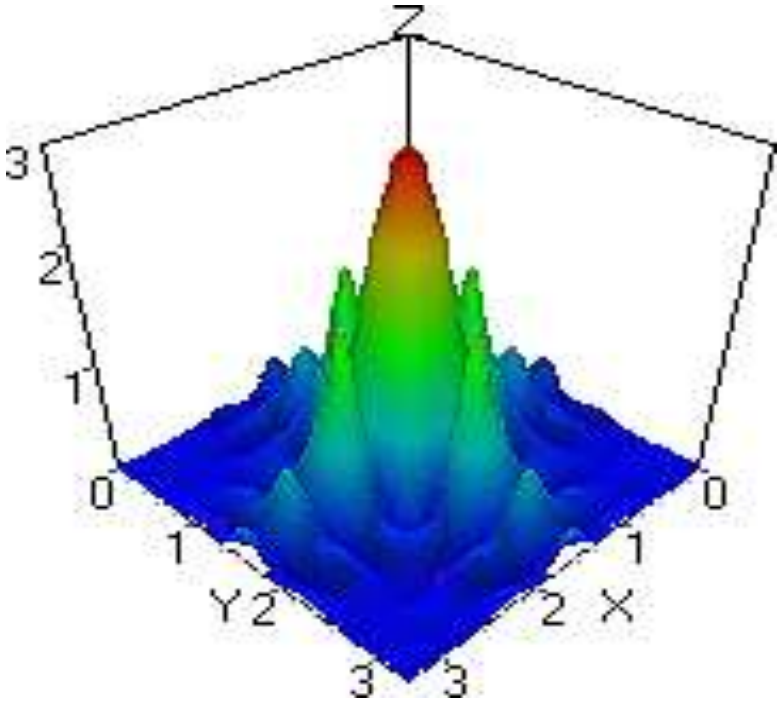

(i)

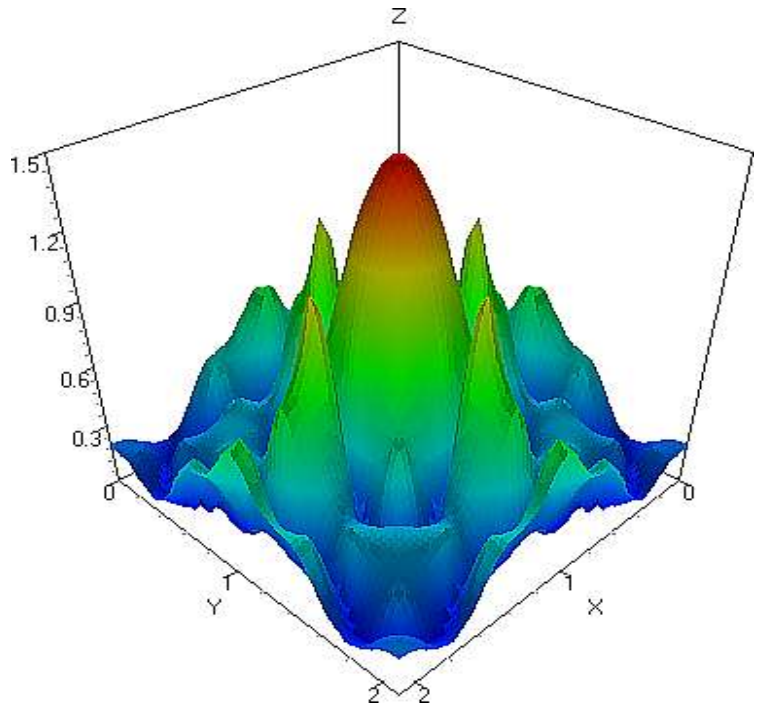

(ii)

Fig. 2.14: Localized defect modes of a square lattice of (i) SiC and (ii) Si dielectric cylinders in air PhC A1cavity: Y- component of electric field (E) amplitude.

The dispersion graph of localized defect mode of SiC PhC A1cavity in figure 2.12 shows a shift of around 3.6nm for the temperature range from 25^0C to 200^0C whereas the Si PhC A1cavity in figure 2.13 exhibits a shift of around 37nm in the same operational window, which is around ten times the variation observed with respect to the SiC based PhC A1cavity. The result depicts that the SiC cavity structures are more temperature resilient as compared to Si based PhC cavity.

2.4.2 Q factor calculation and its optimization

The Q factor [156] or Q of the cavity is defined as the ratio $\frac{\lambda}{\Delta\lambda}$ of the cavity resonance and is a measure of the ratio of the optical energy stored in the micro cavity to the cycle average power radiated out of the cavity. The resonant mode is strongly confined in the micro cavity. Q can be calculated from relative power versus distance curve using transmission function based on the point or transmission function based on the area [58, 156] using relation 1.31.

i.e. $$Q = \frac{\lambda}{\Delta\lambda} = \frac{f_0}{f_2 - f_1} \quad (1.31)$$

Where, f_o is the centre frequency or the resonant frequency, f_1 and f_2 frequencies at full wave at half maximum (FWHM) called the upper and lower cut off frequencies, (f_2 - f_1) is the band width of the resonant system. Quality factor or Q factor is a measure of quality of performance of a resonant system. It indicates the ability of the system to produce a large output at the resonant frequency. Hence, the quality factor for the above mentioned structures has been found out and a maximum value of 224 is obtained for SiC A1 PhC cavity and 213 for Si A1 PhC cavity. It has been found that there is a shift of about 0.3nm in the resonant wavelength peak of the SiC A1 PhC cavity structures when the temperature is varied from 25^0C to 200^0C as shown in figure 2.15. Whereas the Si PhC A1cavity in figure 2.16 exhibits a resonant wavelength peak shift of around 2nm in the same operational window, which is around seven times the variation observed with respect to the SiC based PhC A1cavity. The result indicates that the SiC cavity structures are more temperature resilient as compared to Si based PhC cavity structures [157,158].

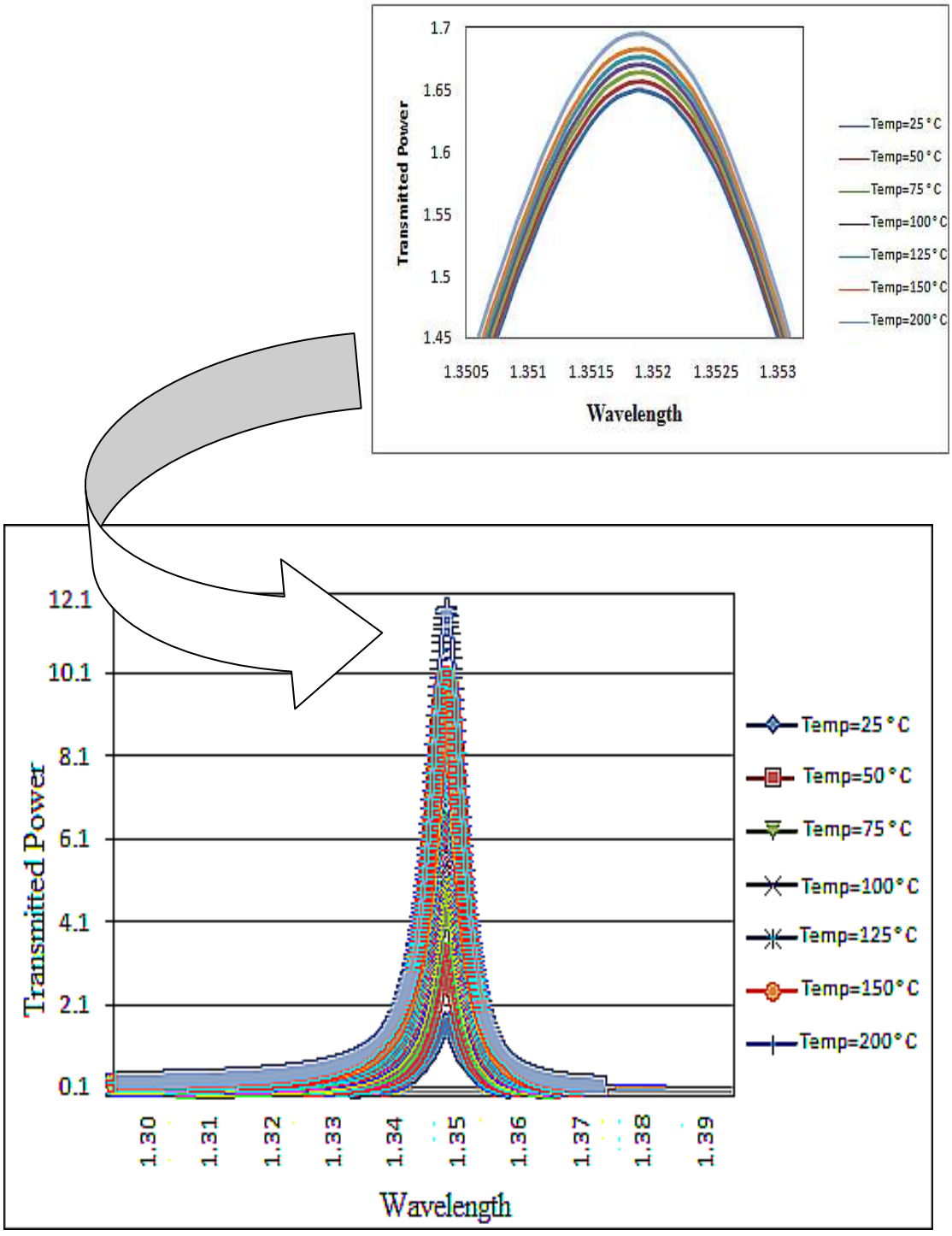

Fig. 2.15: Transmitted Power versus wavelength graph for localized defect mode of SiC PhC A1 defect cavity at different temperatures. Inset: Shift in the resonant peak of the A1 SiC rods in air PhC micro cavity structures for different temperatures.

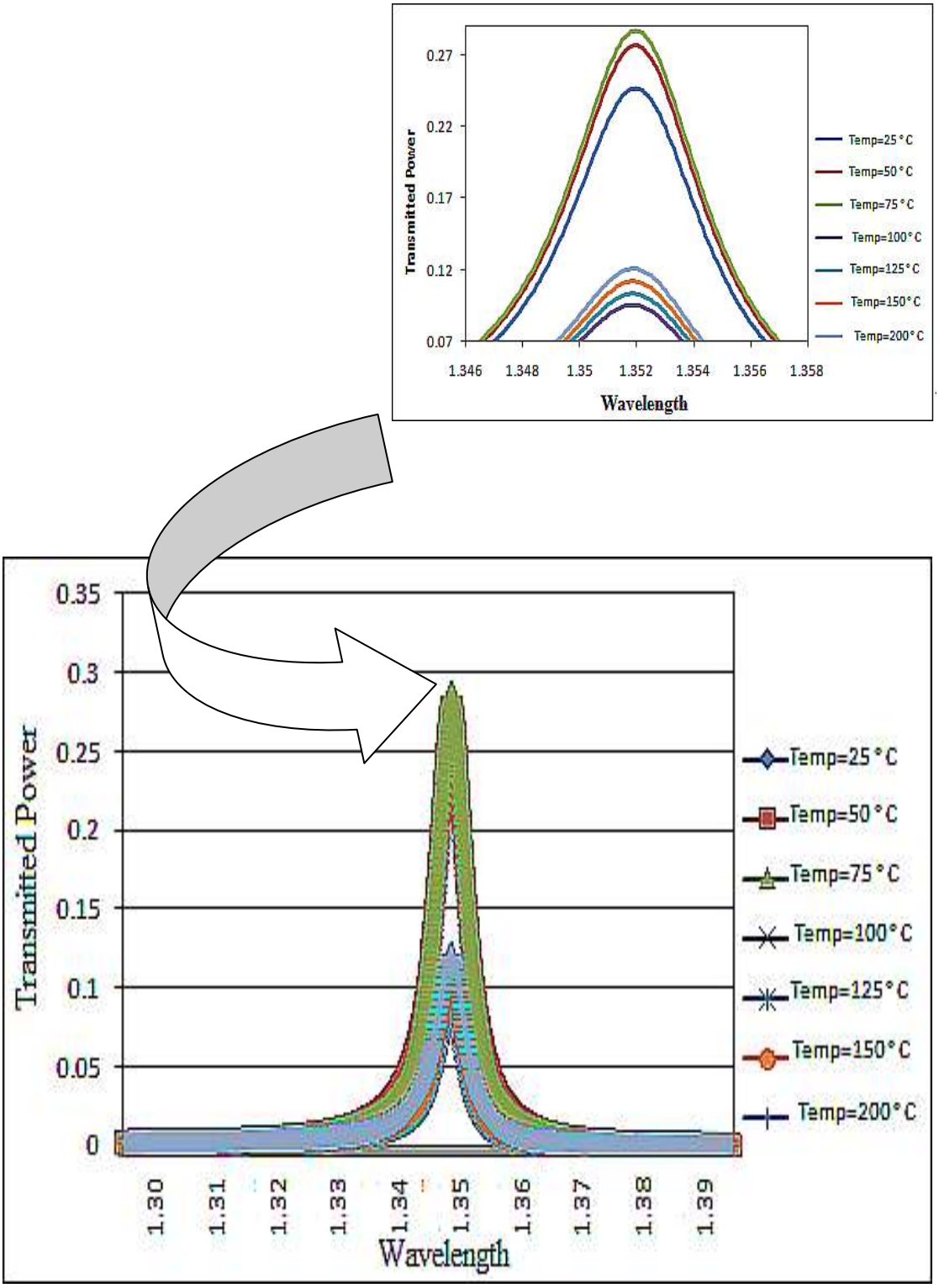

Fig. 2.16: Transmitted Power versus wavelength graph for localized defect mode of Si PhC A1 defect cavity at different temperatures. Inset: Shift in the resonant peak of the A1 Si rods in air PhC micro cavity structures for different temperatures.

2.5 Conclusion

Here, in this chapter, photonic crystal (PhC) based on two dimensional(2D) square and hexagonal lattice periodic arrays of Silicon Carbide (SiC) rods in air structure has been investigated using plane wave expansion (PWE) method. The PhC designs have been optimized for telecommunication wavelength (λ=1.55 μm) by varying the radius of the rods and lattice constant. The result obtained shows that a photonic band gap (PBG) exists for TE-mode propagation. First, the effect of temperature on the width of the photonic band gap in the 2D SiC PhC structure has been investigated and compared with Silicon (Si) PhC. Further, a cavity has been created in the proposed SiC PhC and carried out temperature resiliency study of the defect modes. The dispersion relation for the TE mode of a point defect A1 cavity for both SiC and Si PhC has been plotted. Quality factor (Q) for both these structures have been calculated using finite difference time domain (FDTD) method and found a maximum Q value of 224 for SiC and 213 for Si PhC cavity structures. Thus, we have designed an optimized cavity in temperature resilient material (SiC) and analyzed its PBG and cavity mode characteristics using PWE and FDTD techniques. These analyses are important for fabricating novel PhC cavity designs that may find application in temperature resilient devices. The SiC PhC devices can be used for high temperature and power transmission which is difficult to achieve with Si or GaAs based photonic crystals and devices. Apart from applications in optical communication, various other SiC based devices such as optical filters, switches and lasers etc can be designed which are stable at high power and high temperature, at which the silicon photonics fails, which can lead to the era of silicon carbide power photonics analogous to silicon carbide power electronics.

Chapter-III

Characterization of Fluoropolymer Photonic Crystal Fiber for THz regime

CHAPTER-III

CHARACTERIZATION OF FLUOROPOLYMER PHOTONIC CRYSTAL FIBER FOR THZ REGIME

3.1 Introduction

As discussed in chapter I of this thesis, Photonic Crystals Fiber (PCF) is a new class of fiber also called specialty fiber designed on the basis of the properties of the photonic crystal. Due to it's capacity to confine more light in the core or the confinement characteristics not possible in conventional optical fiber, PCF is finding applications in fiber-optic communication, fiber lasers, nonlinear devices, high power transmission, sensing, fiber to the home applications (FTTH) etc. PCF [10] is a single material optical fiber with an array of periodic air holes across the cross-section running down its entire length. By leaving a single lattice site without an air hole, a localized region of higher refractive index is formed. This localized region acts as a waveguide core in which light can be trapped along the axis of the fiber [63,87]. PCF are usually designed in silica material. In recent past, different materials are used for the formation of PCF using Ge-Se Chalcogenide glass [159], As_2Se_3 chalcogenide glass [160,161], As_2S_3 chalcogenide glass [162] and plastic or polymer [163] due to their unique optical properties and for non linear applications like supercontinuum generation and generation of slow light. Very recently, tellurite [164] and fluoro-tellurite [165] glass have been used to design PCF.

A substantial amount of attention has been given to Fluoropolymer (commercial name Teflon) based PCF [166] because of its unusual and attractive optical properties in THz frequency range [163] like single mode operation [168], large mode area[163], high birefringence[163] and manageable dispersion properties [166,170,171] and possible applications in optical communication[172], nonlinear optics such as optical coherence tomography[106], metrology and spectroscopy[168,169], and can be utilized in construction of compact THz devices and measurement systems[172]. Moreover, the Fluoropolymer (Teflon) based PCF is one of the potential candidates

for a range of optical communication application such as THz imaging systems in THz spectroscopy, laser amplifier, pulse compression, wavelength conversion, all optical switching, supercontinuum(SC) generation and also in optical sensing. These applications require a detailed investigation of the optical properties of Teflon PCFs, which, to our knowledge, have not been investigated much by the research community till today since Goto et al [173] successfully used Teflon to produce a viable PCF THz waveguide followed by Pobre et al [174] conducting modal analysis of Teflon photonic crystal fiber as a terahertz waveguide. These properties include variation of effective index of guided mode with wavelength and dispersion etc.

Fluoropolymer or the fluorinated copolymer is a copolymer of 2,2-bistrifluoromethyl-4,5-difluoro-1,3-dioxole(PDD) and tetrafluoroethylene (TFE) and amorphous in nature [166]. The PDD dioxole monomer in fluoropolymers yields unexpected properties. Teflon or polytetraflourethylene is the trademark brand name of fluoropolymer produced by Dupont. Teflon has outstanding light transmission from the deep UV range including a significant portion of the IR range. Also, as Teflon does not absorb light, it will not deteriorate with exposure to light. These optical properties, over such a wide range of wavelength and possible exposure conditions, are unmatched by any other polymer. The properties of Teflon, including optical clarity, unusually low refractive index, high flexibility and exceptional UV stability and UV transmission capability, make it an ideal material for optical devices. Fluoropolymer PCF can be easily manufactured and has low loss characteristics to be used as a waveguide for terahertz waves i.e. in the frequency regime of 100 GHz (or 0.1THz) to 30 THz [168,169,172] or in the wavelength range of 10 μm to 300 μm.

In optical communication, dispersion plays an important role as it determines the information carrying capacity of the fiber. Therefore it becomes important to study the dispersion properties of PCF. Following these issues, we present the propagation characteristics of Fluoropolymer PCFs exhibiting guiding properties in terahertz region. The variation of effective index of guided mode and dispersion with wavelength in hexagonal lattice Fluoropolymer PCF are investigated by using the fully-vectorial finite element method (FEM).

3.2. Design of Fluoropolymer PCF

A PCF is designed using the highly flexible plastic material Fluoropolymer whose commercial name is Teflon. Figure 3.1 shows the transverse cross-sectional view of the proposed fluoropolymer PCF structure. Here, the fiber cladding consists of a hexagonal lattice of circular air hole with a missing air hole in the centre, in a fluoropolymer background, whose refractive index is considered to be equal to 1.44.

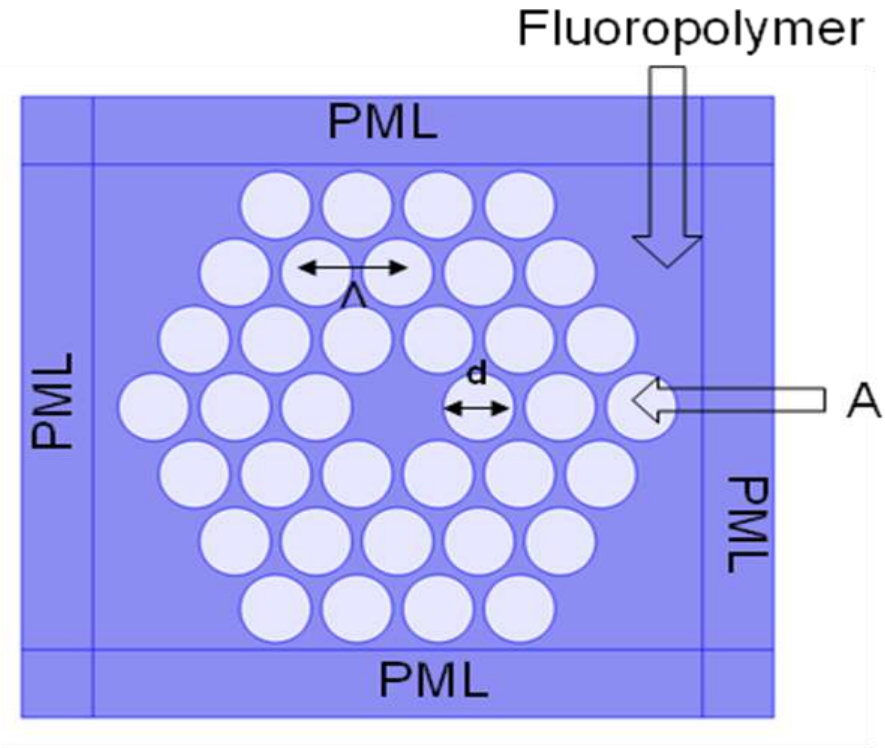

Fig. 3.1: Transverse cross sectional view of the designed Fluoropolymer PCF.

In the design, the pitch, Λ(i.e. the distance between the center's of two consecutive air holes or air hole spacing), is taken to be 750 μm, and the diameter of cladding air hole is varied (from d/Λ=0.3μm to d/Λ=0.6μm) while keeping diameter of the core (d_c=1000 μm) larger than diameter of air holes in the cladding. Following this optimization, finally obtained an optimized asymmetric PCF structure for our calculation having diameter (d/Λ=0.3μm) of air hole in cladding. The mesh diagram and distribution of electric field inside the PCF design is shown in figures 3.2(a) and 3.2(b).

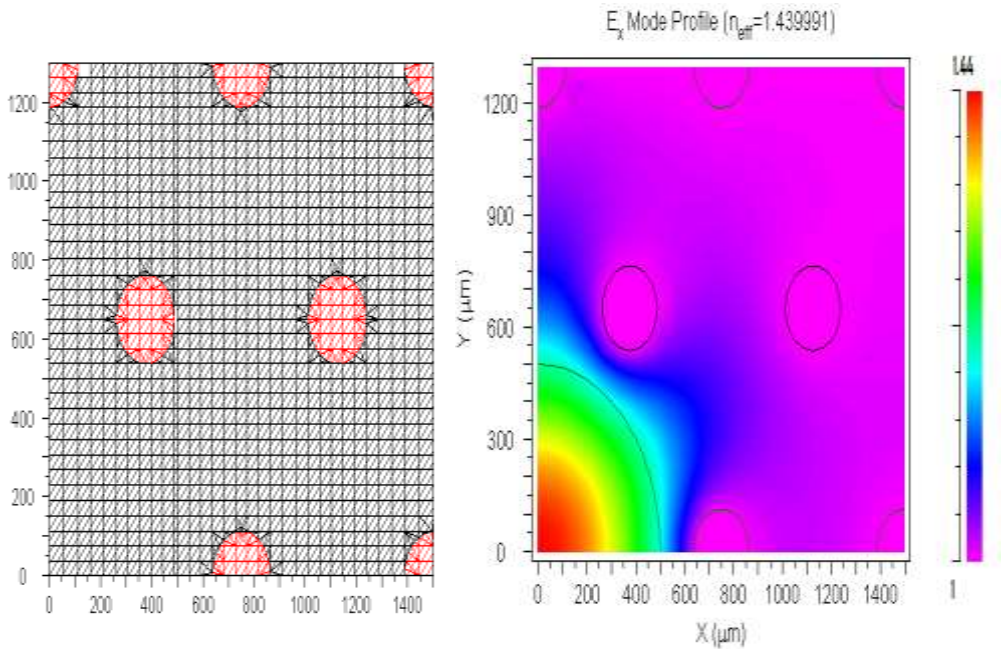

(a) (b)

Fig.3.2: (a) Mesh distribution applied on a quarter of the PCF and (b) Distribution of the electric field of the fundamental mode into a PCF with Λ= 750µm at λ=10 µm on a quarter of Fluoropolymer PCF using Rsoft-FemSIM software tool.

Symmetric Fluoropolymer PCF structures have been created considering similar pitch value for d/Λ value ranging from 0.3 to 0.6, keeping the diameters of the core same as the diameter of the air holes of cladding for corresponding d/Λ value.

3.3. Numerical calculations and results

We calculate the effective index of fundamental polarization modes by using finite element method (FEM) which is highly suited for the analysis of our periodic structure. The chromatic dispersion then deduced from the determination of the effective index. Chromatic dispersion is the main contribute to the optical pulse broadening. Chromatic dispersion D (λ), includes both waveguide and material dispersion, and is proportional to the second derivative of effective index of guided mode with respect to wavelength 'λ' and is given in equation 1.26. Figure 3.3(a) shows the variation of effective index of guided mode, and Figure 3.3(b) shows the variation of chromatic dispersion with wavelength for wavelength range 10 µm to 300 µm for the asymmetric optimized PCF structure.

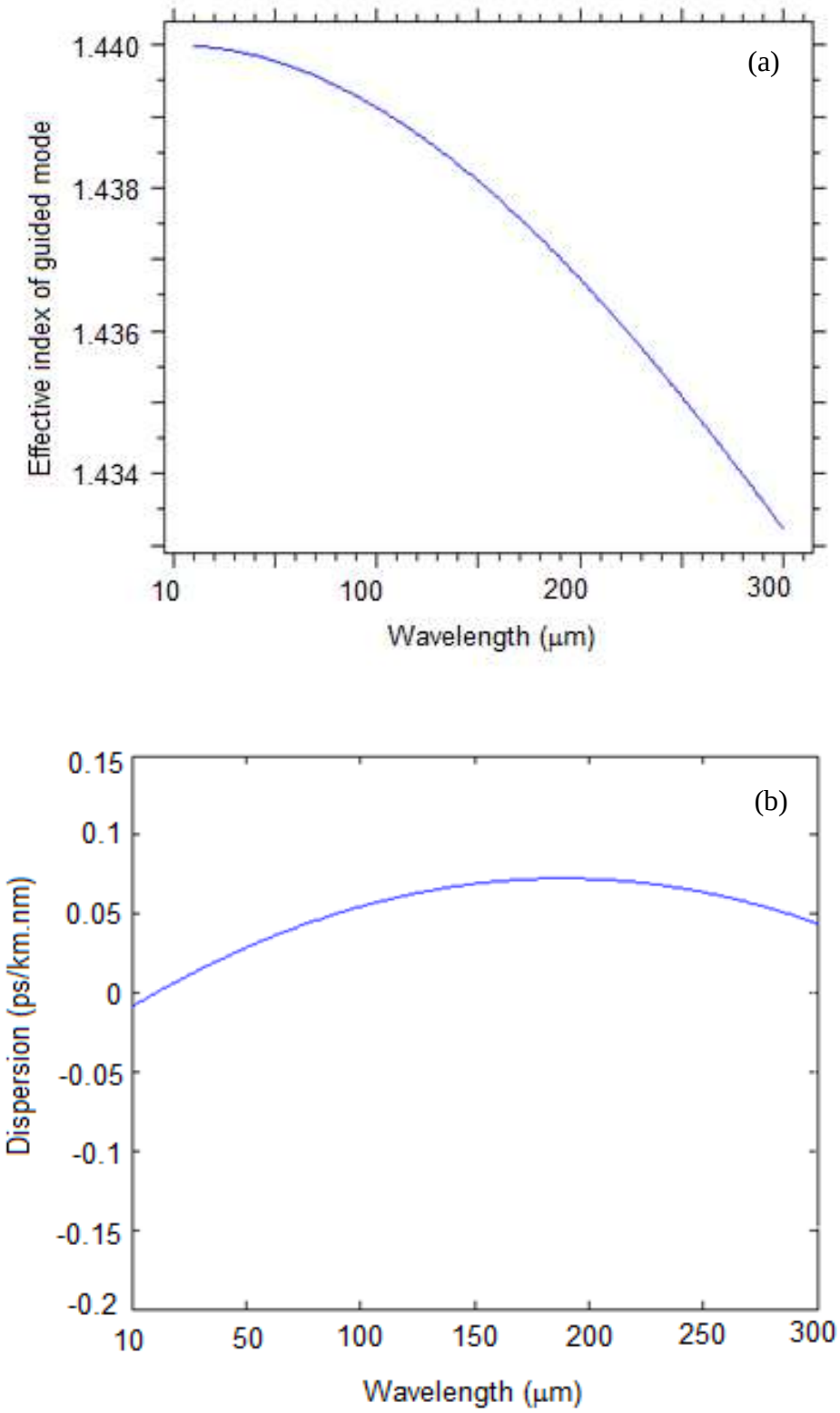

Fig. 3.3: Variation of (a) Effective index of guided mode, and (b) Chromatic dispersion with wavelength in the proposed asymmetric Fluoropolymer PCF.

The variation of effective index (n-eff) of guided mode shows a sharp decrease with wavelength depicts that the effective refractive index of the cladding region relative to the core is reduced due to the presence of the air holes in the higher wavelength range and effective index shows a strong wavelength dependency. The variation of chromatic dispersion graph shows a flattened dispersion thereby opening the door for dispersion flattened PCF.

Further, n-eff for the proposed Fluoropolymer PCF for wavelength range 10 μm to 300 μm for the symmetric optimized PCF structure for d/Λ value ranging from 0.3 to 0.6 has been calculated. Table 3.1 gives the values of n-eff for symmetric Fluoropolymer PCF at different wavelengths and for d/Λ value ranging from 0.3 to 0.6.

Table 3.1: Value of n-eff for Fluoropolymer PCF at different wavelengths and for d/Λ value ranging from 0.3 to 0.6.

Wavelength (μm)	**d/pitch= 0.3**	**d/pitch= 0.4**	**d/pitch= 0.5**	**d/pitch= 0.6**
	n-eff	**n-eff**	**n-eff**	**n-eff**
10	1.439984869	1.43997875	1.439968733	1.439950224
50	1.439626699	1.439474967	1.439227899	1.438782053
100	1.438543288	1.437951642	1.436994587	1.435304205
150	1.436804877	1.435513933	1.433440324	1.429809466
200	1.434461154	1.432234809	1.428685768	1.422497456
250	1.431559202	1.428179724	1.422833218	1.413541005
300	1.428144337	1.423409431	1.415973099	1.403093749

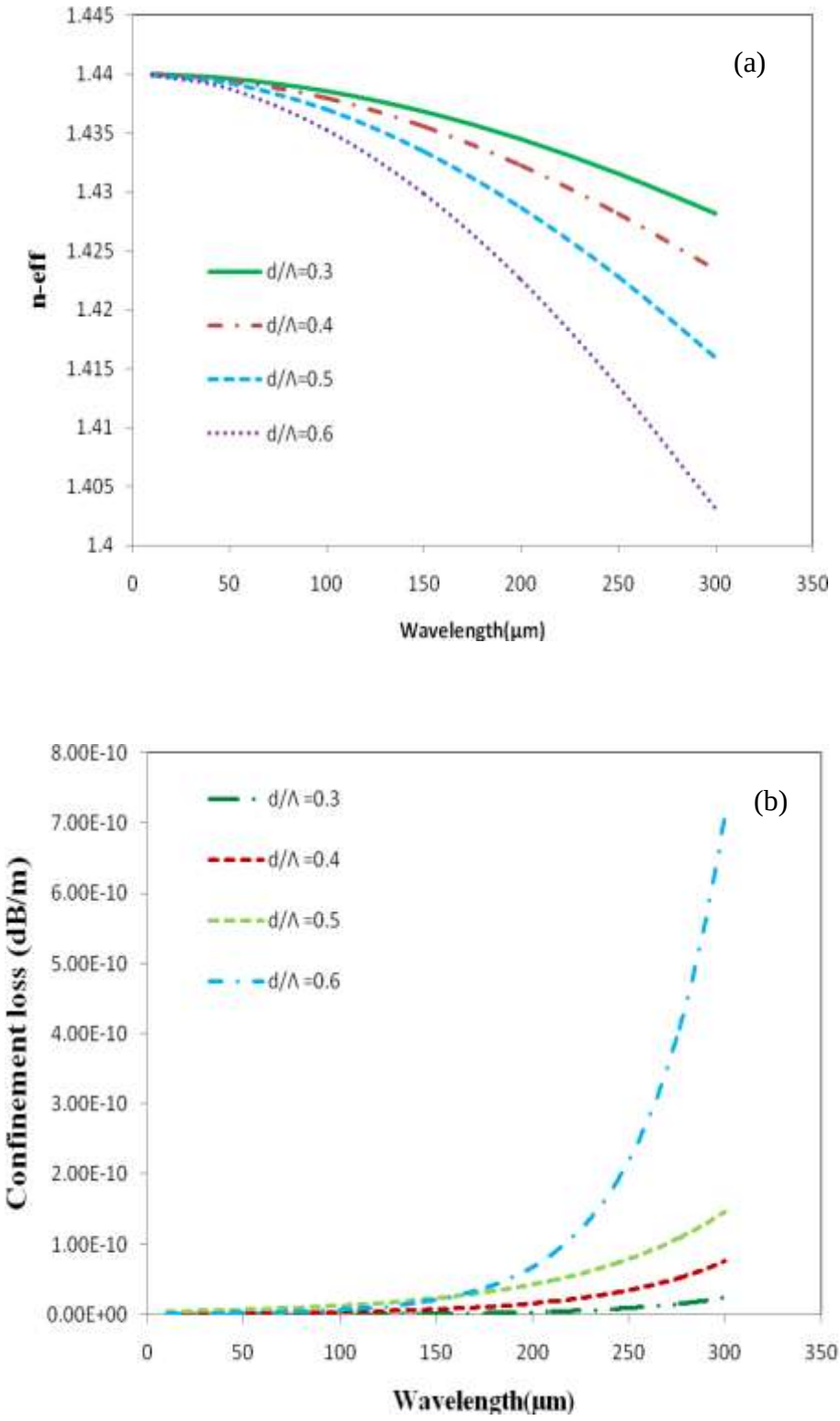

Fig. 3.4: Variation of: (a) Effective index (n-eff) of guided mode with wavelength, and (b) Confinement loss of guided mode with wavelength in the proposed Fluoropolymer PCF for different d/Λ value ranging from 0.3 to 0.6.

The confinement loss of the proposed symmetric Fluoropolymer PCF designs have been calculated using equation 1.29 in chapter I and the confinement loss found increasing exponentially for d/Λ value 0.3 to 0.6 as shown in figure 3.4(b). Due to the increase in diameter of the holes of the cladding as well as the core diameter of the proposed PCF there is less confinement in the central hole or core. As the diameter of holes increased for different d/Λ value from 0.3 to 0.6, the refractive index contrast between core and cladding decreases and also the effective index of guided mode decreases as shown in figure 3.4(a). Both of these, resulting in the increase of the confinement loss of the proposed PCF structures.

3.4. Conclusion

In this chapter, we report the design of a simplified PCF structure based on Fluoropolymer material exhibiting guiding properties in terahertz region i.e. in the wavelength range of 10 µm to 300 µm. The variations of effective index of guided mode, confinement loss and dispersion with wavelength of proposed Fluoropolymer PCF are investigated by using full-vector finite element method. The obtained results add remarkable contribution for the use of Fluoropolymer PCF in numerous applications of sensing, imaging and spectroscopy particularly for terahertz region.

Chapter-IV

Temperature dependent bending loss characteristics of W-type photonic crystal fibers: design and analysis.

CHAPTER-IV

TEMPERATURE DEPENDENT BENDING LOSS CHARACTERISTICS OF W-TYPE PHOTONIC CRYSTAL FIBERS: DESIGN AND ANALYSIS

4.1 Introduction

It has been discussed in previous chapter I and III that photonic crystal fibers (PCFs) or microstructured fibers (MFs) or holey fibers are the single material specialty optical fibers in which arrays of air holes are arranged in a specific arrangement in the cladding region around the core and running along throughout the length [10,63-65, 87]. The effective refractive index of the cladding region relative to the core is reduced due to the presence of these air holes. The presence of the air holes around the core makes the design more flexible. Significant amount of interest has been shown in PCFs because of its unusual and attractive optical properties like single mode operation in wide wavelength range, bending loss characteristics, excitation of non-linear effects at small mode area, and manageable dispersion properties [175-183]. According to the shape, size, orientation and arrangement of the air holes in the cladding region various types of functionalities have been achieved using the PCF structures [175-178]. Recently, a triangular core PCF structure has been reported for all-normal and flat dispersion profile [179,180]. Large-mode-area PCF structure that supports effective mode-area of fundamental mode as large as 794 μm^2 with nominal bend loss of propagating mode 0.064 dB/m at the bend radius of 15cm has been reported for high power applications[175]. In W-type PCF design, the effective index of the cladding region is reduced by varying the diameter of the air holes of different layers to different extent thereby producing a W-type index profile [180,181] and hence is called the W-type PCF [182]. The confinement and guidance of the light in this PCF with relatively high core index occurs via total internal reflection. The single-mode propagation depends on the core radius and the operating wavelength [183, 131].

The study of bending in PCF is an important aspect as PCF like conventional telecom grade optical fibers are needed to be cabled or placed in the forms of coils for its application as transmission medium resulting in bend loss of optical signals in these fibers. In the bend state of the fibers, the field profiles of the propagating modes deform which causes a large bend loss.

In this chapter, bending losses for different bend radii as well as the effect of thermo-optic coefficient on bend loss of W-type-I and W-type-II PCF have been investigated. Mode field diameter (MFD), effective area (A_{eff}) [135] and nonlinearity coefficient [184] of both the proposed PCF structures have been simulated. The thermo-optic effect on bend loss of the proposed PCF structures has been studied and it has been found that the thermo-optic effect overcomes the bend losses at high temperature and there is partial recovery of the fundamental mode thereby making it a potential candidate to be used as temperature-tuned device. Least change in bending loss data has been observed for the proposed PCF designs for macro-bending which implies that the structure is macro-bend insensitive and can be used in fiber-to-the-home applications.

4.2 Modeling of W-type PCF

We have designed two PCF structures. There are three rings of the air holes in the cladding region of the PCF structures. d_1, d_2, and d_3 are the diameters of the air holes in first, second and third ring respectively. The material of the PCFs has been taken as silica.

4.2.1 W-type-I PCF structure

In this PCF structure, the values of the diameters of the air holes are taken as: d_1 = 0.345µm and $d_2 = d_3$ = 0.690 µm. The transverse cross-sectional view of the proposed W-type-I PCF structure has been illustrated in figure 4.1.

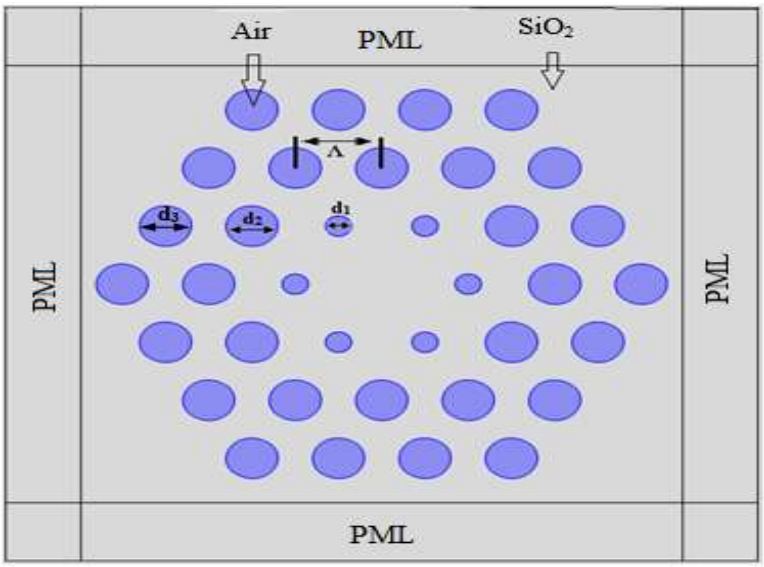

Fig. 4.1: The transverse cross sectional view of W-type-I PCF structure.

4.2.2 W-type-II PCF structure

In this PCF structure, the values of the diameters of the air holes are considered as: d_1 = 0.690 µm and d_2 = d_3 = 0.345µm. The transverse cross-sectional view of the proposed W-type-II PCF structure has been illustrated in figure 4.2. In contrast to step-index fibers the PCF is said to be single-moded if the effective V number is less than approximately the value of the π. [185]. The PCF structures have been analysed for three wavelengths, 0.633µm, 1.33µm and 1.55µm.

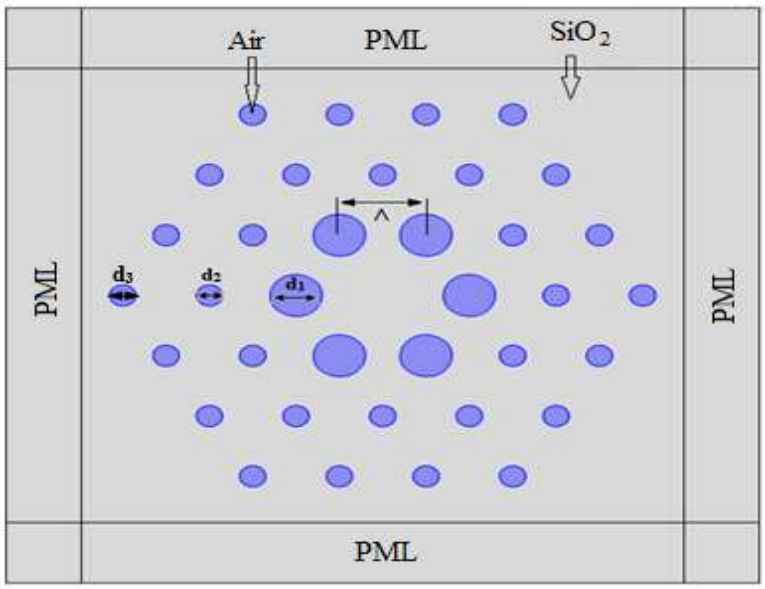

Fig. 4.2: The transverse cross sectional view of W-type II PCF structure.

4.3. Bend loss calculation

The bending loss of the PCF structures plays a vital role in most of the fiber optic applications. Of late several works have been reported on calculation of low bend losses in small mode area PCF [179, 186]. In order to simulate the effects of the bending, the bent PCF is transformed into a straight PCF with an equivalent refractive index profile [141] defined in equation 1.30.

A rectangular perfectly matched layer (PML) has been introduced at the surface of the W-type PCFs to simulate the accurate bend losses. At the bend state of the PCF structure, the propagation constant of the modes of the structure becomes complex. Effective index and the bending loss of the mode have been calculated by using the real and imaginary part of the propagation constant respectively. Bending losses have

been calculated using imaginary part of effective refractive index of the propagating mode by using the following Eq. 1.29.

The bends with different macro bending radii ranging from 2.5cm to 30cm have been applied on the proposed PCF structures in a circular loop with a single-turn and arbitrary angular orientation and bend loss of individual structures have been calculated. The effect of the bending radius on the bending loss of the propagating mode of proposed W-type-I PCF is illustrated in figure 4.3. It is clear from this figure that the bending loss of the propagating mode decreases on increasing the bend radius. In other words, the shift in the modal field towards the bending direction increases with decreasing bend radius. It has been found that at small bending radius, the loss is high and reaches its maximum. However, by increasing the bending radius the bend loss can be dropped to 0.01 dB/m, this is because at large bending radius the scattering loss becomes small.

Table 4.1 shows the calculated refractive index values at different wavelengths using Sellmeier equation for silica at equation 1.25 in chapter I.

Table 4.1: Calculated refractive index values for silica glass at different wavelengths.

Wavelength (μm)	**Calculated refractive index values using Sellmeier equation for Silica**
0.2	1.5505
0.4	1.4701
0.6	1.4580
0.8	1.4533
1	1.4504
1.2	1.4481
1.4	1.4458
1.55	1.4440
1.6	1.4434
1.8	1.4409
2	1.4381
2.2	1.4350
2.4	1.4316

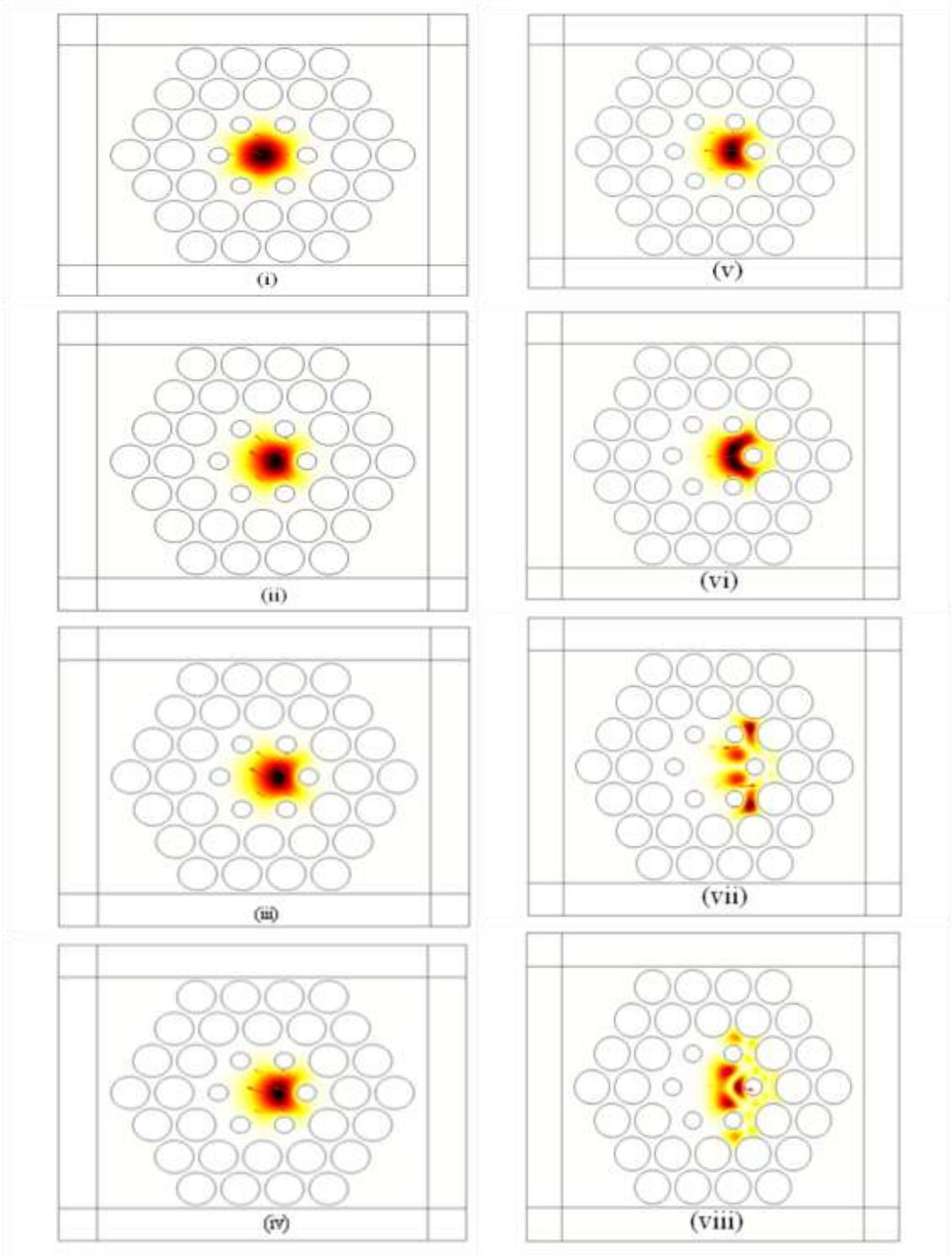

Fig. 4.3: Gradual shift of modal field (electric field intensity profile) along the direction of application of bend for (i) No Bend and for different bend radii from (ii) 30cm,(iii) 25cm, (iv) 20cm, (v) 15cm, (vi) 10cm, (vii) 5cm and (viii) 2.5cm for W-type-I PCF at wavelength 1.55 μm.

4.3.1. Effect of bend radius on bend loss

To study the effect of bend radius on bending loss of the proposed W-type PCF structures, we have calculated bend loss of the propagating mode with different bend radii at 0.633 µm, 1.33 µm, and 1.55 µm wavelengths. This bend loss characteristic of the W-type-I and W-type-II PCF structures have been illustrated in figure. 4.4 and figure 4.5 respectively. Figures 4.4 (a), 4.4 (b), and 4.4 (c) show the variation of bend loss with bend radius of W-type-I PCF for 0.633µm, 1.33µm, and 1.55µm wavelengths respectively. Figures 4.5 (a), 4.5 (b), and 4.5 (c) elucidate the variation of the bend loss with bend radius of W-type-II PCF for 0.633µm, 1.33µm, and 1.55µm wavelengths respectively.

It has been found that the W-type-I PCF is almost insensitive to macro bending. The W-type-I PCF has minimum bending loss of 0.01dB/m, 0.01dB/m and 0.07dB/m at wavelengths of 0.633µm, 1.33 µm and 1.55µm respectively for a 30 cm bend radius. Our simulated results indicate that the bending performances of the proposed PCF structures are better than that of the earlier reported structures in the Refs. [187-190].

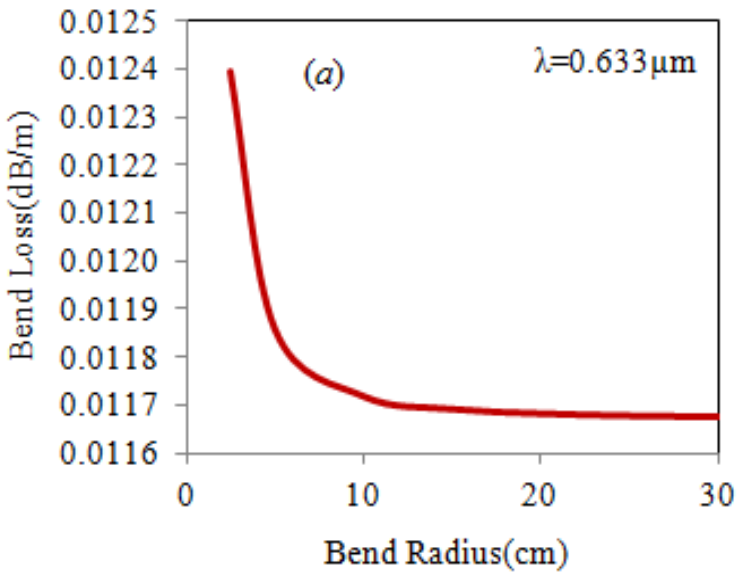

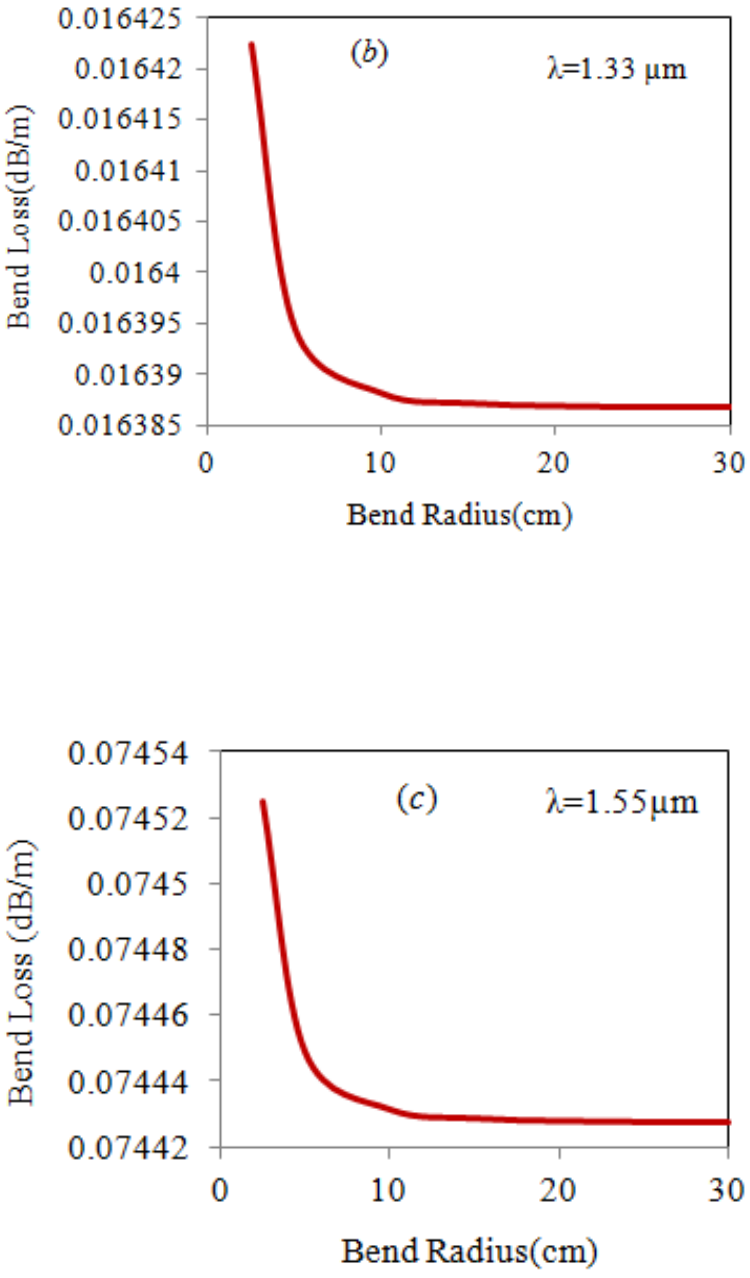

Fig.4.4: Variation of the bend loss on the bend radii at different wavelengths; (a) 0.633µm, (b) 1.33 µm, and (c) 1.55 µm for W-type-I PCF structure.

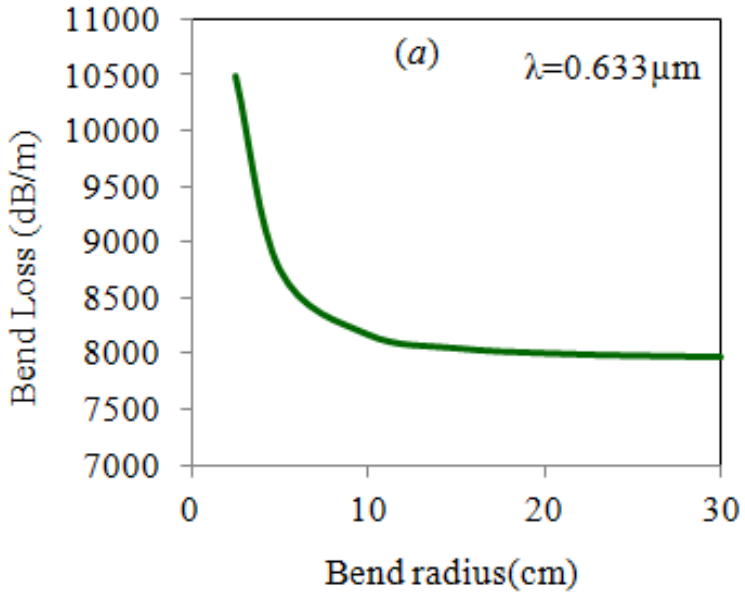
(a)
λ=0.633μm
Bend Loss (dB/m)
11000
10500
10000
9500
9000
8500
8000
7500
7000
0
10
20
30
Bend radius(cm)

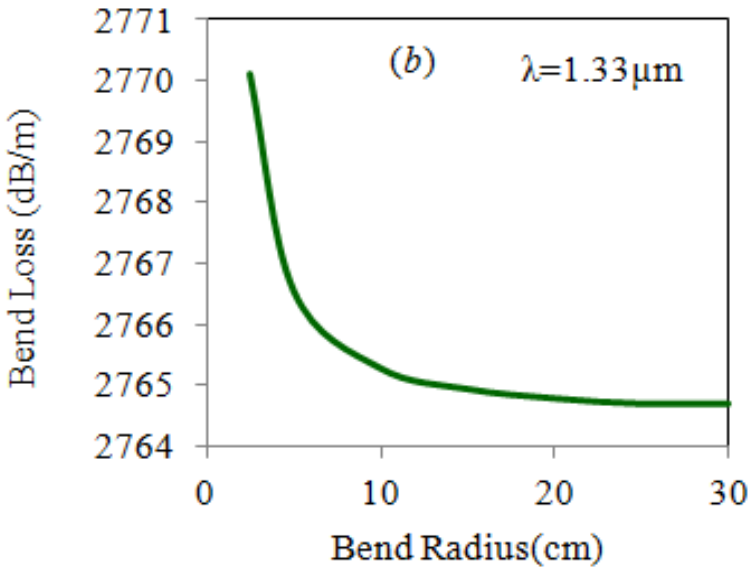
(b)
λ=1.33μm
Bend Loss (dB/m)
2771
2770
2769
2768
2767
2766
2765
2764
0
10
20
30
Bend Radius(cm)

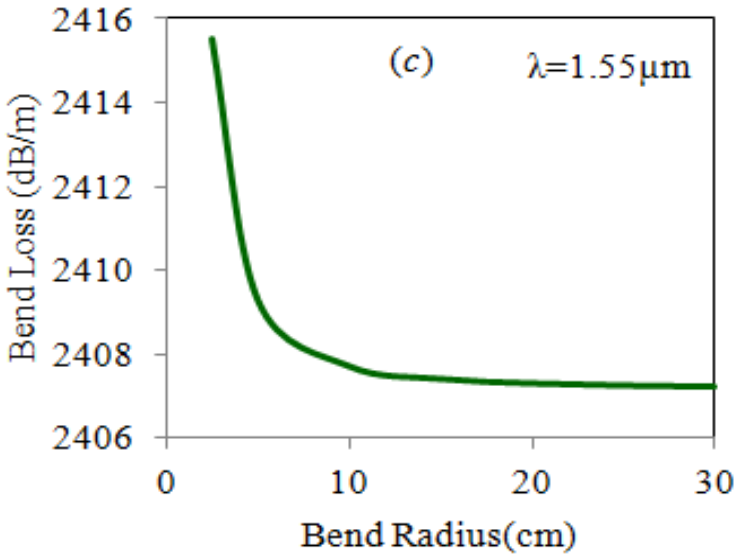

Fig.4.5: Variation of the bend loss on the bend radii at different wavelengths; (a) 0.633μm, (b) 1.33 μm, and (c) 1.55 μm for W-type-II PCF structure.

4.3.2. Effect of temperature on bend loss

The temperature dependence of the refractive index is described by the thermo-optic coefficient (dn/dT), which is a measure of the shift of the value of the refractive index with temperature [191]. To study the effect of thermo-optic coefficient on propagation characteristics of W-type-I and W-type-II PCF, a more practical temperature range of 25 ^{0}C to 200 ^{0}C has been considered. The background material, i.e. silica, used in the PCF design exhibits a highly linear, positive thermo-optic coefficient (TOC) equal to 8.3×10^{-6} / ^{0}C [73].

Based on the change of refractive index with temperature, the corresponding bend losses of the fundamental mode of the proposed PCF structures has been simulated for different temperatures. Further, bend loss calculations have been carried out for different bend radii ranging from 2.5 cm to 30 cm applied on the two proposed PCF structures at 1.55 μm wavelength for different temperatures from 25 ^{0}C to 200 ^{0}C. The variations of the bend loss with temperature for a bend radius of 30 cm at wavelength 1.55μm for both W-type-I and W-type-II PCF structures have been found lowest. Figure 4.6 (i) and 4.6 (ii) show the variation of bend loss with temperature in W-type-I PCF and W-type-II PCF that signifies that due to the positive thermo-optic coefficient (TOC) of Silica, bend loss decreases with temperature in both W-type-I and W-type-II PCF structures.

Due to increase in temperature, the refractive index contrast between cladding and core also increases and that in turn partially reconstruct back the fundamental guiding mode to the core of the fiber. At room temperature, the mode of the bent fiber is asymmetric in shape and shifts towards the outside of the bend but as the temperature increases, the guiding mode starts accumulating at the core. The thermo-optic effect overcome the bend loss at high temperature and there is partial recovery of the fundamental mode for W-type-I PCF for wavelengths 0.633μm, 1.33μm and 1.55μm and is limited for W-type-II PCF. Thus, the W-type-I PCF has the potential to be used for macro-bend sensing and due to the feature of power recovery with temperature the PCF has the ability to act as temperature-tuned device.

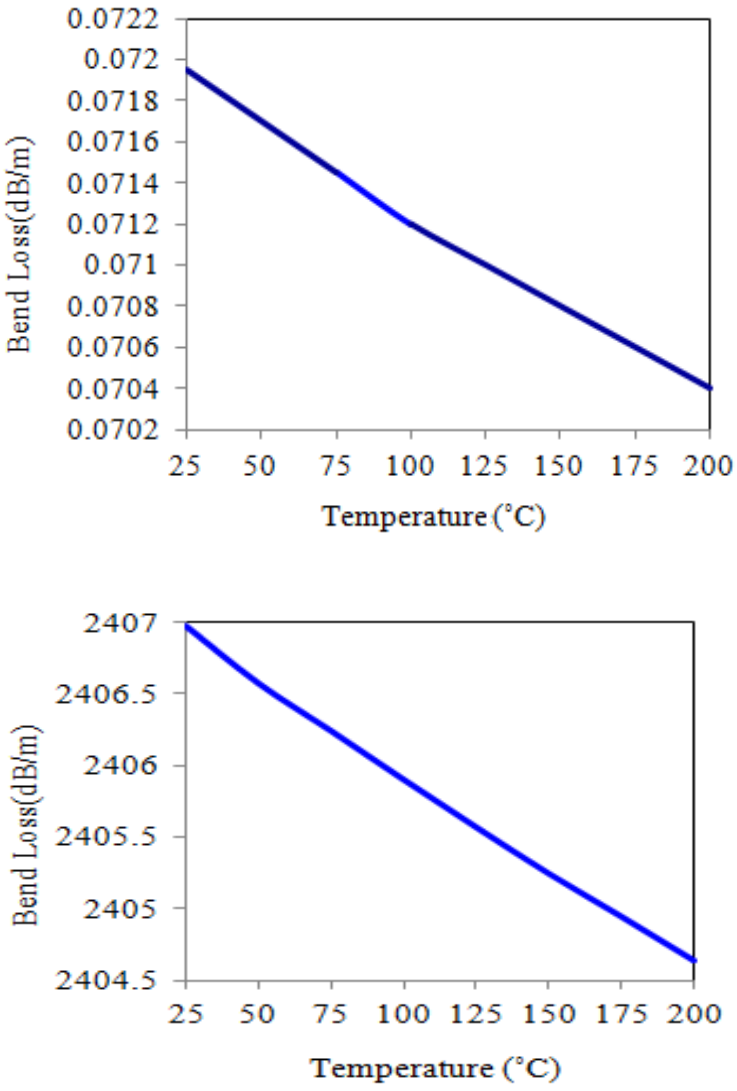

Fig. 4.6: Variation of bend loss with temperature for a bend radius of 30 cm at 1.55μm in: (i) W-type-I PCF, and (ii) W-type-II PCF.

4.4. Nonlinearity study of the PCF designs

The nonlinearity of the proposed PCF designs can be measured by calculating the nonlinear coefficient [192]. A high nonlinearity value of PCF implies ability to confine high-intensity light. Figure 4.7 represents the variation of the nonlinear coefficient as a function of wavelength for the two proposed W-type-I and W-type-II PCF designs that shows the exponential decrease of nonlinear coefficient with the increase of wavelength for a wavelength ranging from 0.4μm to 2.4 μm. The W-type-I PCF has nonlinear coefficient value of $\gamma(\lambda) = 29\ W^{-1}Km^{-1}$, $10W^{-1}Km^{-1}$, and $8W^{-1}Km^{-1}$at a wavelength of 0.633μm,1.33 μm and 1.55μm respectively. On the other hand, the W-type-II PCF has nonlinear coefficient value of $\gamma(\lambda) = 49W^{-1}Km^{-1}$, $16W^{-1}Km^{-1}$, and $14\ W^{-1}Km^{-1}$at a wavelength of 0.633μm, 1.33μm, and 1.55μm respectively. So, the proposed W-type PCF structures can also be applicable for nonlinear applications such as supercontinuum generation in visible and near infrared region.

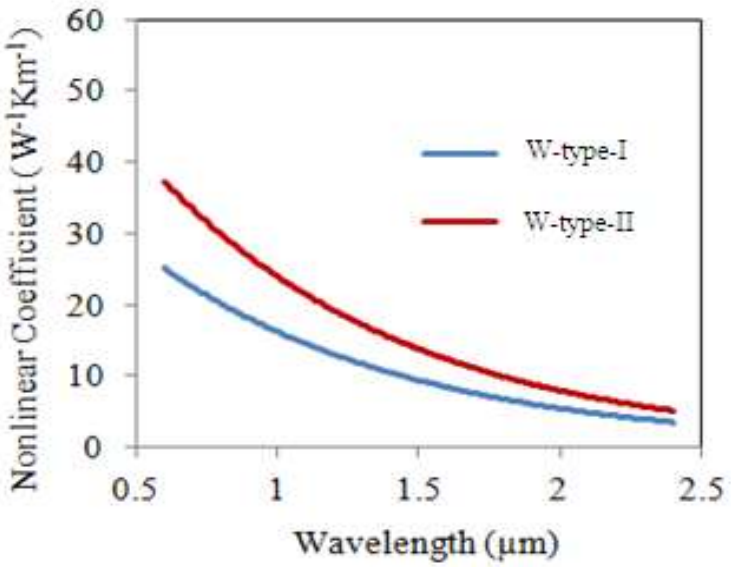

Fig. 4.7: Variation of the nonlinear coefficient with wavelength for W-type-I and W-type-II PCF structures.

4.5. Conclusion

The temperature dependant bending loss characteristics of two solid-core W-type photonic crystal fiber structures have been computed by employing commercially available software 'COMSOL Multiphysics' based on full vectorial finite element

method. Bending performance of the proposed PCF structures have been reported. The bending loss characteristics of W-type-I photonic crystal fiber structure have been found better than that of the W-type-II photonic crystal fiber structure. It has been found that the W-type-I PCF structure offers bend losses of 0.01dB/m, 0.018 dB/m, and 0.07 dB/m at 0.633μm; 1.33μm; and 1.55μm wavelengths respectively for a 30cm bend radius.

The effect of temperature on bend loss of the proposed structures has been studied and it has been found that the proposed PCF structures are sensitive to temperature variations when applied for a temperature range from 25˚C to 200˚C. The proposed structures can be utilized in both telecommunication and macro-bend sensing. Least change in bending loss data observed for the proposed PCF design for macro-bending imply that the structure is macro-bend insensitive and that makes them suitable candidates for fiber to the home applications. Moreover, the proposed photonic crystal fiber structures shows significant nonlinearity and hence can be used in nonlinear applications such as visible to near infrared supercontinum generation as well.

Chapter-V

Design and analyses of cladding doped large mode area W-type photonic crystal fiber for high power delivery devices and sensing applications

CHAPTER-V

DESIGN AND ANALYSIS OF CLADDING DOPED LARGE MODE AREA W-TYPE PHOTONIC CRYSTAL FIBER FOR TELECOM AND SENSING APPLICATIONS

5.1. Introduction

In previous chapters we have discussed about conventional photonic crystal fiber (PCF) and W-type photonic crystal fiber (W-type PCF). A conventional photonic crystal fiber (PCF) is made up of wave guiding parts with a solid core and cladding layers consisting of spatially periodic air holes [65]. The presence of these air holes in the cladding reduces the effective refractive index of the cladding region relative to the core. On the other hand, in W-type PCF design, the effective index of the cladding region is reduced by varying the diameter of the air holes of different layers to different extent thereby producing a W-type index profile [77,180,181] and hence named W-type PCF. The design of large mode area (LMA) [193,194] PCF based on selective material-filling technique [195,207] is a new kind of technique to obtain LMA PCF structures. *Ademgil* et al. proposed endlessly single-mode photonic crystal fiber with improved effective mode area based on introducing higher index material in the cladding region and the ideal overall performance is achieved by adjusting the doping level [133].

In the proposed PCF, the central core is un-doped silica while the second cladding layer of rings have been doped with different concentration of fluorine to drop the refractive index of doped silica [196] rods to below 1.45. This design of PCF structure simultaneously gives large-mode-area with low bending loss. Numerical calculations have been carried out on the proposed PCF design to calculate parameters like confinement loss, bend loss, birefringence, sensitivity, effective mode-area and nonlinear coefficient. The confinement and guiding of light in this PCF with relatively high core index occur via total internal reflection and the single-mode propagation is dependent on the ratio between the core radius and wavelength.

To calculate bend loss, bends of different radii have been applied on the proposed PCF designs. In bent fibers, the field profile deforms outwards in the direction of the bend. In order to simulate the effects of bending, the bent PCF is transformed into a straight PCF with an equivalent refractive index [184,187, 197-200] defined in Eq. 1.30. A rectangular perfectly matched layer (PML) has been introduced at the surface of the W-type PCF to imitate the effect of an infinite domain in the finite element method. With the introduction of the PML the propagation constant of modes of the proposed PCF structure becomes complex [201]. The confinement loss of the guided mode of the PCF can be calculated by using the complex effective index of the proposed PCF designs without the application of bend using equation 1.29. The bending loss [132] of the guided mode has been calculated by using the imaginary part of propagation constant or complex effective index of the bent fiber with the equivalent refractive index obtained using Eq. 1.30.

Birefringence [202] (B) that exists in such asymmetric PCF structures has been calculated using Eq. 1.32.

$$B = \left| n_{eff}(x) - n_{eff}(y) \right| \tag{1.32}$$

where, n_{eff} (x) and n_{eff} (y) are the x and y components of the effective index of the guided mode of the proposed PCF structures.

The sensitivity of the proposed PCF structures can be measured by calculating relative sensitivity co-efficient [203-205] given by Eq. 1.33.

$$r = \frac{n_s}{n_e} f \tag{1.33}$$

where, n_s is the refractive index of the absorbing material (i.e. fluorine in our case) and n_e is the real part of the effective refractive index of the guided mode in the core, f is the percentage of energy present in the holes. According to Poynting's theorem, the percentage of energy present in the holes [203-205] can be expressed as in Eq. 1.34.

$$f = \frac{(sample)\left(\int Real(E_x H_y - E_y H_x)\right) dxdy}{(total)\left(\int Real(E_x H_y - E_y H_x)\right) dxdy} X\ 100 \tag{1.34}$$

The effective mode area [194,132] which is essential feature to suppress the nonlinear effects in the proposed PCF design has been calculated by using the Eq. 1.27. The nonlinearity of the proposed PCF designs can be measured by calculating the nonlinear coefficient [192,206] by utilizing Eq. 1.28 and considering value of the non-linear refractive index of silica as n_2 ($\approx 2.5 \times 10^{-20}$ m^2 W^{-1}).

5.2. Design of cladding doped large mode area W-type PCF

The proposed W-type PCF structures have been created by making the air hole diameter of the first central ring different from the air hole diameter of the outer rings. Due to which, it behaves like two index layers and the structure will have the cladding of W-type refractive index profile. The resulting fiber will be like doubly clad fiber, with refractive index n_2 and n_3 in the cladding. Two types of W-type PCF structures have been designed. In W-type-I PCF the diameter of the rings of first layer is kept at minimum compared to last layers. Whereas, in W-type-II PCF the diameter of the rings of first layer is kept at maximum compared to last layers. The second layer of rings of the proposed W-type PCF has been created with silica rods doped with different concentration of fluorine to vary the refractive index of doped silica rods. The full vectorial finite element method (FEM) has been applied to calculate the effective index of the proposed structure of PCF introducing perfectly matched layers (PML).

5.2.1. Design of W-type -I PCF

A hexagonal lattice solid defect-core W-type-I PCF has been designed having the following parameters: the background material refractive index, n = 1.45, air hole periodicity, Λ = 40μm, width period, (d/Λ) = 0.43μm, perfectly matched layer (PML) width = 35μm and diameter of first ring of air holes d_1= 8.75μm, keeping equal the diameter of second and third ring of air holes, d_2=d_3=17.5μm.

5.2.2. Design of W-type -II PCF

A hexagonal lattice solid defect-core W-type-II PCF has been designed by increasing the width of the rings of first layer to twice of that of the rings of the other layers and keeping the background material refractive index, n = 1.45, air hole periodic, Λ =

40μm, width period, (d/Λ) = 0.43μm, perfectly matched layer (PML) width = 35μm and diameter of first ring of air holes d_1= 17.5μm, keeping equal the diameter of second and third ring of air holes, d_2=d_3=8.75μm.

Further, the second layer of rings of both the proposed W-type-I PCF and W-type-II PCF have been created with silica rods doped with fluorine with different concentration such that the refractive index of fluorine doped silica rods varies from 1.434 to 1.448.

The transverse cross-sectional view of proposed photonic crystal fiber designs are shown in figures 5.1(a) and 5.1 (b) respectively, in which, the triangular array of air holes is drawn in the silica. The diameter of air hole in the cladding is taken as d. The hole to hole distance also called pitch is Λ. The central air hole has been removed to create the defect in the photonic crystal geometry. The rings highlighted in brick red color are the fluorine doped silica rods.

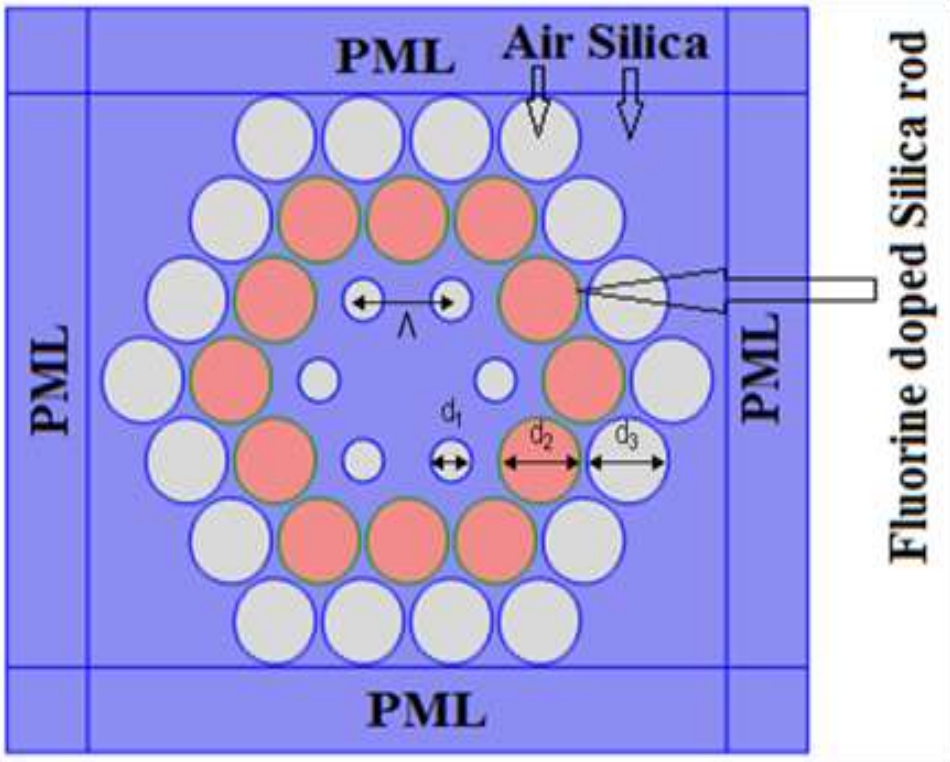

(a)

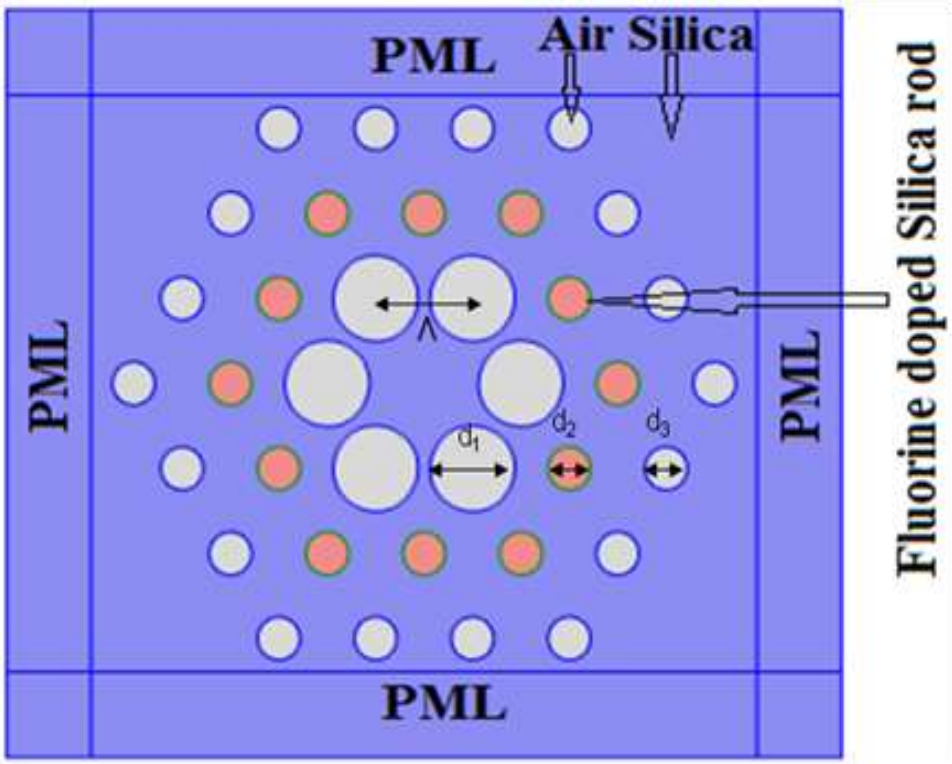

(b)

Fig. 5.1: Transverse cross-sectional view of fluorine doped large mode area (a) W-type-I PCF and (b)W-type-II PCF.

5.3. Numerical Results and Analysis

5.3.1. Confinement loss and effective index calculation

The confinement loss arises due to the leakage of power between and through the holes of PCF. The PCF being a leaky structure has complex effective indices of the modes. The confinement loss can be extracted from the imaginary part of effective index of the guided mode of the proposed PCF structures by using the equation 1.29. First, the confinement loss of the guided mode has been calculated for PCF structure with same size of holes in the cladding and the results has been plotted in figure 5.2(a). Figure 5.2(a) shows gradual decrease in confinement loss for increase in d/Λ value for undoped PCF with same size of air holes in the cladding. The lowest values of confinement loss for this symmetric PCF with same size of air holes in the cladding for d/Λ equal to 0.43 at 1.55μm recorded as 2.24 X 10^{-13} dB/m. Further, the

confinement loss of the guided mode has been calculated for both W-type-I and W-type-II PCF structures without doping the cladding and doping with different concentration of fluorine in the second layer of rings of the cladding such that the refractive index of fluorine doped silica rods varies from 1.434 to 1.448.

The confinement loss as a function of d/Λ graph has been plotted in figure 5.2(b) and 5.2(c) for undoped W-type-I and W-type-II PCF structures. Figures 5.2(b) and 5.2(c) show gradual decrease in confinement loss for increase in d/Λ value for undoped W-type-I PCF and W-type-II PCF structures.

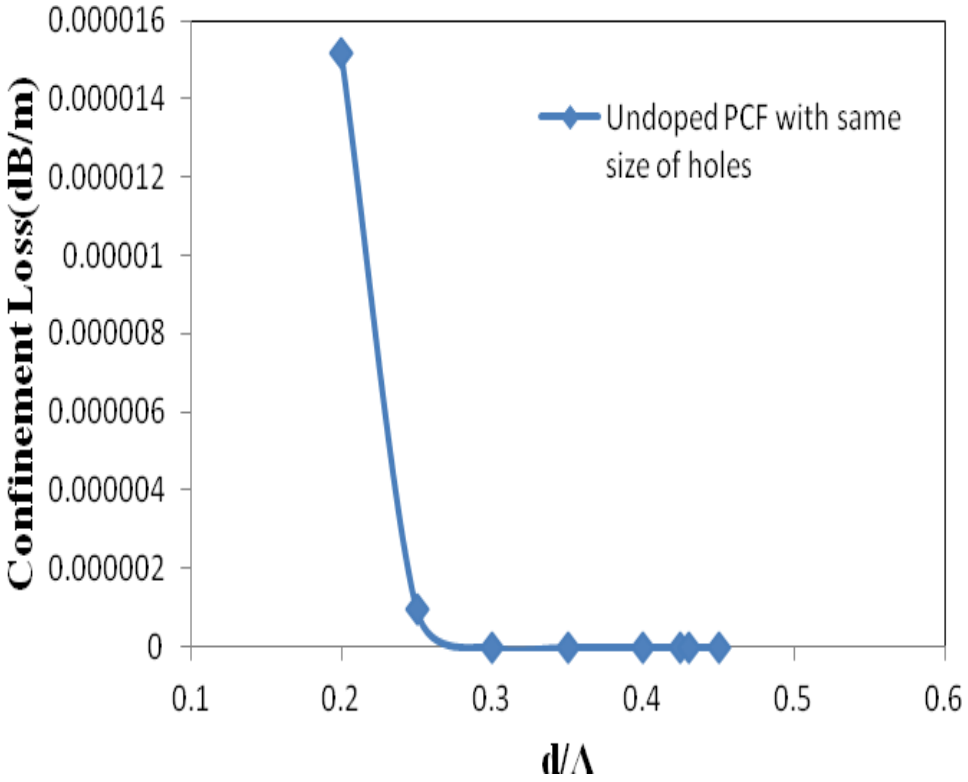

(a)

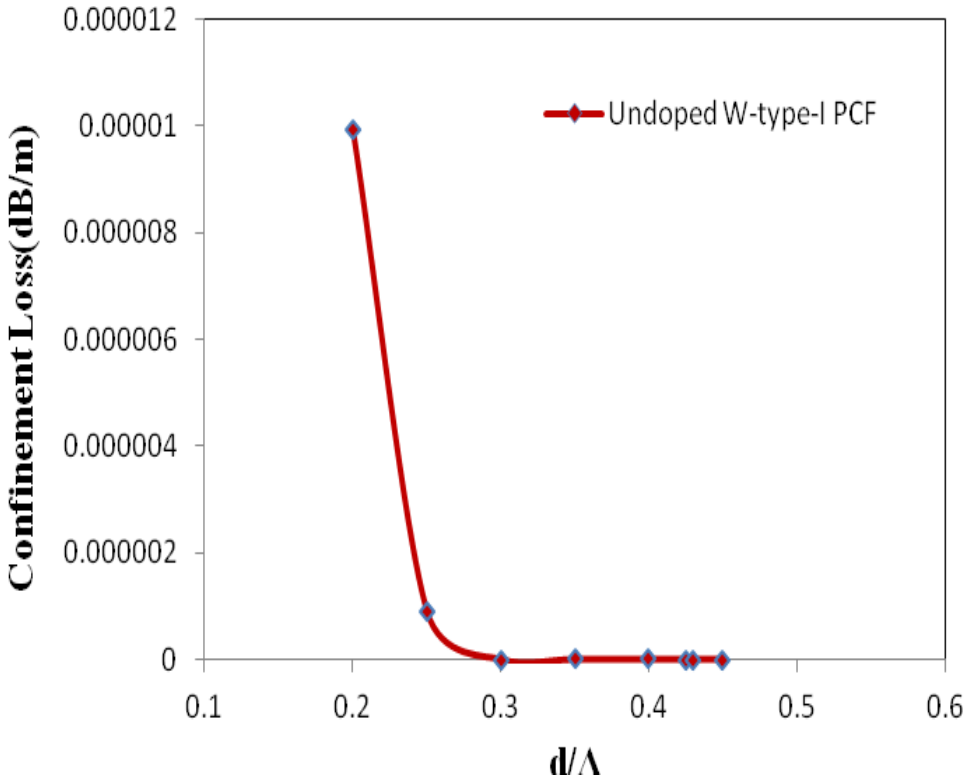

(b)

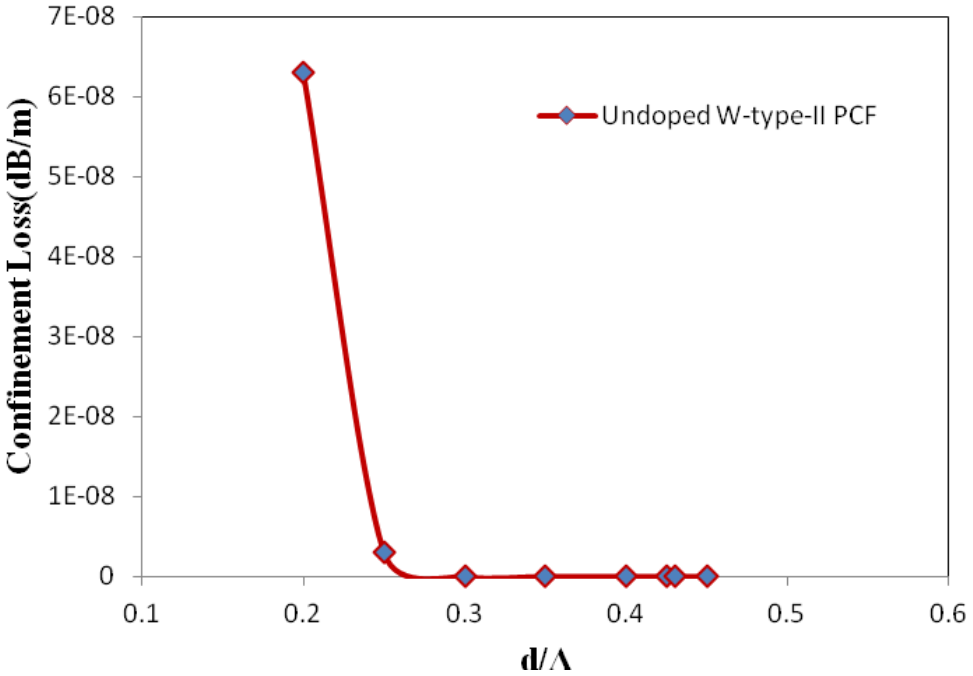

(c)

Fig.5.2: Confinement loss as a function of d/Λ in: (a) Undoped PCF with same size of holes, (b)Undoped W-type-I PCF and (c) Undoped W-type-II PCF.

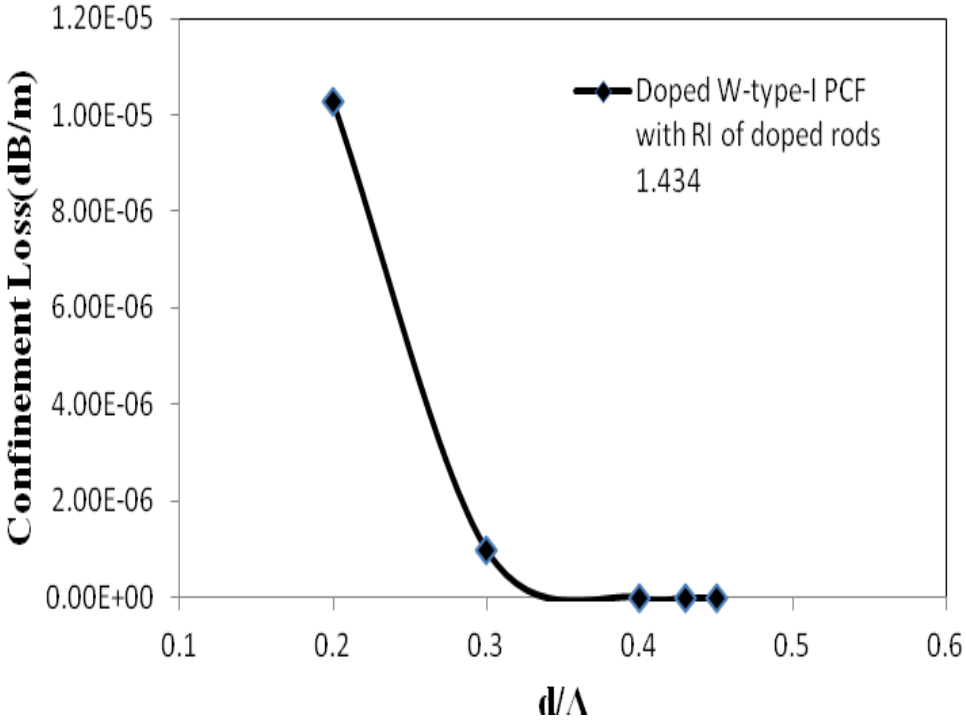

(a)

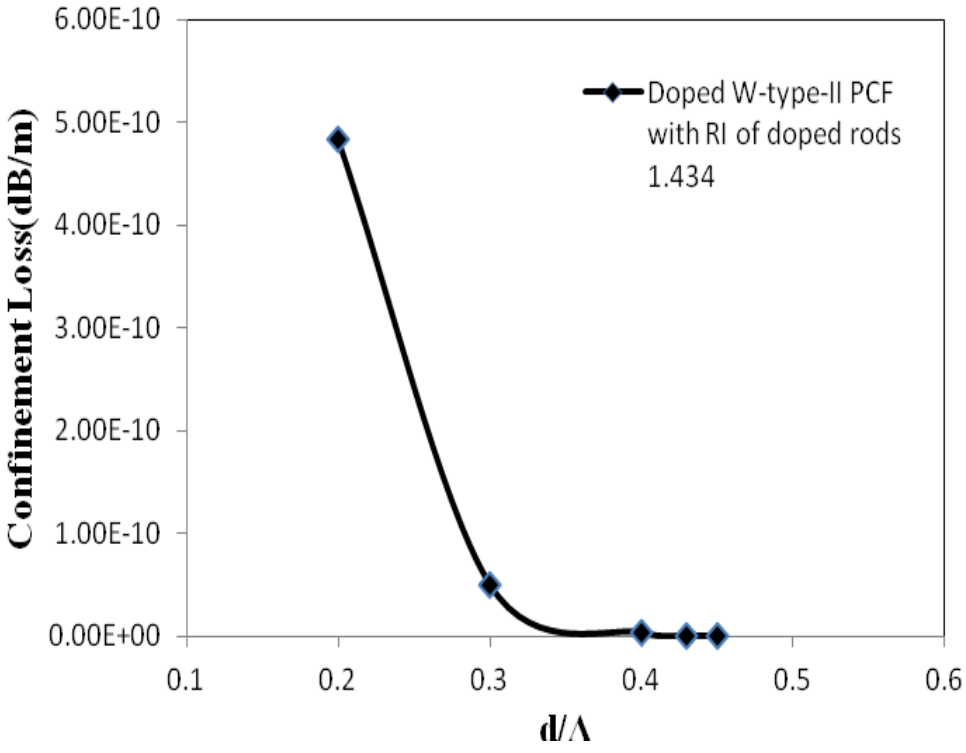

(b)

Fig.5.3: Confinement loss as a function of d/Λ in: (a) Doped W-type-I PCF and (b) Doped W-type-II PCF when refractive index of doped rods 1.434.

The confinement loss for undoped W-type-II PCF structure has been found to be less as compared to undoped PCF structure with same size of holes in the cladding and undoped W-type-I PCF structures. The lowest values of confinement loss for undoped W-type-I and W-type-II PCF structures at 1.55μm recorded as 1.16 X 10^{-10} dB/m, and 1.24 X 10^{-13} dB/m respectively. The increase in the cladding asymmetry in W-type PCF in turn increases the effective index of cladding. This further increases the effective index contrast between the core and cladding and decreases the confinement loss.

In addition to this, the confinement loss of the W-type-I and II PCF structures with doped cladding has been calculated and the results have been plotted in figures 5.3(a) and 5.3(b) for doped cladding rod refractive index 1.434.

The confinement loss decreases as we increase the d/Λ value for both the doped PCF structures. It has been found that the confinement loss in doped W-type-II PCF is less as compared to doped W-type-I PCF. The lowest values of confinement loss for doped W-type-I PCF at 1.55μm recorded as 9.24 X 10^{-15} dB/m when the refractive index of the doped rods 1.434 whereas the lowest values of confinement loss for doped W-type-II PCF at 1.55μm recorded as 1.64 X 10^{-15} dB/m when the refractive index of the doped rods 1.434 respectively. The increase in the doping level decreases the refractive index of the doped rods and that in turn reduces the effective index. This further reduces the effective index contrast between the core and cladding and increases the confinement loss.

Further, we calculate the effective index (n-eff) of fundamental polarization mode of the proposed PCF structures by using finite element method (FEM). Variation of effective index of guided mode with wavelength in the proposed W-type-I PCF and W-type-II PCF has been shown in figure 5.4. The variation of effective index of guided mode shows a sharp decrease with wavelength depicts that the effective refractive index of the cladding region relative to the core is reduced due to the presence of the air holes in the higher wavelength range and effective index shows a strong wavelength dependency which is a measure of dispersion.

From figure 5.4 it has been found that W-type-II PCF is more dispersive compared to its counterpart W-type-II PCF.

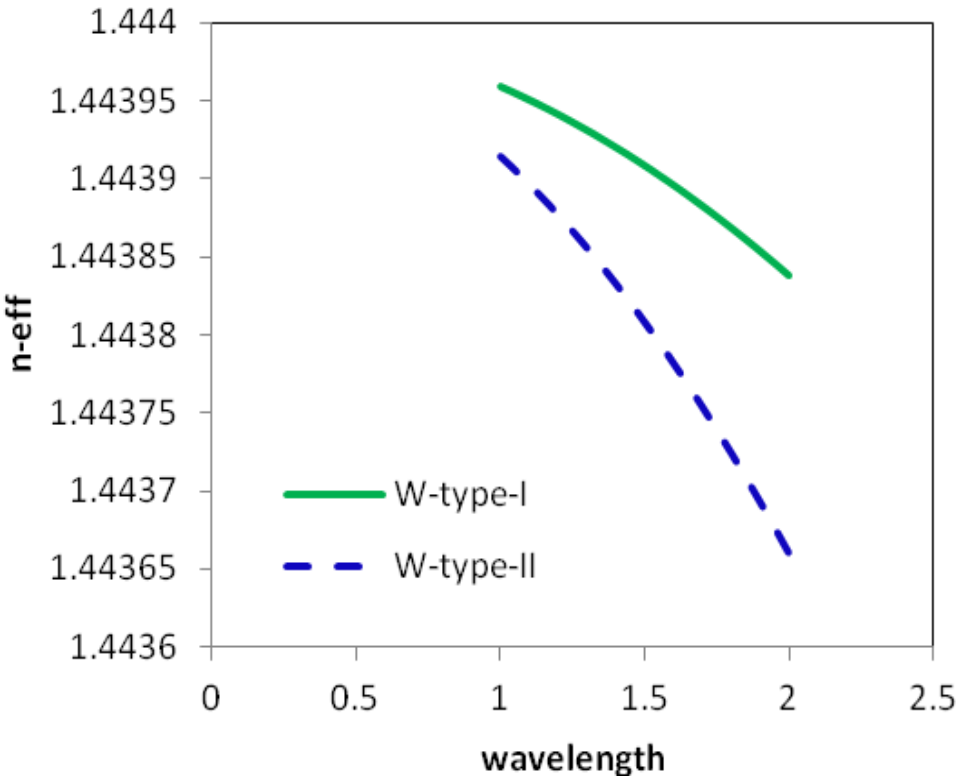

Fig.5.4: Variation of effective index (n-eff) of guided mode with wavelength in the proposed W-type-I PCF and W-type-II PCF.

5.3.2. Bend loss calculation

First, the bend loss of both the W-type-I and W-type-II PCF structures with d/Λ value equal to 0.43, without doping the cladding have been calculated for macro bending radii ranging from 2.5cm to 30cm at operating wavelength 1.55μm and applied in a circular loop with a single-turn of PCF and arbitrary angular orientation. Due to application of bend mode leaking across the PCF is observed which is the cause of bend loss and due to which the modal field in the core region shifts towards the bend. The bend loss is high and reaches it's maximum at small bending radius. Bend loss in undoped W-type-I PCF is less as compared to undoped W-type-II PCF as shown in the figures 5.5(a) and 5.6(a). For W-type-I and W-type-II undoped PCF structures

minimum bending loss values of 7.15 X 10^{-13}dB/m and 2.93 X 10^{-7}dB/m have been obtained for a 30cm bend radius.

To examine the effect of doping on bend loss of the PCF structures, the doping concentration of fluorine in the second layer of rings in the cladding of the proposed PCF structures varied such that the refractive index of fluorine doped silica rods varies from 1.434 to 1.448 at operating wavelength 1.55μm. Bends of different macro bending radii ranging from 2.5cm to 30cm have been applied on these proposed PCF structures. Figures 5.5(b), 5.5(c) and 5.5(d) and 5.6(b), 5.6(c) and 5.6(d) show the variation of bend loss with bend radius of the W-type-I PCF and W-type-II PCF for refractive index of the doped rods 1.434, 1.440 and 1.448 respectively. The bend loss of both the proposed W-type-I and W-type-II PCF structures increases as we increase the refractive index of the doped rods from 1.434 to 1.448 or decrease the doping level in the doped cladding rods. For W-type-I PCF, the minimum bending loss values of 1.35 X 10^{-12}dB/m, 3.89 X 10^{-10}dB/m and 6.68 X 10^{-9}dB/m and for W-type-II PCF, the minimum bending loss values of 1.83 X 10^{-10}dB/m, 1.28 X 10^{-10}dB/m and 6. X 10^{-9}dB/m have been obtained for a 30cm bend radius for refractive index of the doped rods 1.434, 1.440 and 1.448 respectively.

The low bending sensitivity for W-type-II PCF compared to the W-type-I PCF particularly at large bend radii can be clearly seen from these figures. The bend loss decreases as the doping level increases in the second layer of rings in the cladding of the proposed PCF structures. The increase in the doping level decreases the refractive index of the doped rods and that in turn increases the effective index contrast of core and cladding resulting in more confinement of guided mode and that in turn results in less bend loss. Thus, the proposed W-type PCF structures are found to be insensitive to macro bending. The results found are better compared to published results [147,185, 187, 207].

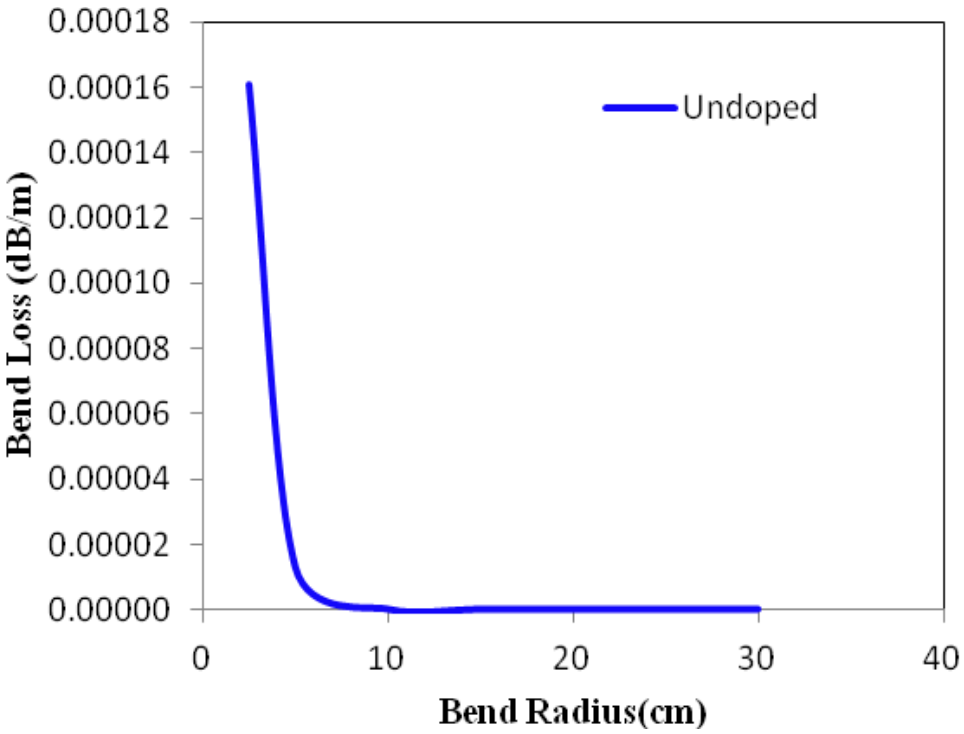
0.00018
0.00016
0.00014
0.00012
0.00010
0.00008
0.00006
0.00004
0.00002
0.00000
Bend Loss (dB/m)
Undoped
0
10
20
30
40
Bend Radius(cm)

(a)

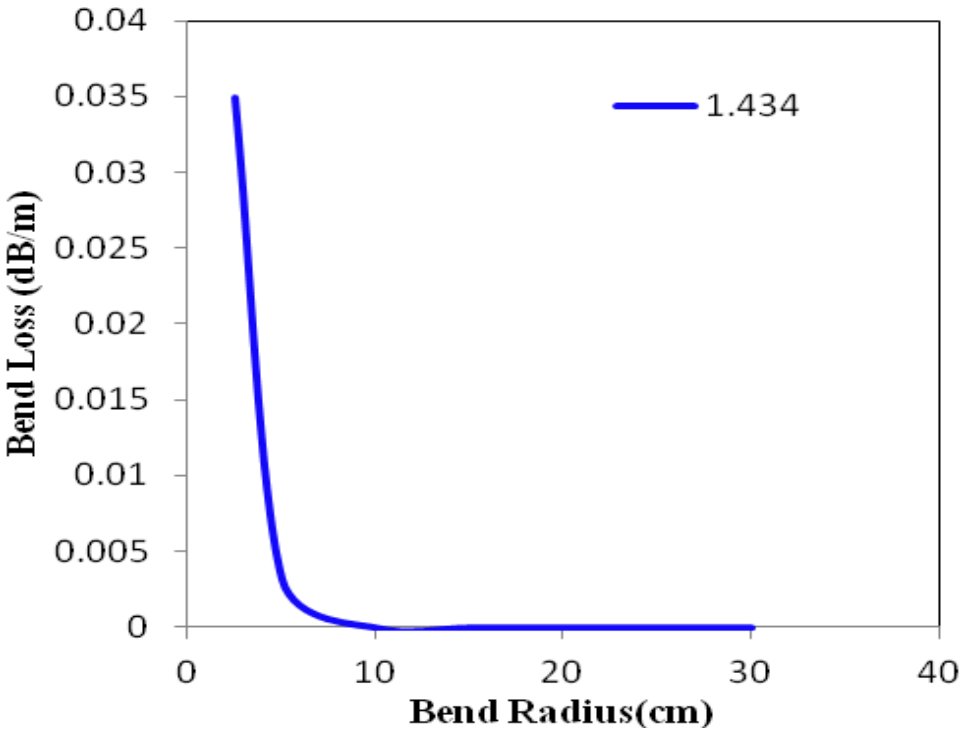
0.04
0.035
0.03
0.025
0.02
0.015
0.01
0.005
0
Bend Loss (dB/m)
1.434
0
10
20
30
40
Bend Radius(cm)

(b)

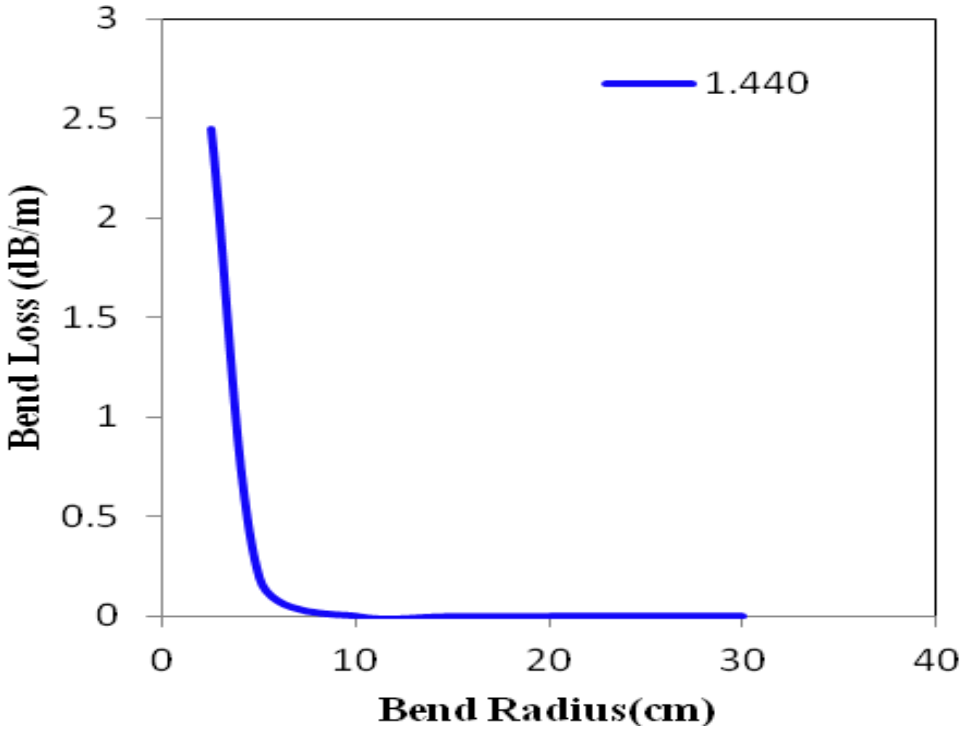

(c)

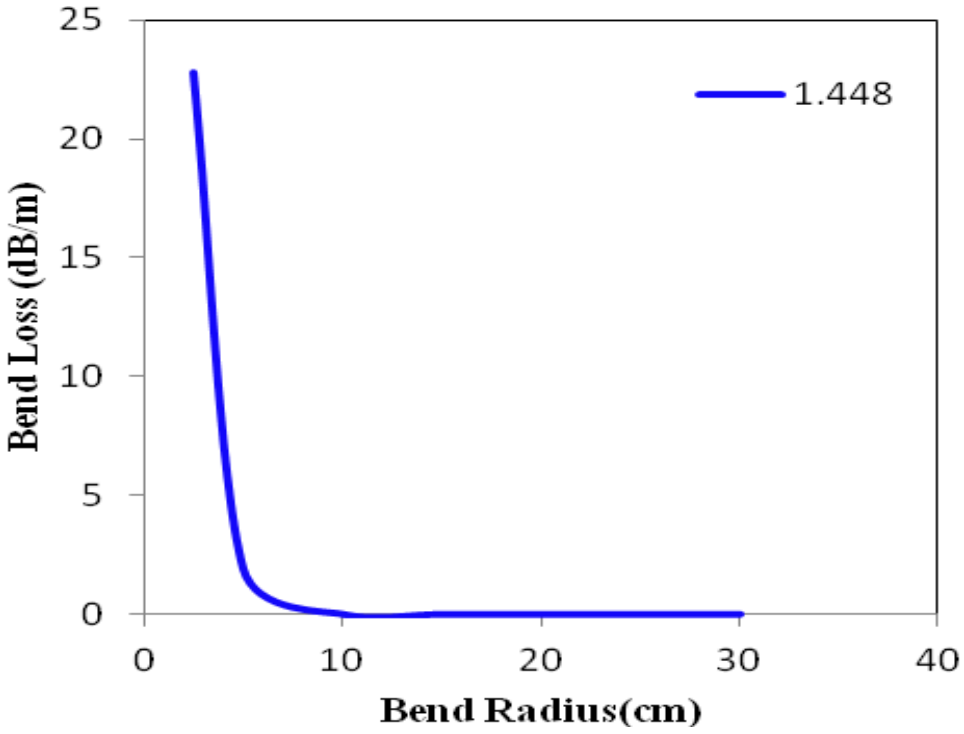

(d)

Fig. 5.5: Bend loss as a function of bend radius for: (a) Undoped W-type-I PCF, (b) Doped W-type-I PCF with RI of rods 1.434, (c) Doped W-type-I PCF with RI of rods 1.440, (d) Doped W-type-I PCF with RI of rods 1.448.

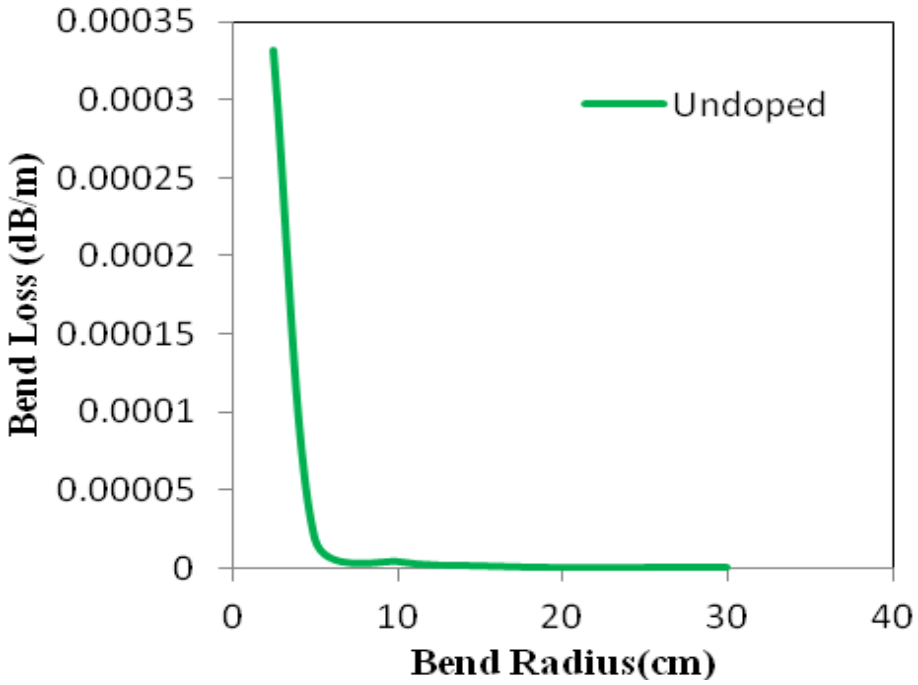
0.00035
0.0003
0.00025
0.0002
0.00015
0.0001
0.00005
0
Bend Loss (dB/m)
Undoped
0
10
20
30
40
Bend Radius(cm)

(a)

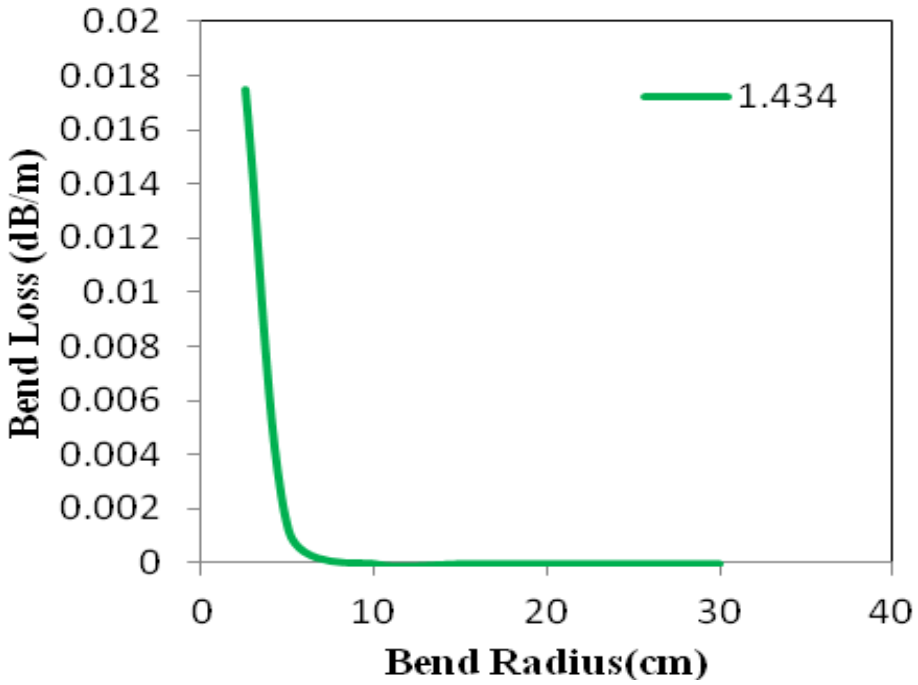
0.02
0.018
0.016
0.014
0.012
0.01
0.008
0.006
0.004
0.002
0
Bend Loss (dB/m)
1.434
0
10
20
30
40
Bend Radius(cm)

(b)

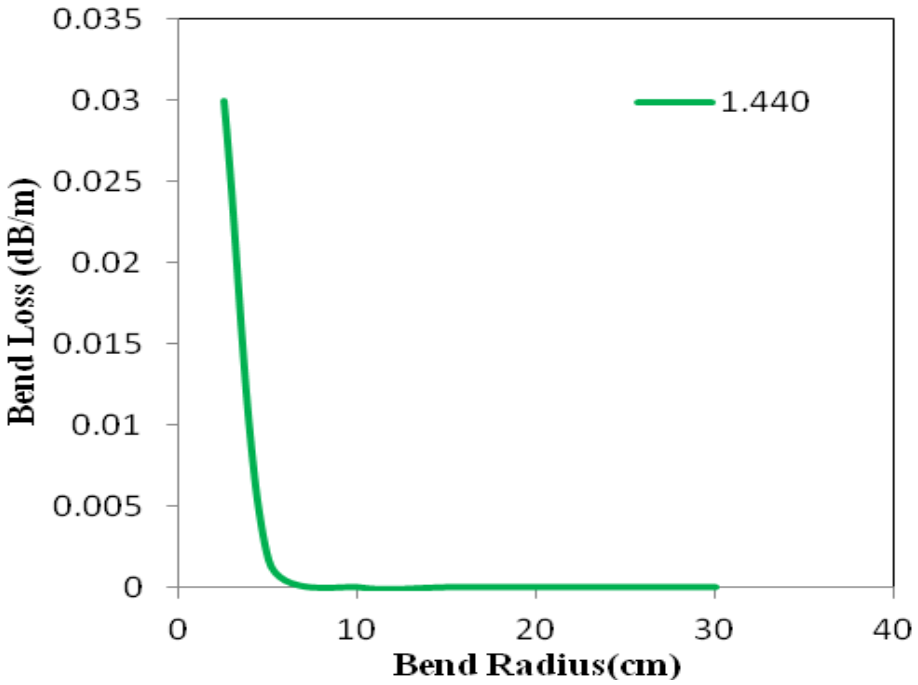

(c)

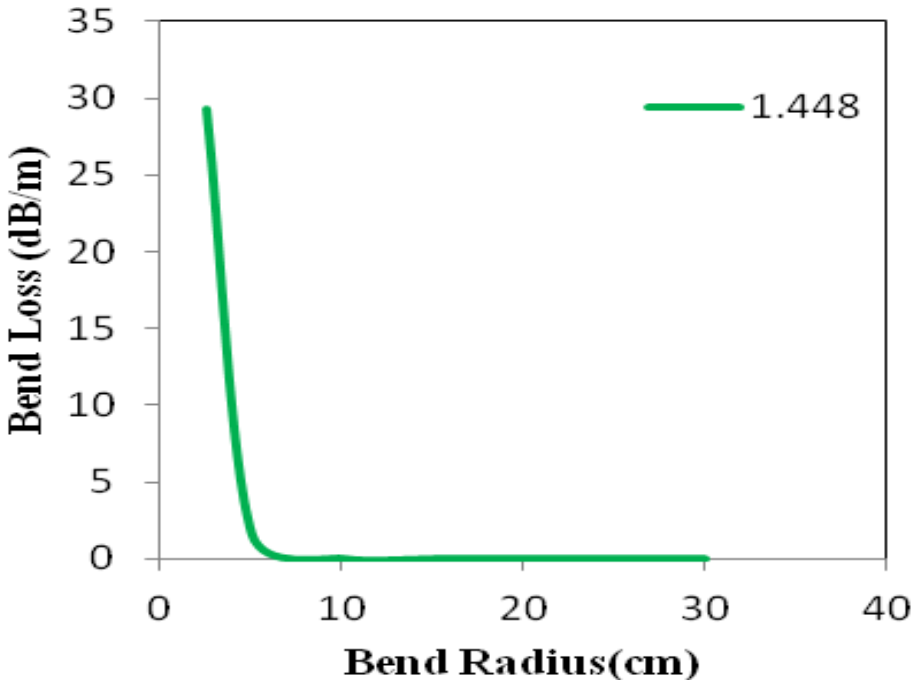

(d)

Fig. 5.6: Bend loss as a function of bend radius for: (a) Undoped W-type-II PCF, (b) Doped W-type-II PCF with RI of rods 1.434,(c) Doped W-type-II PCF with RI of rods 1.440, (d) Doped W-type-II PCF with RI of rods 1.448.

5.3.3. Birefringence and relative sensitivity calculation

The birefringence of the proposed PCF structures for a wavelength range of 0.6μm to 2μm have been calculated changing the doping concentration of fluorine in the second layer of fluorine doped rods in the cladding such that the refractive index of fluorine doped silica rods varies from 1.434 to 1.448. Figure 5.7(a), 5.7(b) shows the variation of the birefringence with wavelength for a wavelength range of 0.6μm to 2μm.

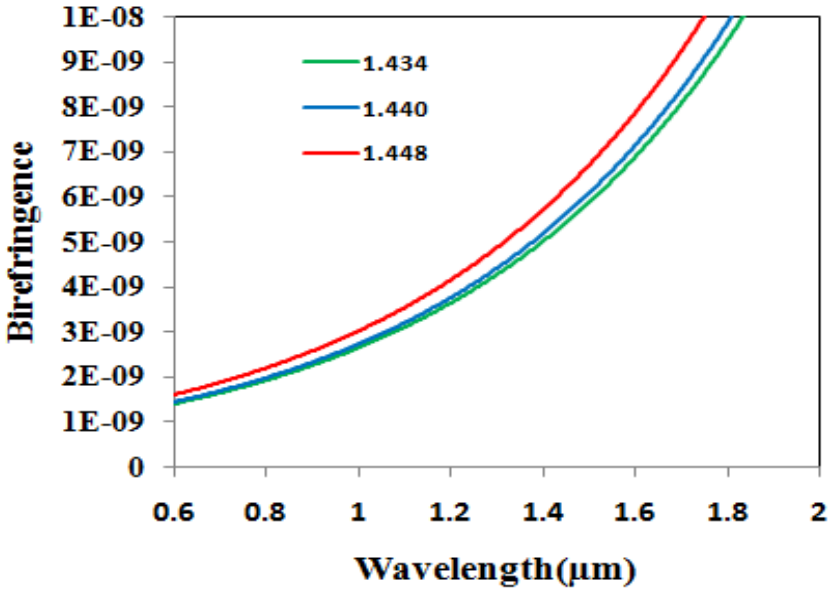

(a)

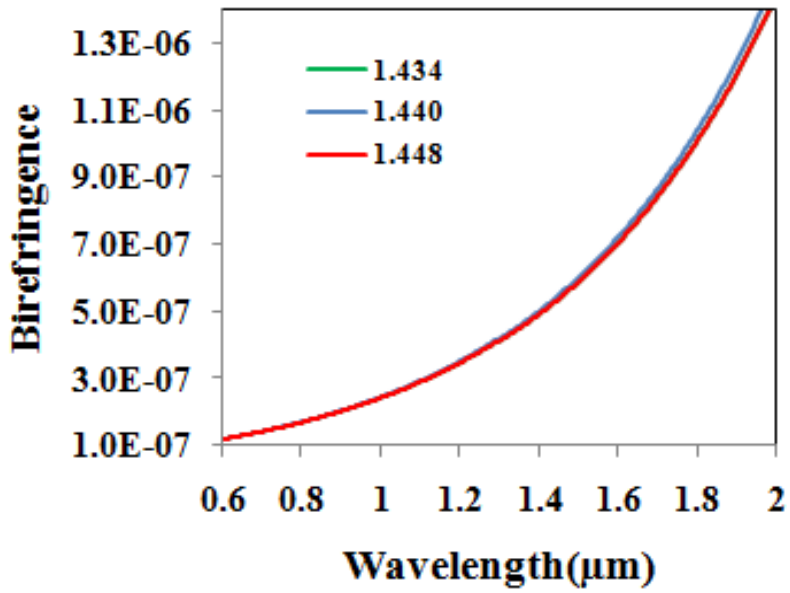

(b)

Fig.5.7: Birefringence as a function of wavelength in: (a) W-type-I PCF and (b) W-type-II PCF.

Figure 5.7(a) shows that birefringence of the proposed W-type-I PCF structure for a wavelength range increases as we increase the refractive index of the doped rods or decrease the doping concentration of fluorine. Figure 5.7(b) shows that birefringence of the proposed W-type-II PCF structure increases for a wavelength range. The maximum birefringence for W-type-I PCF and W-type-II PCF found to be equal to 7.82 X 10^{-8} and 6.91 X 10^{-7} for refractive index of doped rods equal to 1.448 at 1.55μm. Figures 5.8(a) and 5.8(b) show the variation of the relative sensitivity with wavelength for a wavelength range of 0.6μm to 2μm.

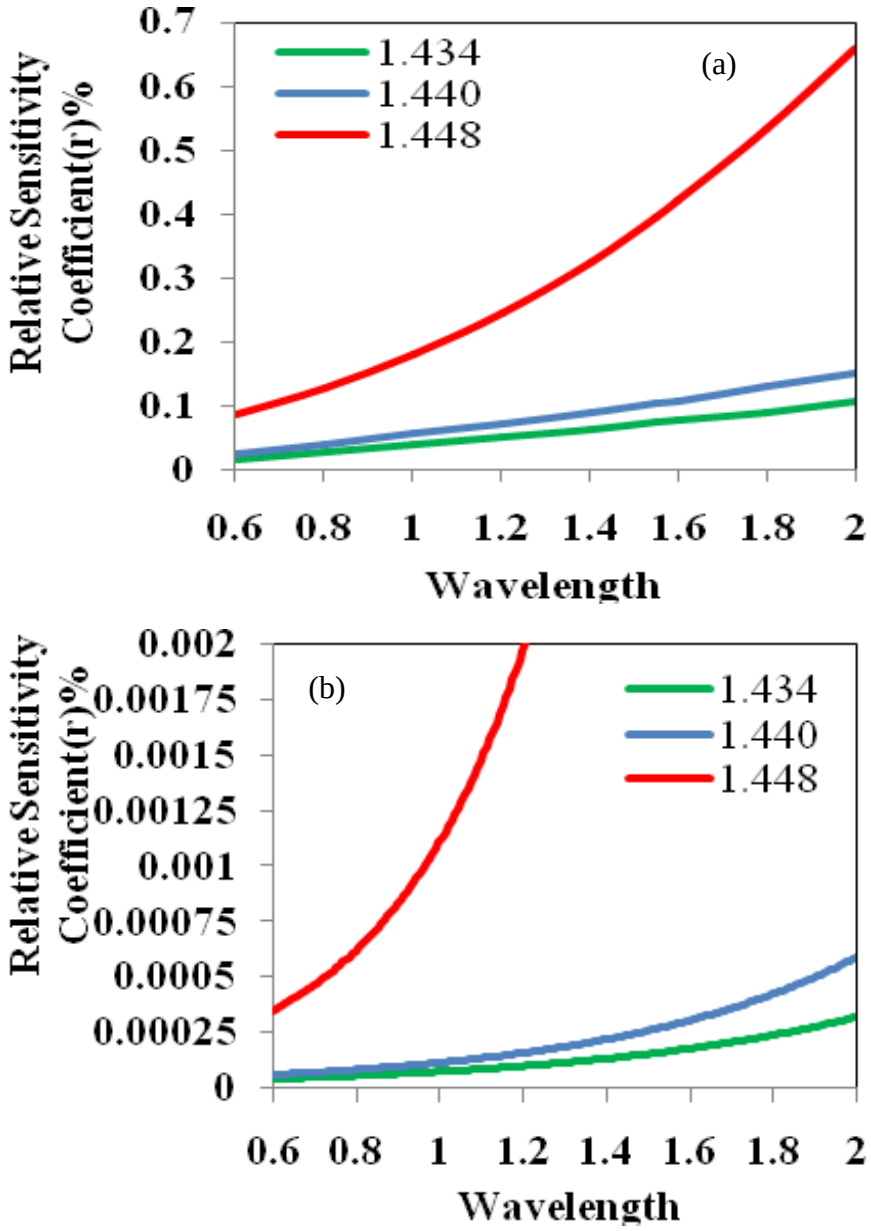

Fig.5.8: Relative sensitivity as a function of wavelength in: (a) W-type-I PCF and (b) W-type-II PCF.

Figure 5.8(a) and 5.8(b) shows that relative sensitivity of the proposed W-type-I PCF structure for a wavelength range increases as we increase the refractive index of the doped rods or decrease the doping concentration of fluorine in the doped rod. The W-type-I PCF is found to be more sensitive compared to W-type-II PCF. The maximum relative sensitivity coefficient values for W-type-I PCF found to be 0.396 for operating wavelength 1.55μm with refractive index of doped rods 1.448. Similarly, the maximum relative sensitivity coefficient values for W-type-II PCF found to be 0.015 for operating wavelength 1.55μm with refractive index of doped rods 1.448.

The W-type-I PCF is found to be more birefringent and sensitive and can be a good candidate for applications in sensing [133, 204].

5.3.4. Effective mode area and non linearity study

The effective mode area (A_{eff}) and nonlinearity of the proposed PCF designs have been calculated. Figure 5.9 and 5.10 represents the effective mode area and the nonlinear coefficient as a function of wavelength graphs of the two proposed W-type-I and W-type-II PCF designs.

It has been found that the cladding doped defect-core large mode area W-type-I PCF has the highest effective mode area 1930μm^2 whereas, cladding doped defect-core large mode area W-type-II PCF has highest effective mode area 901μm^2 for operating wavelength of 1.55μm respectively when the doping concentration of fluorine in the second layer of rings namely the fluorine doped silica rods varied such that the refractive index of the holes or rods becomes equal to 1.434. The cladding doped defect-core large mode area W-type-I PCF has the lowest nonlinear coefficient value of $\gamma(\lambda) = 0.015 W^{-1}Km^{-1}$, whereas, cladding doped defect-core large mode area W-type-II PCF has lowest nonlinear coefficient value of $\gamma(\lambda) = 0.013 W^{-1}Km^{-1}$ respectively for operating wavelength of 1.55μm and when the doping concentration of fluorine in the second layer of rings namely the fluorine doped silica rods varied such that the refractive index of the holes or rods becomes equal to 1.434.

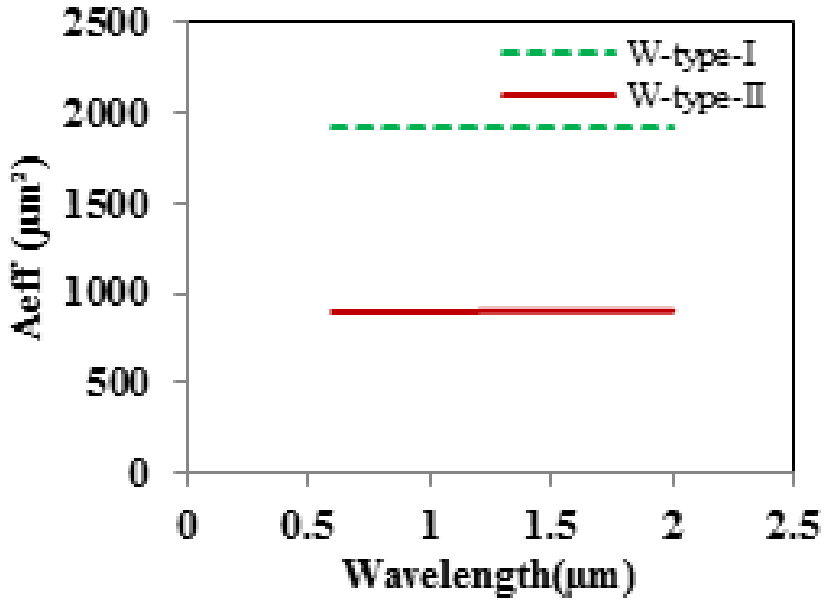

Fig. 5.9 Effective mode Area (Aeff) versus wavelength graphs of W-type-I and W-type-II PCF.

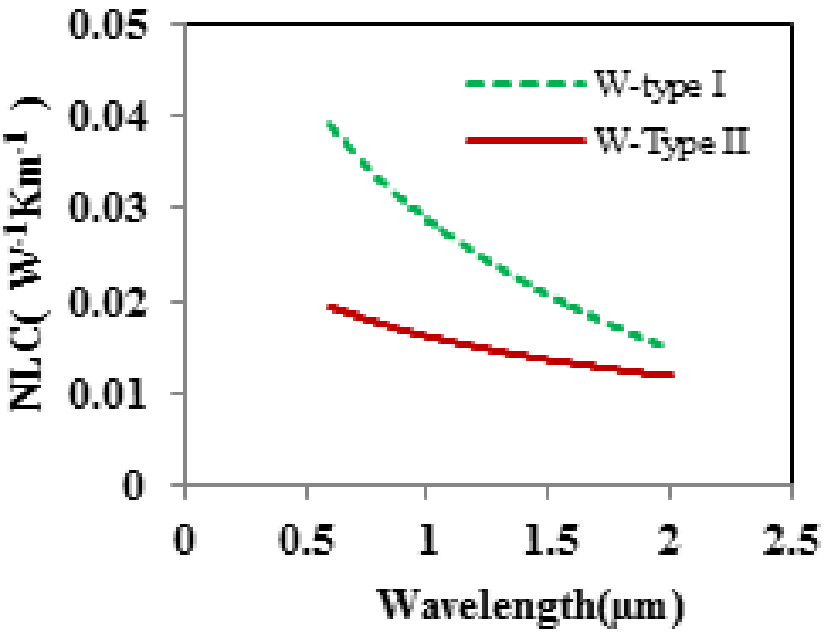

Fig. 5.10: Non-linear coefficient (NLC) versus wavelength graphs of W-type-I and W-type-II PCF.

Low value of nonlinear coefficient implies that the proposed cladding doped defect-core large mode area W-type PCF is free from non linear effects and most suitable for telecommunication and sensing.

5.4. Conclusion

Cladding doped defect-core large mode area W-type-I and W-type-II PCF structures have been designed and propagation characteristics computed by extending the full vectorial finite element method. The W-type PCFs are found to have very low confinement loss. The lowest values of confinement loss for W-type-I PCF and W-type-II PCF at 1.55μm recorded as 1.16 X 10^{-10} dB/m, and 1.24 X 10^{-13} dB/m respectively.

It has been found that the W-type PCFs are insensitive to macro bending. The W-type-I PCF and W-type-II PCF have the minimum bending loss value of 7.15 X 10^{-13}dB/m and 2.93 X 10^{-7}dB/m respectively at operating wavelength 1.55μm for a 30cm bend radius.

The W-type-I PCF is found to be more birefringent and more sensitive compared to W-type-II PCF. The maximum birefringence for W-type-I PCF and W-type-II PCF found to be equal to 7.82 X 10^{-8} and 6.91 X 10^{-7} for refractive index of doped rods equal to 1.448 at 1.55μm. The relative sensitivity coefficient of the W-type-I PCF and W-type-II PCF has been found to be equal to 0.4 and 0.01 respectively.

The W-type-I and W-type-II PCF have the highest effective mode area value of 1930μm^2, and 901μm^2 respectively for operating wavelength of 1.55μm. The cladding doped defect-core large mode area W-type-I and W-type-II PCF have the nonlinear coefficient value as low as 0.015$W^{-1}Km^{-1}$ and 0.013$W^{-1}Km^{-1}$ respectively for operating wavelength of 1.55μm for refractive index of doped rods equal to 1.434.

The structure can thus be utilized for applications in telecommunication and sensing.

Chapter-VI

Low bend loss photonic crystal fiber in Ga-Sb-S based chalcogenide glass for nonlinear applications: design and analysis

CHAPTER-VI

LOW BEND LOSS PHOTONIC CRYSTAL FIBER IN GA-SB-S BASED CHALCOGENIDE GLASS FOR NONLINEAR APPLICATIONS: DESIGN AND ANALYSIS

6.1. Introduction

We have included in the chapter I, III and V about the photonic crystal fiber (PCF) made of waveguiding parts with a solid core and cladding layers consisting of spatially periodic air holes around the core and running along throughout the length [10,63-65, 87]. In such PCFs, the effective refractive index of the cladding region is reduced due to the presence of these air holes. Nowadays, PCFs have been studied by the researchers with lot of attention due to its unusual and attractive optical properties like single mode operation in wide wavelength range, high non-linear coefficient [208], low bending loss characteristics [175], excitation of non-linear effects at small mode area [176], and manageable dispersion properties [177], endlessly single-mode operation [193], large mode area [178], and high birefringence [209]. Among these features, PCF with very high value of nonlinear coefficient is very desirable for the various applications in nonlinear optics. These highly nonlinear PCFs are regarded as candidates for realizing all-optical signal processing devices by means of the nonlinear optical effects. Large nonlinear coefficient in PCFs can be achieved by reducing the diameter of the fiber core and enlarging the air-hole size in cladding. However, the nonlinear coefficient is not the only key parameter affecting the efficiency of a nonlinear interaction, the group velocity dispersion and dispersion slope always strongly affect the nonlinear efficiency either. Recently, an equiangular spiral photonic crystal fiber structure in As_2Se_3 chalcogenide glass has been designed and analyzed to generate an all-normal and flat dispersion characteristic for the applications in supercontinuum generation [210]. A lot of research is being done to achieve highly nonlinearity in PCF structures [81]. Although, these PCFs have been reported to have nonlinear coefficient value less than 80 $W^{-1}km^{-1}$ at 1.55μm wavelength. To achieve larger nonlinear coefficient, some liquid-core PCFs [211] and

slot spiral PCFs [212] have been reported. The nonlinear coefficient at 1.55 μm is as high as $251W^{-1}m^{-1}$, while, ultrahigh nonlinear coefficient up to $3.5 \times 10^4\ W^{-1}km^{-1}$ has been reported in [213]. In conventional silica PCFs, it is difficult to achieve ultrahigh nonlinearity of the order of $10^3\ W^{-1}km^{-1}$.

In order to overcome the above mentioned constraints, we here propose a conventional PCF design in a very recently reported novel Ga-Sb-S chalcogenide glass [214]. The novel Ga-Sb-S chalcogenide glass has a wide transparent window of 0.8 μm to 14 μm, high third-order nonlinear refractive index of the order of $12.4 \times 10^{-14}\ cm^2\ W^{-1}$ at 1.55μm [215]. A design of PCF with such a novel material with above mentioned favourable properties makes them promising candidates for mid-infrared applications like nonlinear optics, and lasers with possible applications in free space communication windows (i.e. 5-8 μm and 13-15 μm), supercontinuum generation, applications in slow light and enhancement of optical forces. The confinement and guiding of light in this PCF with relatively high core index occur via total internal reflection and the single-mode propagation is dependent of the ratio between the core radius and wavelength [183,128,182]. Numerical calculations using finite element method have been carried out on the proposed PCF design to calculate parameters like effective area, nonlinear coefficient, and confinement loss and bend loss for different bend radius regime to judge its propagation characteristics. It has been found that in the proposed structure, the effective area decreases for increasing value of d/Λ whereas increases for increasing value of wavelengths and the nonlinear coefficient increases on increasing d/Λ whereas the nonlinear coefficient decreases for increasing value of wavelengths. The proposed PCF structure with novel Ga-Sb-S chalcogenide glass material is insensitive to macro bending. The structure can be utilized in free space communication windows of 5-8 μm and 13-15 μm, supercontinuum generation, applications in slow light and enhancement of optical forces.

6.2. Method of analysis

The refractive index of the Ga-Sb-S chalcogenide glass material has been calculated by extending the Sellmeier equation for the wavelength dependent refractive index of Ga-Sb-S Chalcogenide glass as given in Eq. 1.25 [214] and the values of the coefficients $a_1 = 6.2563$, $a_2 = 2.9444$, and $b_1 = 0.3425$, $b_2 = 34.28$.

The effective mode area of the propagating mode is a very essential feature to suppress the nonlinear effects and in the proposed PCF design, the effective area has been calculated by using the Eq. 1.27 [215].

The nonlinear coefficient (γ), offered by PCF structure related to the nonlinear refractive index of material of the PCF and represented by the equation 1.28 [216]. The third-order nonlinear nonlinear refractive index (n_2) of Ga-Sb-S Chalcogenide glass material has been considered of the order of 12.4×10^{-14} cm^2W^{-1} at 1.55μm [214].

The confinement loss arises due to the leakage of power between and through the holes of PCF. The PCF being a leaky structure has complex effective indices, n_{eff} of the modes. The confinement loss can be extracted from the imaginary part of the n_{eff} by using the relation at equation 1.29 [194] without the application of bend. While using the fiber for free space communications, bending of the PCF structure is inevitable. The PCF needs to be spooled at certain radius for this purpose and during this the fiber gets bent. Therefore, it is essential to study the bending performance of the design. In bent fibers the field profile deforms outwards in the direction of the bend. The presence of air holes around the core makes the design of effective refractive index more flexible. Bending loss of the proposed PCF has been calculated by using the equivalent index model. In this method, in order to simulate the effects of bending, the bent PCF is transformed into a straight PCF with an equivalent refractive index [184,198,199] defined in equation 1.30.

The bend loss of photonic crystal fiber can be calculated by applying perfectly matched layer (PML) boundary condition. A rectangular perfectly matched layer (PML) has been introduced at the surface of the Ga-Sb-S chalcogenide glass PCF to emulate the effect of an infinite domain in the finite element method. With the introduction of the PML the propagation constant of modes of the proposed PCF structure becomes complex [187,217,201]. The bending loss of the mode has been calculated by using the imaginary part of propagation constant or complex effective index of the bent fiber with the equivalent refractive index using equation 1.29.

The group velocity dispersion $D(\lambda)$ of the reported PCF structure has been calculated from wavelength dependent effective indices of propagating mode by employing the

relation at equation 1.26 considering Sellmeier equation and both material and waveguide dispersion has been included while calculating n_{eff}.

6.3. Design of Ga-Sb-S based chalcogenide glass PCF

The transverse cross-sectional view of the reported PCF structure is illustrated in figure 6.1. A hexagonal lattice solid core PCF structure has been designed by considering Ga-Sb-S based chalcogenide glass as the PCF material. The refractive index of material is equal to 2.75 for operating wavelength of 1.55 μm [214]. The center to center distance of the holes or the pitch is taken constant (i.e. Λ = 2.2 μm) for the proposed PCF structure. The diameter of the each air hole of the PCF structure is represented by d. To calculate the accurate bending loss of the structure, perfectly matched layer (PML) of the width of 2 μm has been applied surrounding the PCF structure. The central air hole has been removed to create the core in the photonic crystal geometry of the PCF.

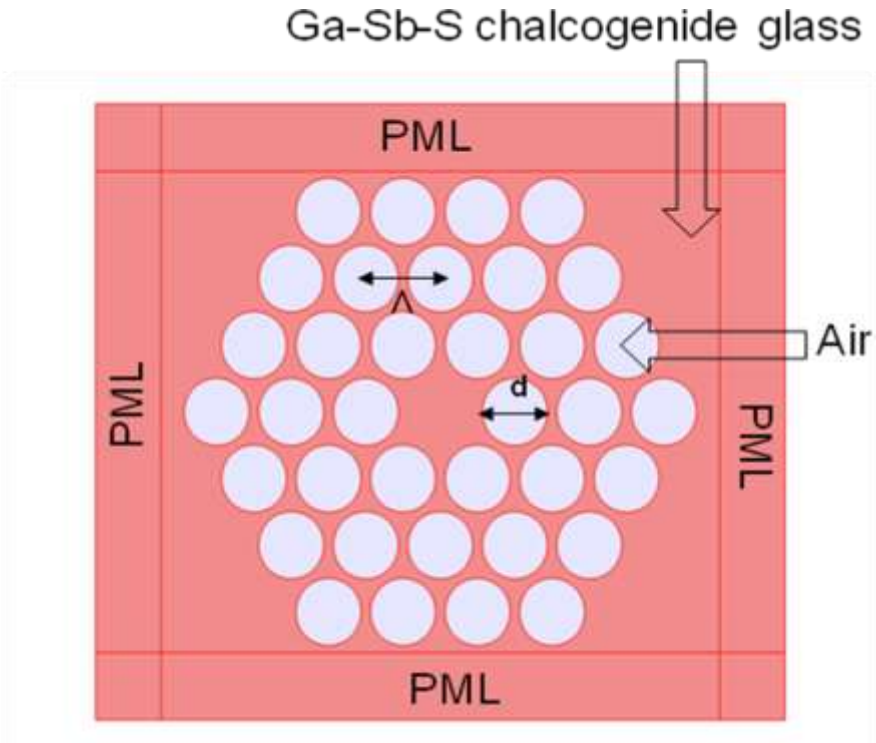

Fig.6.1: Transverse cross-sectional view of Ga-Sb-S based chalcogenide Photonic Crystal Fiber structure.

6.4. Numerical results and analysis

In our simulation, we have used the following parameters unless stated otherwise: d = 880 nm, and Λ = 2.2 μm. To examine the possibility of large nonlinearity with smaller effective mode area of the propagating mode in the proposed structure, the effects of various structural parameters have been investigated. Full vectorial finite element method has been employed to investigate the modal properties of the proposed PCF structure.

6.5. Effective mode area and dispersion characteristics

In PCFs the effective mode area is controlled by tuning the ratio of the diameter of the air holes to the pitch of the air holes (i.e. d/Λ) of the PCF [132,133,120]. To study the influence of d/Λ on the effective mode area (A_{eff}) of propagating mode, the effective mode area of the proposed Ga-Sb-S chalcogenide glass PCF for different d/Λ values ranging from 0.2 to 0.7 have been calculated at the operating wavelength of 1.55 μm as illustrated in Fig.6.2. It is indication from the figure 6.2 that the effective mode area of the propagating mode decreases for increasing value of d/Λ. This is very obvious because on increasing the value of d (with fixed value of Λ) the confinement of the propagating mode in the core of the PCF structure increases and hence the spread of the mode towards the cladding region decreases.

The effective mode area plays a very important role to enhance nonlinear effects in the PCF structures. Narrow core microstructured or photonic crystal fibers are suitable to geometries to get strong nonlinear effects. Use of the different non-silica materials with large values of n_2 such as silicates, chalcogenides, tellurite oxide, and bismuth oxide are also desirable for producing nonlinear effects. The effective mode area plays very important role to enhance nonlinear effects in PCF structures. The spectral variation of the effective mode area has been illustrated in Fig.6.3 for various values of d/Λ. In general, when d/Λ increases from 0.2 to 0.7 the effective mode area decreases as shown in Fig. 6.2. It has been found that the Ga-Sb-S chalcogenide glass PCF has effective mode area of 6.98 μm^2, 3.37 μm^2, 1.49 μm^2 and 0.86 μm^2 for d/Λ values of 0.2, 0.4, 0.6 and 0.7 respectively at operating wavelength 1.55 μm. The maximum effective mode area of 133 μm^2 and nonlinear coefficient of 4183 $W^{-1}Km^{-1}$

has been found for operating wavelength of 14 μm at = 0.7. The effective mode area decreases on increasing d/Λ, because of reduction in the core size on increasing d/Λ.

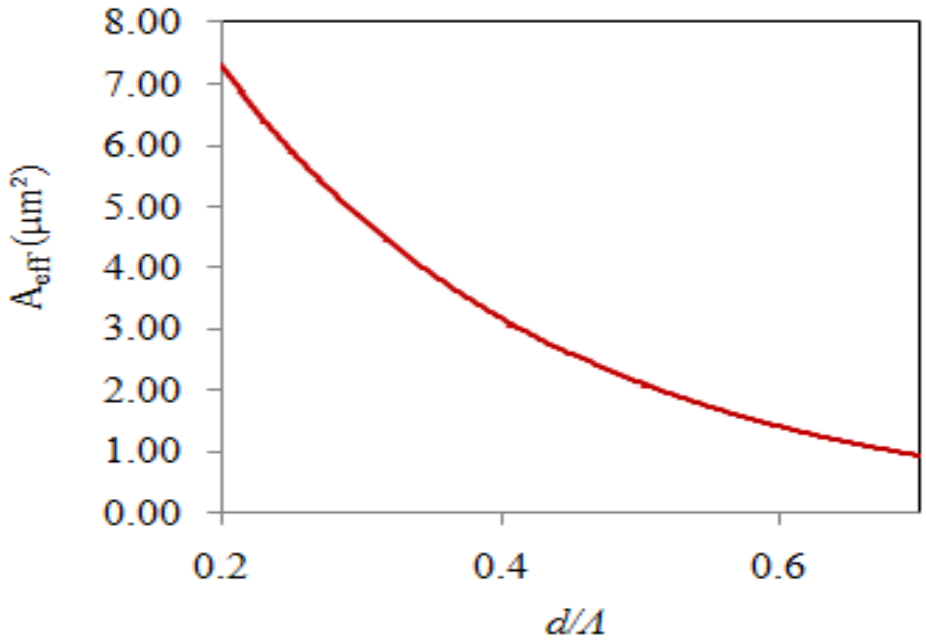

Fig. 6.2: Variation of the effective mode area with various *d/Λ* values of the PCF structure at the operating wavelength of 1.55 μm.

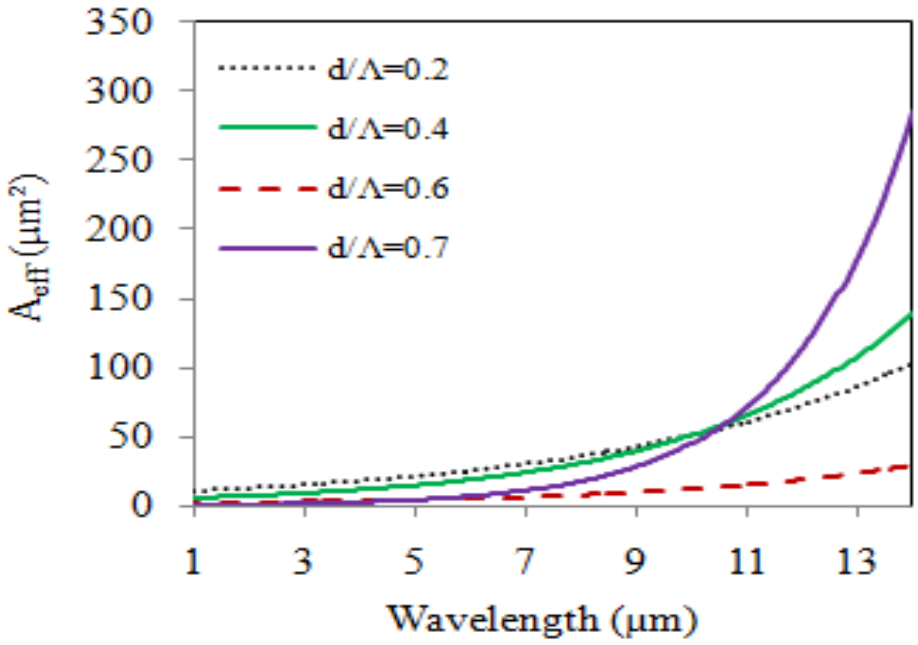

Fig. 6.3: The spectral variation of the effective mode area of the propagating mode for various values of d/Λ at the operating wavelength of 1.55 μm.

The group velocity dispersion, $D(\lambda)$ has been simulated using Eq.1.26 for $d/\Lambda = 0.4$ ($d/\Lambda = 0.4$ has been considered to satisfy the single-mode condition of the PCF). As shown in Fig.6.4, the dispersion curve exhibit normal dispersion characteristic at lower wavelengths and anomalous dispersion for higher wavelengths with zero dispersion wavelength (ZDW) at 2.6 μm. The dispersion curve is almost flat between 2.4 μm to 2.7 μm with dispersion variation of 20 ps/nm km. Such dispersion profile of the PCF structure is very suitable for mid-infrared supercontinuum generation. Therefore, one can choose the pump wavelength near about 2.6 μm wavelength for getting efficient broad supercontinuum generation in mid-infrared regime.

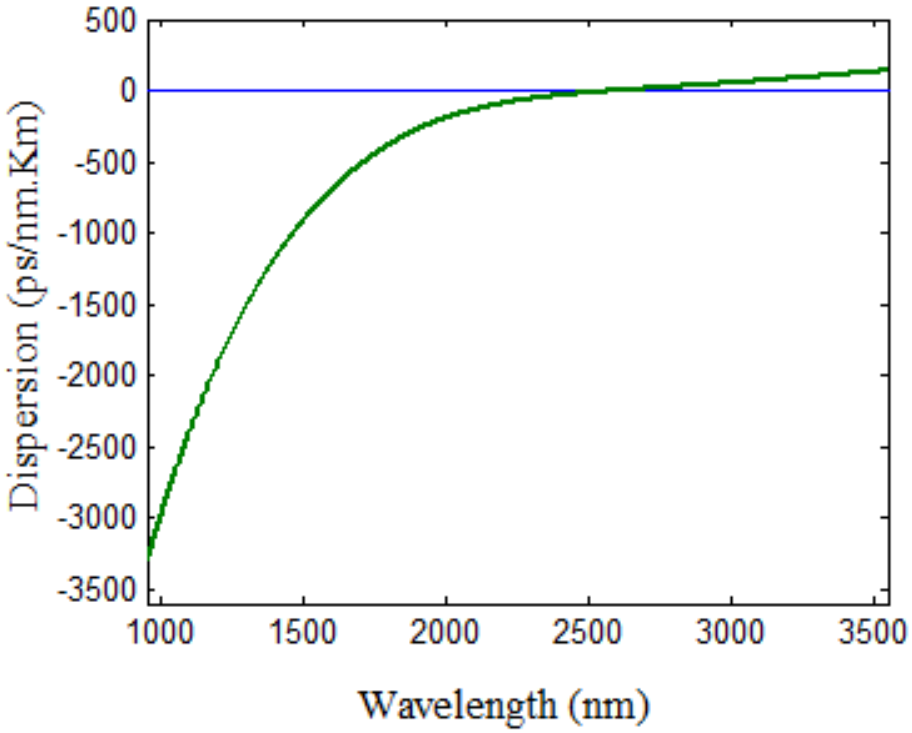

Fig. 6.4: Dispersion characteristics of proposed Ga-Sb-S chalcogenide glass PCF structure when $d/\Lambda = 0.4$.

Table 6.1 shows the calculated refractive index values at different wavelengths using Sellmeier equation for Ga-Sb-S chalcogenide glass.

Table 6.1: Calculated refractive index values for Ga-Sb-S chalcogenide glass at different wavelengths.

Wavelength (μm)	**Calculated refractive index values using Sellmeier equation for Ga-Sb-S chalcogenide glass**
0.8	2.942579497
1.55	2.751622005
2	2.726767746
4	2.69478467
6	2.680242494
8	2.664243226
10	2.643819233
12	2.617289232
14	2.582757522

6.6. Nonlinear characteristic of the PCF Design

The nonlinearity of the proposed PCF designs has been measured by calculating the nonlinear coefficient using the Eq. 1.27 [192,206,218,219]. A high nonlinearity value of PCF implies ability to confine high-intensity light. Many nonlinear effects inside the photonic crystal fiber depend on the nonlinear parameter [i.e. $\gamma = 2\pi n_2/(\lambda A_{eff})$], where, n_2 is the nonlinear refractive index of the material of PCF, λ represents the operating wavelength, and A_{eff} denotes the effective area of propagating mode in the core of the PCF. Therefore, in addition to the intensity of input pump the geometrical parameters of PCF are also play very important role to create the nonlinear effects. For better perfection of the nonlinear effects, the effective mode area of the propagating mode must be as small as possible and the PCF material must be highly nonlinear. Instantaneous nature of the nonlinear effects can be used for high speed switching and ultrafast signal processing.

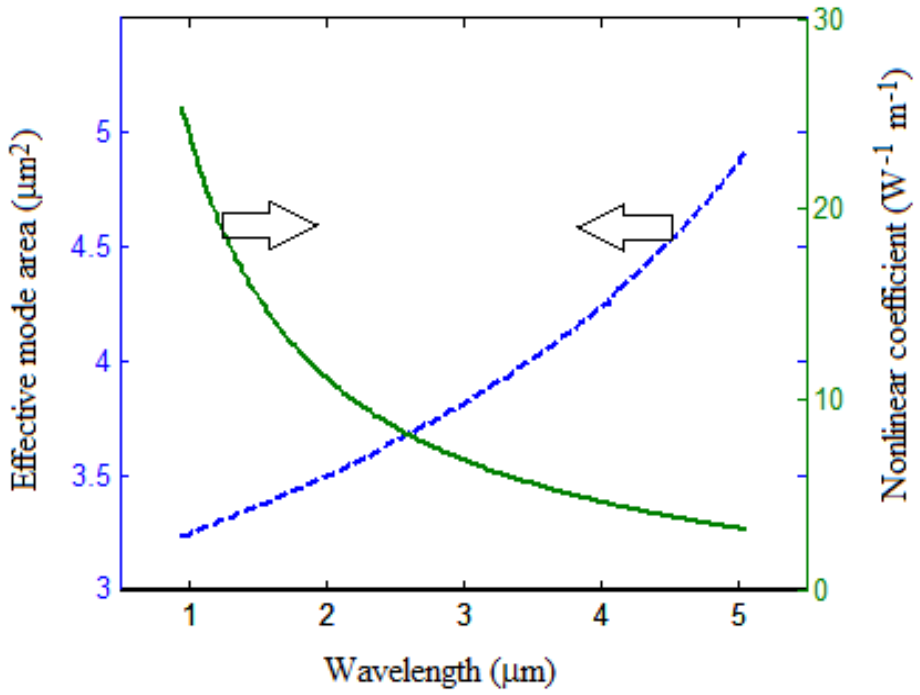

Fig. 6.5: The spectral dependence of the nonlinear coefficient along with the effective-mode-area of the propagating mode in the PCF structure at $d/\Lambda = 0.4$.

The spectral variation of the nonlinear coefficient and effective mode area of the propagating mode have been depicted in Fig.6.5 for $d/\Lambda = 0.4$. Fig.6.5 reveals that the nonlinear coefficient decreases with the increase in wavelength. Since, the nonlinearity is inversely proportional to the effective mode area, the effective mode area increases on increasing wavelength. The proposed Ga-Sb-S chalcogenide glass PCF structure possesses nonlinear coefficient as high as 14.92 W^{-1} m^{-1} with the effective mode of propagating mode of 3.37 μm^2 at the operating wavelength of 1.55 μm. Such highly nonlinear PCF structure in Ga-Sb-S chalcogenide glass is suitable candidate for nonlinear applications such as mid-infrared supercontinuum generation, slow-light generation. Supercontinuum generation has attracted most attention because of its applications for Wavelength Division Multiplexer (WDM) sources, metrology, spectroscopy, and optical coherence tomography.

6.7. Bending Loss Performance of the proposed PCF structure

Bends of different macro bending radii ranging from 2.5cm to 30cm have been applied on the proposed Ga-Sb-S Chalcogenide PCF structure with different values of d/Λ ranging from 0.2 to 0.7 and bend loss of individual structures have been calculated and the results have been plotted in figures 6.6 and 6.7 respectively. The effect of bending on the proposed Ga-Sb-S Chalcogenide PCF structure PCF can be observed by examining the cross-sectional view of transverse mode profile of electric field intensity or the modal field variations, which signifies that due to the application of various bend radii the modal field gets dispersed along the direction of application of bend compared with the modal field of the structure without bending and the shift in the modal field increases with decreasing bend radius from 30cm, 20cm, 15cm, 10cm, 5cm and 2.5cm. The mode leaking across the PCF is the cause of bending losses and as a result of this the modal field in the core region shifted towards the bend. It has been found that at small bending radius, the loss is high and reaches its maximum. However, by increasing the bending radius the bend loss can be dropped 0.22dB/m at 30 cm bend radii for d/Λ value of 0.2 at 1.55μm, this is because at large bending radius, the scattering loss becomes small.

Bending loss of the proposed PCF has been calculated. The output modal field variations for various bend radii, applied in a circular loop with a single-turn of PCF and arbitrary angular orientation has been investigated. Figure 6.6 shows the variation of bend loss with bend radius of the proposed PCF type for wavelength 1.55μm at d/Λ value of 0.2. The low bending sensitivity for the proposed PCF compared to the conventional silica PCF particularly at short wavelengths has been observed. It has been found that the PCF structure for d/Λ value equal to 0.4, 0.6, 0.7 are bend insensitive for bending radii regime of 2.5cm to 30cm. Instead of that the PCF is bend sensitive for a bend radii of 50 μm and less for d/Λ value 0.4 making the PCF a good candidate of bend insensitive PCF in the 1.55μm telecom window.

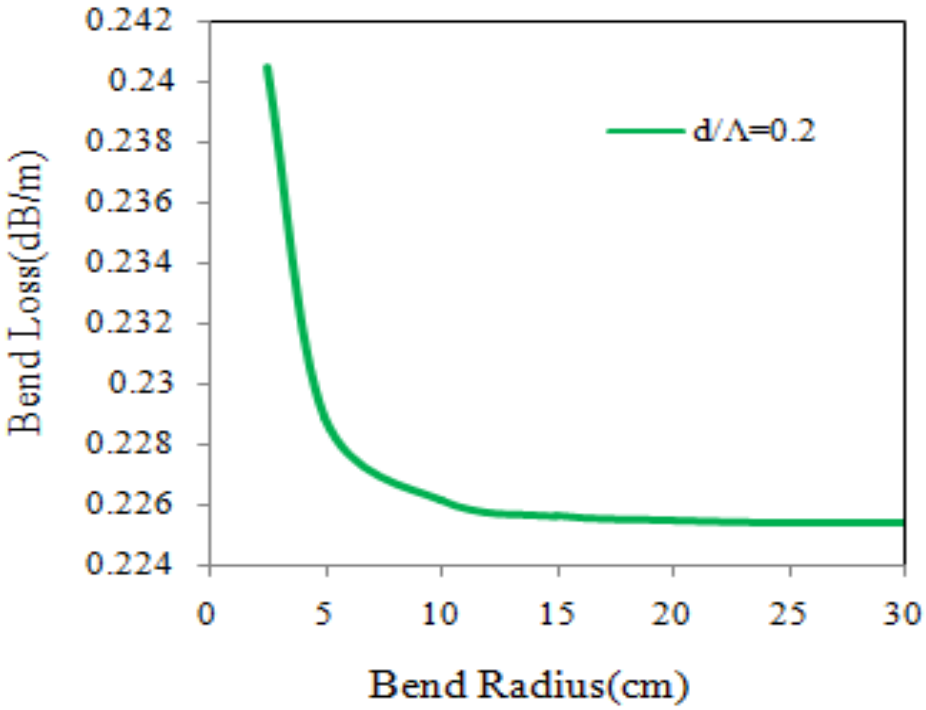

Fig. 6.6: Bend loss in Ga-Sb-S Chalcogenide glass PCF for d/Λ value of 0.2 at 1.55μm for different bend radii.

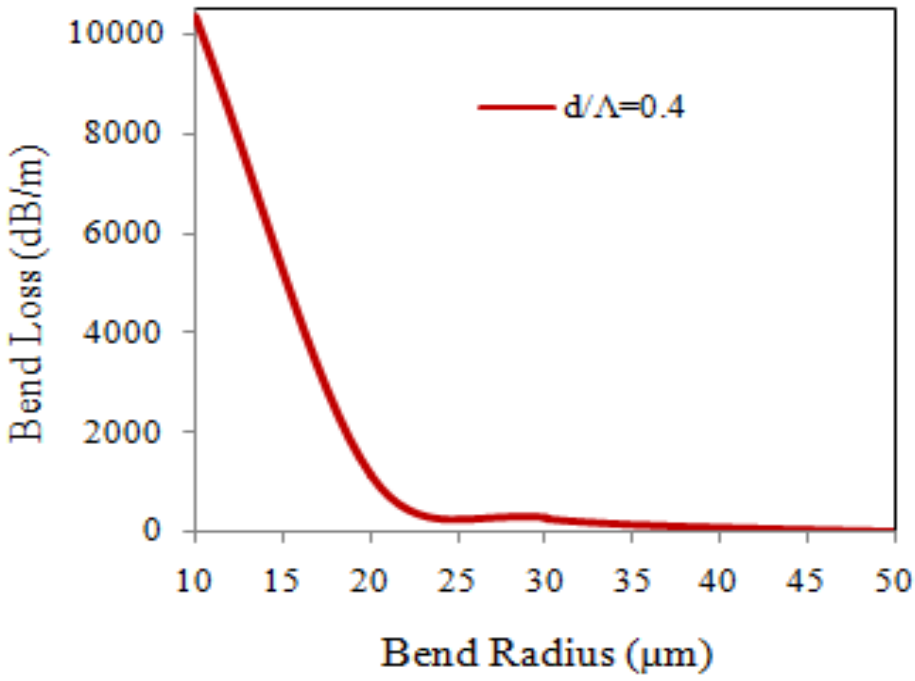

Fig. 6.7: Bend loss in Ga-Sb-S chalcogenide glass PCF for d/Λ value of 0.4 at 1.55μm for different bend radii.

Figure 6.7 shows the variation of bend loss with bend radius of the proposed PCF type for wavelength 1.55μm at d/Λ value of 0.4 for a bend radii regime of 10μm to 50μm. At 50 μm bend radii minimum bend loss recorded as 0.0144dB/m for d/Λ value of 0.4 at 1.55μm. The PCF structure for d/Λ value 0.6 is bending insensitive even for bending radii of 50μm and less depicting bend insensitive PCF design for the 1.55μm telecom window. The PCF is slightly sensitive to bending for a bend radius of 2.5μm and lower. For bend radii of 2μm the fundamental mode has zero bend loss. Again for PCF design with d/Λ value 0.7 the fundamental mode has zero bend loss even in the micrometer range bend radii. However, application of micrometer level bend radii or radius of curvature to the proposed PCF structure is impractical as that may lead to breakage of the fiber. Hence, the PCF may be depicted as bend insensitive for d/Λ value above 0.2 and is a good candidate for use in free space communication windows of 5-8 μm and 13-15 μm.

6.8. Conclusion

A photonic crystal fiber structure has been designed and analyzed for first time in recently reported Ga-Sb-S based chalcogenide glass material for nonlinear applications. The linear and nonlinear propagation characteristics have been investigated for the proposed PCF structure. The proposed Ga-Sb-S chalcogenide glass PCF has nonlinear coefficient as high as 14.92 $W^{-1}m^{-1}$ with effective mode area of 3.37 μm^2 for d/Λ values of 0.4 at operating wavelength of 1.55μm. It has been found that the Ga-Sb-S chalcogenide glass PCF is insensitive to macro bending above d/Λ value equal to 0.2 at operating wavelength of 1.55μm. At 50 μm bend radii minimum bend loss recorded as 0.0144 dB/m for d/Λ value of 0.4 for operating wavelength of 1.55μm. The Ga-Sb-S chalcogenide glass PCF has minimum bending loss value of 0.22dB/m for d/Λ value equal to 0.2 at the operating wavelength of 1.55μm for a 30cm bend radius. The structure is a promising candidate for mid-infrared applications in nonlinear optics such as supercontinuum generation, slow-light generation and mid-infrared fiber lasers.

Chapter-VII
Summary and future scope of the research work

CHAPTER-VII

SUMMARY AND FUTURE SCOPE OF THE RESEARCH WORK

In this thesis, the importance of photonic crystal and photonic crystal fiber based photonic devices for potential applications in telecommunication, sensing and photonic circuits has been discussed. In addition to this, detailed literature review on the advances in the area of photonic crystal and the photonic crystal fiber based photonic devices for potential applications and different methods of their fabrication have been discussed in chapter 1. The theory, analytical techniques and numerical methods used for the design of photonic crystal and the photonic crystal fiber based photonic devices also described.

This is followed by designing of a 2D photonic crystal on temperature resilient silicon carbide (SiC) material and further creation of point defect cavity structure in the SiC based PhC have been done. Effect of temperature on different parameters of the proposed PhC and cavity designs like band gap width, defect cavity mode dispersion, the resonance mode and quality factor of resonant mode using plane wave expansion (PWE) method and finite difference time domain (FDTD) method for telecommunication applications, are carried out in chapter II. The results obtained were found better compared to Si based PhC. The SiC PhC devices can be used for high temperature and power transmission which is difficult to achieve with Si or GaAs based photonic crystals and devices. Apart from applications in optical communication, various other SiC based devices such as optical filters, switches and lasers etc can be designed which are stable at high power and high temperature, at which the silicon photonics fails. This can lead to a future era of silicon carbide power photonics analogous to silicon carbide power electronics.

The chapter III discussed about the design of fluoropolymer photonic crystal fiber and analyses of the same in terms of the parameters like effective refractive index of the guided mode and dispersion for wavelength range 10μm to 300μm using full vectorial FEM and found transmission characteristics of fluoropolymer photonic crystal fiber

comparable with the earlier published result. The proposed fluoropolymer PCF may find applications in long distance telecommunication and in mid-infrared region.

Chapter IV included the design and analyses of W-type photonic crystal fibers (W-Type PCF) in terms of the parameters like effective refractive index of the guided mode and dispersion using full vectorial FEM. The transmission characteristics of W-Type PCF obtained with the simulation are found better compared with the earlier published results. The power coupling in W-type PCF is more compared to conventional PCF. The bend insensitive nature of the proposed W-type PCF structures makes them good candidate for large mode area fiber design and fit for fiber to home applications.

In chapter V, the designing of large mode area W-type photonic crystal fibers with doped cladding and analyses of the proposed structures in terms of the parameters like effective refractive index of the guided mode, effective area, non-linear co-efficient, dispersion and sensitivity using full vectorial FEM for possible applications in high power delivery devices and sensing have been done. The proposed W-type PCF structures possesses very low confinement loss and W-type-I PCF structures are found to be less bend sensitive compared to W-type-II PCF.

The chapter VI discusses about the design and analyses of novel Ga-Sb-S based chalcogenide glass photonic crystal fiber (Ga-Sb-S-PCF) in terms of the parameters like effective refractive index of the guided mode, dispersion, effective area, non-linear co-efficient using full vectorial FEM. The transmission characteristics of Ga-Sb-S-PCF have been studied for wavelength range 0.8μm to 14μm. This novel Ga-Sb-S material PCF structure has been studied for the first time since the inception of novel material Ga-Sb-S and can be a promising candidate for nonlinear applications such as supercontinuum generation, slow light generation, and mid-infrared fiber lasers.

This research is directed at achieving a higher level of understanding of the PhC and PCF based devices to predict and explain their behavior which eventually will help in finding more accurate and reliable devices that are made possible by PhC and PCF. The study has been undertaken by considering the most relevant principles supporting the application of PhC and PCF and also considering the present situation and trends. Different PhC and PCF structures for different applications have been explored looking for trends towards future developments and applications. Following possible

future works can be predicted further on the subject matters discussed in the previous chapters from chapter II to VI:

1. The resonant PhC cavity in high temperature resilient SiC discussed in chapter II can further be used to:
    - Design of 2D and 3D SiC PhC waveguide micro cavity on air holes in SiC PhC slab microstructures.
    - Design of 2D and 3D SiC PhC waveguide on air holes in SiC PhC slab microstructures which are more practical structures from fabrication point of view.
    - Design of coupled cavity waveguide in SiC for low dispersion applications.
    - Design of DWDM demultiplexer using resonance cavity in SIC.
2. The Fluoropolymer PCF discussed in chapter III may further find use in the design of metal coated defect core PCF for THz propagation and sensing and imaging applications. The Fluoropolymer PCF structures can be a promising candidate for nonlinear applications such as supercontinuum generation.
3. The proposed structures of W-type PCF discussed in chapter IV can be utilized in both telecommunication and macro-bend sensing. The W-type PCF structures can be a promising candidate for nonlinear applications such as supercontinuum generation.
4. The proposed structures of cladding doped W-type PCF discussed in chapter V can be a good candidate for temperature and pressure sensor designing.
5. The proposed structures of novel Ga-Sb-S chalcogenide glass PCF discussed in chapter VI can be a promising candidate for nonlinear applications such as supercontinuum generation, slow light generation, and mid-infrared fiber lasers.

Moreover, the thesis has been written keeping in mind the requirement of a basic researcher in the field of PhC and PCF. Therefore, every details of theory of PhC and PCF has been tried to be incorporated in this thesis work including the books, computational methods that can be utilized, along with latest topic references in the relevant field of PhC and PCF that may be helpful in future for all beginners in research in this field.

References

REFERENCES

[1] S. G. Johnson, and J. D. Joannopoulos, Introduction to Photonic Crystals: Bloch's Theorem, Band Diagrams, and Gaps (But No Defects), MIT, 2003.

[2] J. D. Joannopoulos, R. D. Meade, and J. N. Winn, Photonic Crystals: Molding the flow of light, 2E, Princeton Univ. Press, New Jersey, 2008.

[3] K. Inoue, and K. Ohtaka, Photonic Crystals: Physics, Fabrication and applications, Springer Series in Optical Sciences, 2004.

[4] C. Kittel, Introduction to Solid State Physics, 7E, Wiley India Pvt Ltd., 2007.

[5] A. J. Dekker, Solid State Physics, 1E, Macmillan India, 2000.

[6] C. Sibilia, T.M. Benson, M. Marciniak, and T. Szoplik, Photonic Crystals: Physics and Technology, Springer-Verlag, 2008.

[7] K. Busch, S. Lolkes, R.B. Wehrspohn and H. Foll, Photonic Crystals: Advances in design, Fabrication and Characterization, Wiley-VCH, 2004.

[8] J. M. Lourtioz, Henry Benisty, Vincent Berger, Jean-Michel Gerard, Daniel Maystre, and Alexis Tchelnokov, Photonic Crystals: Towards Nanoscale Photonic Devices, Springer, New York, 2005.

[9] D. J. Griffiths, Introduction to Electrodynamics, 3E, Pearson Education, 2006.

[10] E. Yablonovitch, "Inhibited spontaneous emission in solid state physics and electronics", Physical. Review Letters, 58, 2059–2062, 1987.

[11] S. John, "Strong localization of photons in certain disordered dielectric superlattices", Physical Review Letters, 58, 2486-2489, 1987.

[12] T. Baba, D. Mori, K. Inoshita, and Y. Kuroki, "Light localization in line defect photonic waveguides", IEEE Journal of Quantum Electronics, 10, 484-491, 2004.

[13] J. S. Foresi, P. R. Villeneuve, J. Ferrera, E. R. Thoen, G. Steinmeyer, S. Fan, J. D. Joannopoulos, et al, Photonic-band gap microcavities in optical waveguides, Nature, 390, 143-145, 1997.

[14] M. Qi, E. Lidorikis, P. T. Rakich, S. G. Johnson, J. D. Joannopoulos, E. P. Ippen, and H. I. Smith, "A three-dimensional optical photonic crystal with designed point defects" Nature, 429, 538-542, 2004.

[15] M. Qiu, M. Mulot, M. Swillo, S. Anand, B. Jaskorzynska, and A. Karlsson, "Photonic crystal optical filter based on contra-directional waveguide coupling" Appl. Phys. Lett. 83, 5121, 2003.

[16] Y. Nagpal, and R.K. Sinha, "Polarization Dependent Analysis of Photonic Crystal Directional Coupler" Journal of Microwaves and Optoelectronics, 3 (4), 2004.

[17] Y. Nagpal, and R. K. Sinha, "Modeling of photonic bandgap directional couplers", Microwave and Optical Technology Letters, 43, 47-50, 2004.

[18] T. Tanabe, M. Notomi, S. Mitsugi, A. Shinya, and E. Kuramochi "All-optical switches on a silicon chip realized using photonic crystal nanocavities" Appl. Phys. Lett., 87, 151112, 2005.

[19] R. K. Sinha, and Y. Kalra, "Design of optical waveguide polarizer using photonic bandgap", Optics Express, 14, 10790-10794, 2006.

[20] Y. Cui, Q. Wu, E. Schonbrun, M. Tinker, J-B Lee, and W. Park, "Silicon based 2D slab photonic crystal TM polarizer at telecommunication wavelength", IEEE Photonic Technology Letters, 20, 641-643, 2008.

[21] K. Bayat, S. K. Chaudhuri, S. S. Naeini, and M. F. Baroughi, "Design and Simulation of Photonic Crystal Based Polarization Converter", IEEE Journal of Lightwave Technology, 27, 5483-5491, 2009.

[22] A. Camargo, and R. M. De La Rue, "Photonic crystal channel guide Y-junction beam splitter based on an AlGaAs/GaAs epitaxial structure", Integrated Photonics Research, San Francisco, CA, 2004.

[23] C. C. Chen, H. D. Chien, and P. G. Luan, "Photonic Crystal Beam Splitters" Applied Optics, 43, 6188-6190, 2004.

[24] W. Huang, Y. Zhang, and B. Li, "Ultracompact wavelength and polarization beam splitters in periodic dielectric waveguides", Optics Express, 16, 1600-1609, 2008.

[25] E. Centeno, B. Guizal, and D. Felbacq, "Multiplexing and Demultiplexing with Photonic Crystals", Pure and Applied Optics, 1, 10-13, 1999.

[26] F. S.-S. Chien, Y. J. Hsu, W. F. Hsieh, and S.-C. Cheng, "Dual wavelength demultiplexing by coupling and decoupling of photonic crystal waveguides", Optics Express, 12, 1119-1125, 2004.

[27] F. S. Chien, S. C. Cheng, Y. J. Hsu, and W. F. Hsieh, "Dual band multiplexer/demultiplexer with photonic crystal waveguide couplers for bidirectional communications", Optics Communication, 226, 592-597, 2006.

[28] L. W. Chung, and S. L. Lee, "Photonic crystal based dual band demultiplexers on silicon materials", Optical and Quantum Electronics, 39, 677-687, 2007.

[29] K. T. V. Grattan, and B. T. Meggitt, Optical Fiber sensor Technology Fundamentals, Kluwer Academic Publishers, London, 2000.

[30] J. Dakin, and B. Culshaw, Optical Fiber Sensors: principles and components, Vol I, Artech House, 1988.

[31] J. M. Lopez-Higuera, Handbook of optical fiber sensing technology, John Wiley & Sons Ltd, 2002.

[32] M. Notomi, A. Shinya, K. Yamda, C. Takahashi, and I. Yokohama, "Single mode transmission within photonic bandgap of width varied single line defect photonic crystal waveguides on SOI substrates", Electronic Letters, 37, 293-295, 2001.

[33] M. Plihal, and A. A. Maradudin, "Photonic band structures of two dimensional systems – The Triangular lattice", Physics Review B, 44, 1865-8571, 1991.

[34] M. Qui, "Bandgap effects in asymmetric crystal slabs", Physical Review B, 66, 033103, 2002.

[35] B. S. Song, S. Yamada, T. Asano, and S. Noda, Demonstration of two–dimensional photonic crystals based on silicon carbide, Opt. Express, 19, 11084-1089, 2011.

[36] A. Baron, A. Ryasnyanskiy, N. Dubreuil, P. Delaye, Q. Vy Tran, S. Combrie, S. Alfredo De Rossi, R. Frey, and G. Roosen, "Light localization induced enhancement of third order nonlinearities in a GaAs photonic crystal waveguide", Optics Express, 17, 552-557, 2009.

[37] N. Kawai, K. Inou, N. Carlsson, N. Ikeda, Y. Sugimoto, K. Asakawa, and T. Takemori, "Confined Band Gap in an Air-Bridge Type of Two-Dimensional AlGaAs Photonic Crystal", Physical Review Letters, 86, 2289-2292, 2001.

[38] V. R. Almeida, C. A. Barrios, R. R. Panepucci, and M. Lipson, "All optical control of light on a silicon chip", Nature, 481, 1081-1084, 2004.

[39] J. Bravo-Abad, A. Rodriguez, P. Bermel , S. G. Johnson, J. D. Joannopoulos, and M. Soljacic "Enhanced nonlinear optics in photonic-crystal microcavities" Optics Express, 15(24), 16161- 16176, 2007.

[40] S. Combrie, S. Alfredo De Rossi, Q. V. Tran, and H. Benisty, "GaAs photonic crystal cavity with ultrahigh Q: microwatt nonlinearity at 1.55 μm", Optics Letters, 33, 1908-1910, 2008.

[41] V. N. Astrov, R. M. Stevenson, I.S. Culshaw, D. M. Whittaker, M. S. Skolnick, T. F. Krauss, and R.M. De La Rue, "Heavy photon dispersion in photonic crystal waveguides', Applied Physics Letters, 77, 178-180, 2000.

[42] S. Assefa, and Y. A. Vlasov, "High order dispersion in photonic crystal waveguides," Optics Express, 15, 17562, 2007.

[43] C. Luo, S. G. Johnson, J. D. Joannopoulos, and J. D. Pendry, "All angle negative refraction without negative effective index", Physical Review B, 65, 201104, 2002.

[44] K. Kishor, M. N. Baitha, R. K. Sinha, and B. Lahiri, "Tunable negative refractive index metamaterial from "V" shaped SRP structure: Fabrication and Characterization", Journal of the Optical Society of America B (OSA) Vol. 31 No. 7, 1410-1414, 2014.

[45] T. Baba, D. Mori, "Slow light engineering in photonic crystals', Journal of Physics D: Applied Physics, 40, 2659-2665, 2007.

[46] T. F. Krauss, "Slow light in photonic crystal waveguides," Journal of Physics D: Applied Physics, 40, 2666-2670, 2007.

[47] T. F. Krauss, "Why do we need slow light?," Nature Photonics, 2, 448-450, 2008.

[48] W. Ding, C. Benton, A. V. Gorbnach, W. J. Wadsworth, J. C. Knight, D. V. Skryabin, M. Gnan, M. Sorrel, and R. M. De La Rue, "Solitons and spectral broadening in long silicon-on-insulator photonic wires", Optics Express, 16, 3310-3319, 2008.

[49] P. Rani, Y. Kalra, and R. K. Sinha, "Design and analysis of polarization independent all-optical logic gates in silicon-on-insulator photonic crystal" Optics Communications, 374, 148-155, 2016.

[50] P. Rani, Y. Kalra, and R. K. Sinha, "Design of all optical logic gates in photonic crystal waveguides" Optik - International Journal for Light and Electron Optics, 126(9-10), 950-955, 2015.

[51] G. P. Agrawal, Fiber Optic Communication systems, Hoboken, NJ: Wiley Interscience, 1997.

[52] Y. Kalra, and R.K. Sinha, Photonic Band gap Engineering in 2D Photonic Crystals, Pramana- Journal of Physics ,India, Springer, 67 (6) 1155-1164, 2006.

[53] S. G. Johnson, and J. D. Joannopoulous, "Block iterative frequency domain methods for Maxwell's equations in plane wave basis", Optics Express, 8, 173-190, 2001.

[54] User guide of bandSOLVE 9 software of Rsoft Design Group, Inc (2009).

[55] S. G. Johnson, and J. D. Joannopoulos, Photonic crystals: The road from theory to practice, Kluwer Academic Publishers, 2001.

[56] User guides of optiFDTD 8 software of Optiwave (2008).

[57] User guide of RF module of COMSOL multiphysics, 4.3 software (2013).

[58] H. Benisty, J.-M. Gerard, R. Houdre, J. Rarity, and C. Weisbuch, Confined Photon Systems: Fundamentals and applications, Springer, New York, 2005.

[59] G. Subramania, and S. Y. Lin, "Fabrication of three dimensional photonic crystal with alignment based on electron beam lithography", Applied Physics Letters, 85, 5037-5039, 2004.

[60] M. Campbell, et. al., "Fabrication of photonic crystals for visible spectrum by holographic lithography", Nature, 404, 53-56, 2000.

[61] Y. A. Vlasov, X. Bo, J. C. Sturm, and D. J. Norris "On-chip natural assembly of silicon photonic bandgap crystals" Nature, 414, 2001.

[62] M. Kawakami, "Photonic crystals for the visible range fabricated by autocloning technique and their applications", Optical and Quantum Electronics, 34, 63-70, 2002.

[63] J. C. Knight, T. A. Birks, P. S. J. Russell, and D. M. Atkin, "All-silica single-mode optical fiber with photonic crystal cladding," Opt. Lett. 21, 1547-549, 1996.

[64] J. C. Knight, "Photonic crystal fibres," Nature, 424, 847-851, 2003.

[65] P. S. J. Russell, "Photonic-crystal fibers," J. Lightwave Technol., 24(2), 4729-4749, 2006.

[66] A. Ghatak, and K. Thygarajan, Introduction to fiber optics, Cambridge University Press, 1999.

[67] J. M. Senior, Optical Fiber Communications: Principles and Practice, 2E, Preentice Hall Europe, 1992.

[68] G. Keiser, Optical fiber communication, 3E, Mc-Graw-Hill International Editions, Electrical Engineering Series, 2000.

[69] J. A. Buck, Fundamentals of Optical Fibers, 2E, John Wiley & Sons, Inc., Publication, 2004.

[70] H. Kolimbiris, Fiber Optics Communication, 4E, Pearson Education, 2004.

[71] J. Crisp, and B. Elliot, Introduction to Fiber Optics, 3E, Newnes, Elsevier, 2005.

[72] F. A. Jenkins, and H. E. White, Fundamentals of Optics, 4E, Mc-Graw-Hill International Editions, Physics Series, 2011.

[73] A. Yariv, and P. Yeh, Photonics: optical electronics in modern communications, Oxford University Press, New York, 2007.

[74] J. Broeng, G. Mogilevtsev, S. Barkou, and A. Bjarklev, "Photonic crystal fibers: a new class of optical waveguides", Optical Fiber technology, Vol. 5, 305-330, 1999.

[75] J. Arriaga, J. C. Knight, and P. S. J. Russell, "Modelling photonic crystal fibers", Physica E, 17, 440-442, 2003.

[76] J. C. Knight, J. Broeng, T. Birks, and P. S. J. Russell, "Photonic bandgap guidance in optical fibers", Science, Vol. 282, 1476-1478, 1998.

[77] F. Mitschke, Fiber Optics: Physics and Technology, Springer, 2009.

[78] J. K. Ranka, R. S. Windeler, and A. J. Stentz, "Optical properties of high-delta air-silica microstructure optical fibers", Opt. Lett., 25, 796-798, 2000.

[79] J. C. Knight, T. A. Birks, R. F. Cregan, P. S. J. Russell, and J. P. de Sandro, "Large mode area photonic crystal fiber", Elect. Lett. 34, 1347-1348, 1998.

[80] N. G. R. Broderick, T. M. Monro, P. J. Bennett, and D. J. Richardson, "Nonlinearity in holey optical fibers: measurement and future opportunities", Opt. Lett., 24, 1395-1397, 1999.

[81] J. K. Ranka, and R. S. Windeler, "Nonlinear interactions in air-silica microstructure optical fibers", Opt. & Photon. News, 20-25, 2000.

[82] I. A. Sukhoivanov, and I. V. Guryev, Photonic Crystals: Physics and Practical modeling, Springer, 2009.

[83] F. Benabid, and P. J.Roberts, "linear and nonlinear optical properties of hollow core photonic crystal fiber" Journal of Modern Optics, 58 (2), 87-124, 2011.

[84] C. Martijn de Sterke, and I. M. Bassett "Differential losses in Bragg fibers" Journal of Applied Physics 76, 680, 1994.

[85] M. F. S. Ferreira, E. Castro-Camus, D. J Ottaway, J. M. López-Higuera, X. Feng, W. Jin, Y. Jeong, N. Picqué, L. Tong, B. M. Reinhard, "Roadmap on optical sensors" Journal of Optics, Vol.19, No.8, IOP Publishing Ltd, Published 24 July, 2017.

[86] E. Wolf, Progresses in Optics, vol. 49, 1E, Elsevier, 2006.

[87] T. A. Birks, J. C. Knight, and P. S. J. Russell "Endlessly single-mode photonic crystal fiber," Opt. Lett. 22, 961-963, 1997.

[88] D. Mogilevtsev, T. A. Birks, and P. S. J. Russell "Group-velocity dispersion in photonic crystal fibers", Opt. Lett., 23, 1662-1664, 1998.

[89] M. Bass, C. Macdonald, G. Li, C.M. DeCusatis, and V.N. Mahajan, Handbook of Optics, Vol. 5, 3E, Mc Graw- Hill companies, Inc, 2010.

[90] P. P. Banerjee, Nonlinear Optics: Theory, Numerical Modeling and Applications, Marcel Dekker, Inc, New York, 2004.

[91] J. K. Ranka, R. S. Windeler, and A. J. Stentz, "Visible continuum generation in air-silica microstructure optical fibers with anomalous dispersion at 800 nm", Opt. Lett., 25, 25-27, 2000.

[92] T. A. Birks, W. J. Wadsworth, and P. S. J. Russell, "Supercontinuum generation in tapered fibers", Opt. Lett., 25, 1415-1417, 2000.

[93] S. Coen, A. H. L. Chau, R. Leonhardt, J. D. Harvey, J. C. Knight, W. J. Wadsworth, and P. St. J. Russell, "White-light supercontinuum generation with 60-ps pump pulses in a photonic crystal fiber", Opt. Lett., 26, 1356-1358, 2001.

[94] A. V. Husakou, and J. Herrmann, "Supercontinuum generation of higher-order solitons by fission in photonic crystal fibers", Phys. Rev. Lett., 87, 203901, 2001.

[95] A. L. Gaeta, "Nonlinear propagation and continuum generation in microstructured optical fibers", Opt. Lett., 27, 924-926, 2002.

[96] S. Coen, A. H. L. Chau, R. Leonhardt, and J. D. Harvey, "Super continuum generation via stimulated raman scattering and parametric four wave mixing in photonic crystal fibers", The journal of Optical Society of America B, Vol. 26, 753, 2002.

[97] P. A. Champert, S. V. Popov, and J. R. Taylor, "Generation of multiwatt, broadband continua in holey fibers", Optics Letters, Vol. 27, 122-124, 2002.

[98] J. Hermann, U. Griebner, N. Zhavoronkov, A. Husakao, D. Nickel, J. C. Knight, W. J. Wardsworth, P. St. J. Russel, and G. Korn, "Experimental evidence for supercontinuum generation by fission of higher order solitons in photonic crystal fibers", Physical Review Letters, Vol. 88, 173901, April 2002.

[99] A. V. Husakao and J. Hermann, "Supercontinuum generation of higher order solitons by fission in photonic crystal fibers", Physical Review Letters, Vol. 87, 203901, 2001.

[100] T. P. Hansen, J. Broeng, S. E. B. Libori, E. Knudsen, A. Bjarklev, J. R. Jensen, and H. Simonsen, "Highly birefringent index-guiding photonic crystal fibers", IEEE Photon. Techno. Lett., 13, 588-590, 2001.

[101] A. Ortigosa-Blanch, J. C. Knight, W. J. Wadsworth, B. J. Mangan, T. A. Birks and P. St. J. Russell, "Highly birefringent photonic crystal fibers", Opt. Lett., 25, 1325-1327, 2000.

[102] A. Ortigosa-Blanch, A. Diez, M. Delgado-Pinar, J. L. Cruz, and M. V. Andres, "Ultrahigh birefringent nonlinear microstructured fiber", IEEE Photon. Technol. Lett. 16, 1667-1669, 2004.

[103] D. Chen and L. Shen, "Ultrahigh Birefringent Photonic Crystal Fiber with Ultralow Confinement Loss" IEEE Photonics Technology Letters, 19, 185-187, 2007.

[104] K. Suzuki, H. Kubota, S. Kawanishi, M. Tanaka, and M. Fujita, "Optical properties of a low-loss polarization-maintaining photonic crystal fiber", Opt. Exp., 9, 676-680, 2001.

[105] E. Hecht, Optics, 4E, Pearson Education, 2008.

[106] I. Hartl, X. D. Li, C. Chudoba, R. K. Ghanta, T. H. Ko, J. G. Fujimoto, J. K. Ranka, and R. S. Windeler, "Ultrahigh-resolution optical coherence tomography using continuum generation in air-silica microstructure fiber", Opt. Lett., 26, 608-610, 2001.

[107] R. Holzwarth, Th. Udem, and T. W. Hansch, J. C. Knight, W. J. Wadsworth, and P. St. J. Russell, "Optical Frequency Synthesizer for Precision Spectroscopy" Physical Review Letter, Vol. 85, No. 11, 2264-2267, 2000.

[108] A. Bjarklev, J. Broeng, and A. S. Bjarklev, Photonic Crystal Fibres, Springer, Boston, MA, 2003.

[109] F. C. Favero, R. Spittel, F. Just, J. Kobelke, M. Rothhardt, and H. Bartelt, "A miniature temperature high germanium doped PCF interferometer sensor" Optics Express, 21(25), 30266-30274, 2013.

[110] G. Tang, T. Zhu, W. Lin, T. Qiao, Z. Zhang, X. Shan, D. Chen, Q. Qian, and Z. Yang, "Single-Mode Large Mode-Field-Area Tm^{3+}-Doped Lead-Silicate Glass Photonic Crystal Fibers" IEEE Photonics Technology Letters, 29(5), 450-453, 2017.

[111] A. Agrawal, M. Tiwari, Y.O. Azabi, V. Janyani, B.M.A. Rahman, and K.T.V. Grattan, "Ultrabroad supercontinuum generation in tellurite equiangular spiral photonic crystal fiber" Journal of Modern Optics, Vol. 60, No. 12 956-962, 2013.

[112] C. Jin, L. Rao, J. H. Yuan, X. W. Shen, and C.X. Yu, "Investigation on bismuth-oxide photonic crystal fiber for optical parametric amplification" Optoelectronics Letters, 7(3), 194–197, 2011.

[113] C. Markos, I. Kubat, and O. Bang, "Hybrid polymer photonic crystal fiber with integrated chalcogenide glass nanofilms" Nature, Scientific Reports, 4, 6057, 2014.

[114] T. M. Monro, Y. D. West, D. W. Hewark, N. G. R. Borderick, and D. J. Richardson, "Chalcogenide holey fibres", IEE Electronics Letters, Vol. 36, No. 24,1998-2000, Nov. 2000.

[115] V. I. Beloglazov, M.V. Chainikov, Yu. S. Skibina, and V.V. Tuchin, "Spectral properties of a soft glass photonic crystal fiber" Journal of X-Ray Science and Technology, Vol. 13, No. 4, pp. 171-177, 2005.

[116] T. P. White, R. C. McPhedran, C. M. de Sterke, L. C. Botten, and M. J. Steel, "Confinement losses in microstructured optical fibers", Optics Letters, Vol. 26, Iss. 21, pp. 1660-1662, 2001.

[117] G. P. Agrawal, Applications of nonlinear fiber optics, 2E, Academic Press, Elsevier, 2007.

[118] K. Xie et al., "Fiber guiding at the Dirac frequency beyond photonic bandgaps", Light: Science & Applications, 4, e304, 2015. doi:10.1038/lsa.2015.77.

[119] F. Poli, A. Cucinotta, and S. Selleri, Photonic Crystal Fibers: Properties and Applications, Published by Springer, 2007.

[120] G. P. Agrawal, Nonlinear Fiber Optics, 5th ed., CA: Academic, San Diego, 2013.

[121] A. Ferrando, E. Silvestre, J. J. Miret, J. A Monsoriu, M. V. Andres, and P. S. J. Russell, "Designing a photonic crystal fiber with flattened chromatic dispersion", Electron. Lett., 35, 325-326, 1999.

[122] M. J. Gander, R. McBride, J. D. C. Jones, D. Mogilevtsev, T. A. Birks, J. C. Knight, and P. St. J. Russell "Experimental measurement of group velocity dispersion in photonic crystal fibre", Electron, Lett., 35, 63-64, 1999.

[123] T. A. Birks, D. Mogilevstev, J. C. Knight and P. St. J. Russell, "Dispersion compensation using single material fibers", IEEE Photon. Technol. Lett., 11, 674-676, 1999.

[124] J. C. Knight, J. Arriaga, T. A. Birks, A. Ortigosa-Blanch, W. J. Wadsworth, and P. St. J Russell "Anomalous dispersion in photonic crystal fiber", IEEE Photon. Technol. Lett., 12, 807-809, 2000.

[125] A. Ferrando, E. Sylvestre, J. J. Miret, and P. Andres "Nearly zero ultraflattened dispersion in photonic crystal fibers", Opt. Lett., 25, 790-792, 2000.

[126] A. Ferrando, E. Sylvestre, P. Andres, J. Miret, and M. V. Andres "Designing the properties of dispersion-flattened photonic crystal fibers", Opt. Exp., 9, 687-697, 2001.

[127] W. H. Reeves, J. C. Knight, P. St. J. Russell and P. J. Roberts, "Demonstration of ultra-flattened dispersion in photonic crystal fibers", Opt. Exp., 10, 609-613, 2002.

[128] R. K. Sinha, S. K. Varshney, "Dispersion Properties of Photonic crystal Fibers", Microwave Opt. Technol. Lett., Vol. 37, pp. 129-132, 2003.

[129] K. Saitoh, M. Koshiba, T. Hasegawa, and E. Sasaoka, "Chromatic dispersion control in photonic crystal fibers: application to ultra-flattened dispersion", Optics Express, 11, 843-852, 2003.

[130] N. A. Mortensen, "Effective area of photonic crystal fibers", Opt. Exp., 10, 341-348, 2002.

[131] M. Koshiba and K. Saitoh, "Structural dependence of effective area and mode field diameter for holey fibers", Opt. Express, 11, 1746-1756, 2003.

[132] I. Abdelaziz, F. Abdelmalek, H. Ademgil, S. Haxha, T. Gorman, and H. Bouchriha, "Enhanced effective area photonic crystal fiber with novel air hole design", Journal of Light wave Technology, Vol. 28, No. 19, 2010.

[133] H. Ademgil and S. Haxha, "Endlessly single mode photonic crystal fiber with improved effective mode area", Opt. Comm. 285, 1514-1518, 2012.

[134] M. Koshiba, and K. Saitoh, "Simple evaluation of confinement losses in holey fibers" Opt. Commun., 253, 95-98, 2005.

[135] T. Sorensen, J. Broeng, A. Bjarklev, E. Knudsen, and S. E. Barkou Libori, "Macrobending loss properties of photonic crystal fibre", Electron. Lett., 37, 287-289, 2001.

[136] J. I. Sakai, and T. Kimura, "Bending loss of propagation modes in arbitrary-index profile fibers", Appl. Opt., 17, 1499, 1978.

[137] T. Martynkien, J. Olszewski, M. Szpulak, G. Golojuch, W. Urbanczyk, T. Nasilowski, F. Berghmans, and H. Thienpont, "Experimental investigations of bending loss oscillations in large mode area photonic crystal fibers" Opt. Express, 15, 13547-13556, 2007.

[138] T. S. Saini, A. Kumar, and R. K. Sinha, "Design and analysis of large-core multitrench channel waveguide for high-power applications" Applied Optics, Vol. 54, No. 19, 6134-6139, 2015.

[139] M. Koshiba and K. Saitoh, "Finite-element analysis of birefringence and dispersion properties in actual and idealized holey fiber structures", Appl. Opt., 42, 6267-6275, 2003.

[140] F. Brechet, J. Marcou, D. Pagnoux and P. Roy, "Complete analysis of characteristics of propagation into photonic crystal fibers by the finite element method", Opt. Fiber Technol. 6, 181-191, 2000.

[141] M. Qiu, "Analysis of guided modes in photonic crystal fibers using the finite-difference time-domain method" , Microwave and Optical Technology Letters, Vol. 30, No. 5, pp. 327-330, 2001.

[142] Z. Zhu, T. Brown, "Full-vectorial finite-difference analysis of microstructured optical fibers", Optics Express, Vol. 10 Issue 17, pp. 853-864, 2002.

[143] C. E. Kerbage, B. J. Eggleton, P. S. Westbrook, and R. S. Windeler, "Experimental and scalar beam propagation analysis of an air-silica microstructure fiber", Opt. Exp., 7, 113-122, 2000.

[144] F. Fogli, L. Saccomandi, and P. Bassi, "Full vectorial BPM modeling of index-guiding photonic crystal fibers and couplers", Opt. Exp., 10, 54-59, 2001.

[145] J. C. Knight, T. A. Birks, P. St. J. Russell and J. P. de Sandro, "Properties of photonic crystal fiber and the effective index model", J. Opt. Soc. Am. A, 15, 748-752, 1998.

[146] K. Kishor, R. K. Sinha, and A. D. Varshney, "Experimental verification of improved effective index method for endlessly single mode photonic crystal fiber" Optics and Lasers in Engineering, 50 (2), 182-186, 2012.

[147] R. K. Sinha, and A. D. Varshney, "Dispersion properties of photonic crystal fiber: comparison by scalar and fully vectorial effective index methods" Optical and Quantum Electronics, 37, 711-722, 2005.

[148] R. Pratap, Getting started with MATLAB 7: A quick introduction for Scientists and Engineers, Oxford University press, 2006.

[149] S. J. Chapman, MATLAB programming for Engineers, 2E, Thomson Asia Pte Ltd, Singapore, 2002.

[150] G. L. Harris, Properties of Silicon Carbide, Inspec, Institution of Electrical Engineers, London, 1995.

[151] L. Pavesi, and D. J. Lockwood, Silicon photonics, Springer, 2003.

[152] S. G. Johnson, S. Fan, P.R. Villeneuve, and J. D. Joannopoulos, "Guided modes in photonic crystal slabs", Phys. Rev. B, 60, 5751-5758, 1999.

[153] S. Yamada, B.S. Song, T. Asano, and S. Noda, "Experimental investigation of thermo-optic effects in SiC and Si photonic crystal nanocavities", Opt. Lett., OSA, 36, 3981-3983, 2011.

[154] E. Chow, S. Y. Lin, S. G. Johnson, P. R. Villeneuve, J. D. Joannopoulos et al, "Three-dimensional control of light in a two-dimensional photonic crystal slab", Nature, 407, 983-986, 2000.

[155] J. Zhou, H. Li, L. Ye, J. Liu, J. Wang, T. Zhao, L. Jiang, and Y. Song, "Facile fabrication of Tough SiC inverse opal photonic crystals", J. Phys. Chem. C, 114, 22303, 2010.

[156] M. Ziaei-Moayyed, M. F. Su, C. M. Reinke, I. El-Kady, and R. H. Olsson, "Silicon Carbide Phononic Crystals for high f.Q Micromechanical Resonators", IEEE IUS Proceedings, ULTSY M. , 162-166, 2010.

[157] B. Wild, R. Ferrini, R. Houdré, M. Mulot, S. Anand, and C. J. M. Smith, "Temperature tuning of the optical properties of planar photonic crystal micro cavities", Proceedings of SPIE, Bellingham, WA, 5450, 311-317, 2004.

[158] S. M. Weiss, M. Molinari, and P. M. Fauchet, "Temperature stability for silicon-based photonic band-gap structures", Applied Physics Letters, 83 (10), 1980-1982, 2003.

[159] T. Katsuyama, K. Ishida, S. Satoh, and H. Matsumura, "Low loss Ge-Se chalcogenide glass optical fibers" Appl. Phys. Lett., 45, 925, 1984.

[160] B. Dabas, and R. K. Sinha, "Dispersion Characteristic of Hexagonal and Square Lattice Chalcogenide $A_{s2}S_{e3}$ Glass Photonic Crystal Fiber", Opt. Comm., 283, 1331-1337, 2010.

[161] J. Hu , C. R. Menyuk , L. B. Shaw , J. S. Sanghera , and I. D. Aggarwal , " Maximizing the bandwidth of supercontinuum generation in As_2Se_3 chalcogenide fibers" Opt. Express, 18(7), 6722–6739, 2010.

[162] M. El-Amraoui , G. Gadret , J. C. Jules , J. Fatome , C. Fortier , and J. Troles , " Microstructured chalcogenide optical fibers from As_2S_3 glass: Towards new IR broadband sources" Opt. Express, 18, 26655–26665, 2010.

[163] M. A. V. Eijkelenborg, A. Argyros, G. Barton, I. M. Bassett, M. Fellew, G. Henry, N. A. Issa, M. C. J. Large, S. Manos, W. Padden, L. Poladian, and J. Zagari, "Recent progress in microstructured polymer optical fibre fabrication and characterisation" Optical Fiber Technology, 9, 199–209, 2003.

[164] H. Shi, X. Feng, F. Tan, P. Wang, and P. Wang, "Multi-watt mid-infrared supercontinuum generated from a dehydrated large-core tellurite glass fiber" Opt. Mat. Exp., 6, 12, 3967, 2016.

[165] Z. Jia, C. Yao, S. Jia, F. Wang, S. Wang, Z. Zhao, G. Qin, Y. Ohishi, and W. Qin, "4.5 W supercontinuum generation from 1017 to 3438 nm in an all-solid fluorotellurite fiber" Appl. Phys. Lett., 110, 261106, 2017.

[166] M. K. Yang, R. H. French, and E. W. Tokarsky, "Optical properties of Teflon AF amorphous fluoropolymers" Journal of Micro, Nanolithography, MEMS, and MOEMS , 7(3), 2008.

[167] P. Shumyatsky, and R. R. Alfanso "Terahertz Sources", Journal of Biomedical Optics, SPIE, 16, 033001, 2011.

[168] S. Kim, C. S. Kee, and J. Lee, "Single – mode Condition and Dispersion of Terahertz Photonic Crystal Fiber" Journal of optical society of Korea, 11(3), 97-100, 2007.

[169] Z. Y. Chen, H. Su, C.-D. Wang, Q.-Z. Chen, and S.-C. Ruan, "Transmission characteristics of Teflon solid-core PCF for Terahertz region by using Finite Element Method" Proc. of SPIE Vol. 8195, 81950, 2011.

[170] K. Saitoh, and M. Koshiba, "Leakage loss and group velocity dispersion in air-core photonic band-gap fibers", Opt. Exp.11, 3100–3109, 2003.

[171] R. K. Sinha, and S. K. Varshney, "Dispersion Properties of Photonic crystal Fibers", Microwave Opt. Technol. Lett. 37, 129-132, 2003.

[172] N. Muduli, J. S. N. Achary, and H. K. Padhy, "Grade-2 Teflon (AF1601) PCF for optical communication using 2D FDTD technique: a simplest design" Journal of Modern Optics, ISSN: 0950-0340 (Print), 1362-3044 (Online), 2015.

[173] M. Goto, A. Quema, H. Takahashi, S. Ono, and N. Sarukura "Polarization-preserving teflon photonic crystal fiber waveguide for THz radiation" Joint 29th Int. Conf. on Infrared and Millimeter Waves and 12th Int. Conf. on Terahertz Electronics, Novel Devices and Components, IEEE, 139-140, 2004.

[174] R. Pobre, A. Quemal, E. Estacio, H. Murakami, S. Ono, and N. Sarukura, "Modal analysis of Teflon photonic crystal fiber as a terahertz waveguide" Joint 30th Int. Conf. on Infrared and Millimeter Waves and 13th Int. Conf. on Terahertz Electronics, Novel Devices and Components, IEEE, 103-104, 2005.

[175] T. S. Saini, A. Kumar, and R. K. Sinha, "Triangular-core large-mode-area photonic crystal fiber with low bending loss for high power applications," Appl. Opt., 53(31), 7246-7251, 2014.

[176] T. S. Saini, A. Kumar, and R. K. Sinha, "Broadband mid-infrared supercontinuum spectra spanning 2-15 μm using As_2Se_3 chalcogenide glass triangular-core graded-index photonic crystal fiber", J. Lightwave Technol., 33(18), 3914 - 3920, 2015.

[177] R. K. Sinha, A. Kumar, and T. S. Saini, "Analysis and Design of single-mode As_2Se_3-chalcogenide photonic crystal fiber for generation of slow light with tunable features," IEEE J. Sel. Topics Quant. Electron., 22(2), 4900706, 2016.

[178] T. S. Saini, A. Kumar, and R. K. Sinha, "Asymmetric large-mode-area photonic crystal fiber structure with effective single-mode operation: design and analysis," Appl. Opt., 55(9), 2306 – 2311, 2016.

[179] A. Kumar, T.S. Saini, K.D. Naik, and R. K. Sinha, "Large-mode-area single-polarization single-mode photonic crystal fiber: design and analysis" Applied Optics, 55(19), 4995-5000, 2016.

[180] S. Kawakami, S. Nishida, and M. Sumi, "Transmission characteristics of W-type optical fibers", Proc. IEE, 123(6), 586-590, 1976.

[181] A. T. Andreev, A. B. Grudinin, E. M. Dianov, A. M. Prokhorov, A. N. Guryanov, G. G. Devjatykh, S. V. Ignatjev, and V. F. Hopin, "Experimental study of single-mode W-Type Optical Fiber", Electronics Lett., 17(12), 416-417, 1981.

[182] K. Thyagarajan, R. K. Varshney, P. Palai, A. K. Ghatak, and I. C. Goyal, "A novel design of a dispersion compensating fiber", IEEE Photonics Technology Letters, Vol. 8, No. 11, November, 1996.

[183] K. Saitoh, and M. Koshiba, "Single-polarization single-mode photonic crystal fibers," IEEE Photonics Tech. Lett. 15, 1384-1386, 2003.

[184] J. Boruah, "Propagation characteristics of solid defect-core W-Type photonic crystal fiber", Workshop on Recent Advances in Photonics (WRAP), 17-18 Dec' 2013, IITD, New Delhi, India and published in IEEE Xplore, 14663368, 09 Oct' 2014.

[185] E. K. Akowuah, H. Ademgil, S. Haxha, and F. Abdelmalek, "An endlessly single-mode photonic crystal Fiber with low chromatic dispersion and bend and rotational insensitivity", J. of Light wave Technol., 27(17), 3940-3947, 2009.

[186] B. G. Ward, "Bend performance-enhanced photonic crystal fibers with anisotropic numerical aperture", Opt. Express, 16(12), 8532-8548, 2008.

[187] N. H. Vu, I. Hwang, and Y. Lee, "Bending loss analyses of photonic crystal fibers based on the finite-difference time-domain method", Opt. Lett., Vol. 33, No. 2 , 119-121, January 15, 2008.

[188] S. K. Varshney, M. P. Singh, and R.K. Sinha, "Propagation characteristics of Photonic Crystal Fibers", J. of Opt. Commun., 24, 856, 2003.

[189] K. Saitoh, Y. Tsuchida, M. Koshiba, and N. A. Mortensen, "Endlessly single-mode holey fibers: the influence of core design", Opt. Express, 13(26): 10833-10839, 2005.

[190] C. Markos, K. Vlachos, and G. Kakarantzas, "Bending loss and thermo-optic effect of a hybrid PDMS/silica photonic crystal fiber", Opt. Express, 18(23), 24344-24351, 2010.

[191] G. H. Ames et al., "Fiber-Optic Hydrophone Arrays: Radial Temperature Compensation Package for Bragg Gratings", NUWC-NPT Technical Report, 11,112, 1999.

[192] X. Li, Z. Xu, W. Ling, and P. Liu, "Design of highly nonlinear photonic crystal fibers with flattened chromatic dispersion," Appl. Opt., 53 (29) 6682-6687, 2014.

[193] N. A. Mortensen, et al., "Improved large-mode-area endlessly single mode photonic crystal fibers", Opt. Express, 28(6), 393, 2003.

[194] M. Napierała, et al., "Extremely large-mode-area photonic crystal fibre with low bending loss", Opt. Express, 18, 15408–15418, 2010.

[195] J. Li et al., "Novel large mode area photonic crystal fibers with selectively material-filled structure", Opt. & Laser Tech., 48, 375-380, 2013.

[196] J. W. Fleming, and D. L. Wood, "Refractive index dispersion and related properties in fluorine doped silica", Appl. Opt., 22, 19, 3102-3104, 1983.

[197] D. Kundu, and S. Sarkar, "Prediction of propagation characteristics of photonic crystal fibers by a simpler, more complete and versatile formulation of their effective cladding indices", Opt. Eng., 53(5), 056111, 2014.

[198] J. Boruah, Y. Kalra, and R. K. Sinha, "Cladding doped defect-core large mode area W-type photonic crystal fiber", Proc. SPIE, 9958, 2016.

[199] J. Boruah et al., "Temperature-dependent bending loss characteristics of W-type photonic crystal fibres: design and analysis", J. of Modern Opt., 1-6, 2016. [doi: 10.1080/09500340.2016.1262916].

[200] J. Boruah, T. S. Saini, and R. K. Sinha, "Low bend loss photonic crystal fiber in Ga-Sb-S based chalcogenide glass for nonlinear applications: design and analysis", J. of Nanophotonics, 11(3), 036002-1–036002-8, 2017.

[201] H. C. Park et al., "Analyses of cladding modes in photonic crystal fiber", Opt. Express, 15(23), 15154, 2007.

[202] G. Singh, S. Sahu, and P. Chaurasia, "Modeling of photonic crystal fibers with Fibonacci-patterned circular and elliptical air holes", Opt. Eng., 51(11), 115001, 2012.

[203] H. Ademgil, and S. Haxha, "PCF based sensor with high sensitivity, high birefringence and low confinement losses for liquid analyte sensing applications", Sensors, 15, 31833–31842, 2015.

[204] D. K. C. Wu et al., "Performance of refractive index sensors based on directional couplers in photonic crystal fibers", J. of Light wave Technol., 31, 22, 3500-3510, 2013.

[205] S. Padidar, V. Ahmadi, and M. Ebnali-Heidari, "Design of high sensitive pressure and temperature sensor using photonic crystal fiber for downhole application", IEEE Photonics J., 4(5), 1590-1599, 2012.

[206] K. Saitoh, and M. Koshiba, "Highly nonlinear dispersion-flattened photonic crystal fibers for supercontinuum generation in a telecommunication window", Opt. Express, 12(10), 2027, 2004.

[207] M. Ebnali-Heidari et al., "Dispersion engineering of photonic crystal fibers by means of fluidic infiltration", J. of Modern Opt., 59(16), 1384–1390, 2012.

[208] H. Ademgil, and S. Haxha, "Highly nonlinear birefringent photonic crystal fiber", Opt. Commun., 282, 2831–2835, 2009.

[209] H. Ademgil, and S. Haxha, "Ultrahigh-birefringent bending-insensitive nonlinear Photonic crystal fiber with low losses", IEEE Journal of Quantum Electronics, Vol. 45, No. 4, 351-358, 2009.

[210] T. S. Saini, A. Bailli, A. Kumar, R. Cherif, M. Zghal, and R. K. Sinha, "Design and analysis of equiangular spiral photonic crystal fiber for mid-infrared supercontinuum generation," J. Modern Optics, 62(19), 1570 – 1576, 2015.

[211] J. Liao, J. Sun, M. Du, and Y. Qin, "Highly nonlinear dispersion-flattened slotted spiral photonic crystal fibers", IEEE Photonics Technology Letters, Vol. 26, No. 4, 380-383, February 15, 2014.

[212] R. Zhang, J. Teiple, and H. Giessen, "Theoretical design of a liquid core photonic crystal fiber for supercontinuum generation," Opt. Express, Vol. 14, No. 15, pp. 6800-6812, July, 2006.

[213] J. Liao, and T. Huang, "Highly nonlinear photonic crystal fiber with ultrahigh birefringence using a nano-scale slot core", Optical Fiber Technology, 22, 107–112, 2015.

[214] A. Yang, M. Zhang, L. Li, Y. Wang, B. Zhang, Z. Yang, and D. Tang, "Ga–Sb–S Chalcogenide Glasses for Mid-Infrared Applications", J. Am. Ceram. Soc., 1–4, 2015. DOI: 10.1111/jace.14025.

[215] M. Y. Chen, Y. R. Li, J. Zhou, and Y. K. Zhang, "Design of Asymmetric Large-mode Area Optical Fiber With Low-bending Loss", J. Lightwave Tech., 31(3), 2013.

[216] X. Wang, S. Lou, and W. Lu, "Bending orientation insensitive large mode area photonic crystal fiber with triangular core", IEEE Photonics Journal, 5(4), 2013.

[217] R. Guobin, W. Zhi, L. Shuqin, and J. Shuisheng, "Mode classification and degeneracy in photonic crystal fibers", Optics Express, Vol. 11, No. 11, 1310, 2003.

[218] F. Oskooi, J. D. Joannopoulos, and S. G. Johnson, "Zero–group-velocity modes in chalcogenide holey photonic-crystal fibers", Optics Express, Vol. 17, No. 12, 10082, 2009.

[219] S. T. Chu, and S.K. Chaudhuri, "A finite-difference time-domain method for the design and analysis of guided-wave optical structures", Journal of Lightwave Technology, 7(12), 2033-2038, 1989.